AD_____

Award Number: W81XWH-06-1-0271

TITLE: Development of a Smart Diagnostics Platform for Early-Stage Screening of Breast Cancer

PRINCIPAL INVESTIGATOR: Joerg Lahann

CONTRACTING ORGANIZATION: University of Michigan
Ann Arbor, MI 48109

REPORT DATE: April 2008

TYPE OF REPORT: Annual

PREPARED FOR: U.S. Army Medical Research and Materiel Command
Fort Detrick, Maryland 21702-5012

DISTRIBUTION STATEMENT: Approved for Public Release;
Distribution Unlimited

REPORT DOCUMENTATION PAGE

Form Approved
OMB No. 0704-0188

1. REPORT DATE	2. REPORT TYPE	3. DATES COVERED
01-04-2007	Annual	1 Apr 2007 – 31Mar 2008

4. TITLE AND SUBTITLE

Development of a Smart Diagnostics Platform for Early-Stage Screening of Breast Cancer

5a. CONTRACT NUMBER

5b. GRANT NUMBER
W81XWH-06-1-0271

5c. PROGRAM ELEMENT NUMBER

6. AUTHOR(S)

Joerg Lahann

Email: lahann@umich.edu

5d. PROJECT NUMBER

5e. TASK NUMBER

5f. WORK UNIT NUMBER

7. PERFORMING ORGANIZATION NAME(S) AND ADDRESS(ES)

University of Michigan
Ann Arbor, MI 48109

8. PERFORMING ORGANIZATION REPORT NUMBER

9. SPONSORING / MONITORING AGENCY NAME(S) AND ADDRESS(ES)
U.S. Army Medical Research and Materiel Command
Fort Detrick, Maryland 21702-5012

10. SPONSOR/MONITOR'S ACRONYM(S)

11. SPONSOR/MONITOR'S REPORT NUMBER(S)

12. DISTRIBUTION / AVAILABILITY STATEMENT
Approved for Public Release; Distribution Unlimited

13. SUPPLEMENTARY NOTES

14. ABSTRACT

The proposed research aims to develop innovative technology that could ultimately lead to new breast cancer screening tests — ones, which will not require expensive equipment for read-out, but rather will be compatible with miniaturized systems integrated in cheap handheld devices. Towards this goal, we have designed and realized in practice a surface that can act as detection unit. This opens the door for further work that will be geared towards testing of biomarkers.

15. SUBJECT TERMS
No subject terms provided.

16. SECURITY CLASSIFICATION OF:			17. LIMITATION OF ABSTRACT	18. NUMBER OF PAGES	19a. NAME OF RESPONSIBLE PERSON
a. REPORT	b. ABSTRACT	c. THIS PAGE			USAMRMC
U	U	U	UU	58	19b. TELEPHONE NUMBER *(include area code)*

Table of Contents

Page

A. INTRODUCTION.

In the last thirty years, the fight against breast cancer has made impressive strides in diagnosis and treatment. Because of the essential importance that early detection has for successful therapy, the American Cancer Society currently recommends that women over the age of 20 should have a clinical breast exam every three years and that women over the age of 40 should have annual screening mammograms and clinical breast exams. Although current screening methods save thousands of lives each year, they are costly and in some cases ineffective. The proposed research aims to develop innovative technology that could ultimately lead to new breast cancer screening tests which will be compatible with miniaturized systems integrated in cheap handheld devices suitable for widespread screening of large population groups. Ultimately, the technology may allow for screening of cancer-indicative biomarkers in the urine or the breath, thereby establishing non-invasive avenues for screening. The bioindicators that we are targeting are apolar metabolites indicative of early-stage breast cancer. The unique structure of our low-density self-assembled monolayers provides a nano-porous structure that can capture such hydrophobic target molecules, causing measurable changes in surface properties (e.g., changes in the electrical resistance or impedance). Modification of the functional groups may allow customized selectivity to be engineered into the surfaces. If required, the unique switching function of "smart surfaces" can potentially be used to regenerate the sensor surface and confer re-usability to the device. The mono-molecular thickness of the sensor surface also yields the potential for part-per-million sensitivity. The current methods used to analyze bioindicators in urine and breath include high-performance liquid chromatography, gas chromatography, mass spectrometry, and enzyme-linked immunosorbent assay. All of these methods require sophisticated laboratory instrumentation and are not compatible with widespread, in-home screening of large population groups. It's the ultimate goal of this *Idea Award* proposal to conduct a proof-of-concept study of the first-time design and evaluation of switchable signal transduction units for screening of breast-cancer indicative biomarkers.

B. Body.

Under this *Idea Award* proposal, we intend to develop basic technology for screening of metabolites in a complex environment such as breath or urine. This goal shall be achieved by designing surfaces with nano-scale architecture and porosity ("smart surfaces") that can undergo conformational switching due to the application of external stimuli. Our specific design hypothesis is that the proper molecular design of these "smart surfaces" will lead to surfaces with dynamically controlled binding events of metabolites indicative of early-stage breast cancer (Figure 1). In contrast to conventional screening approaches, a screening platform that relies on "smart surfaces" for signal transduction will have improved ability to be operated in a complicated environment, such as urine or breath, and thus will be amenable to widespread screening of large population groups. Moreover, the proposed "smart surfaces" can be recharged to ensure continuous sampling. This feature may prove to be critical when sensing metabolites, which may undergo less specific binding events than proteins or DNA, currently used in blood tests.

Proposed Approach.

In accordance with the guidelines of the *Idea Award*, this project has been developed as a pilot study to evaluate the feasibility of "smart surfaces" for screening of early-stage breast cancer markers**.** While the potential impact of such a technology would be enormous, the proposal is associated with considerable risk. However, we believe that the anticipated progress towards the overarching goal of our program - the development of widely-applicable, non-invasive, and cost-effective diagnostic tools for early-stage metabolic indicators of breast cancer – will far outweigh these risks. One of the major scientific limitations of this project is that it focuses solely on *in vitro* studies. Any meaningful effort in the field requires confirmation by animal studies, and eventually also by clinical

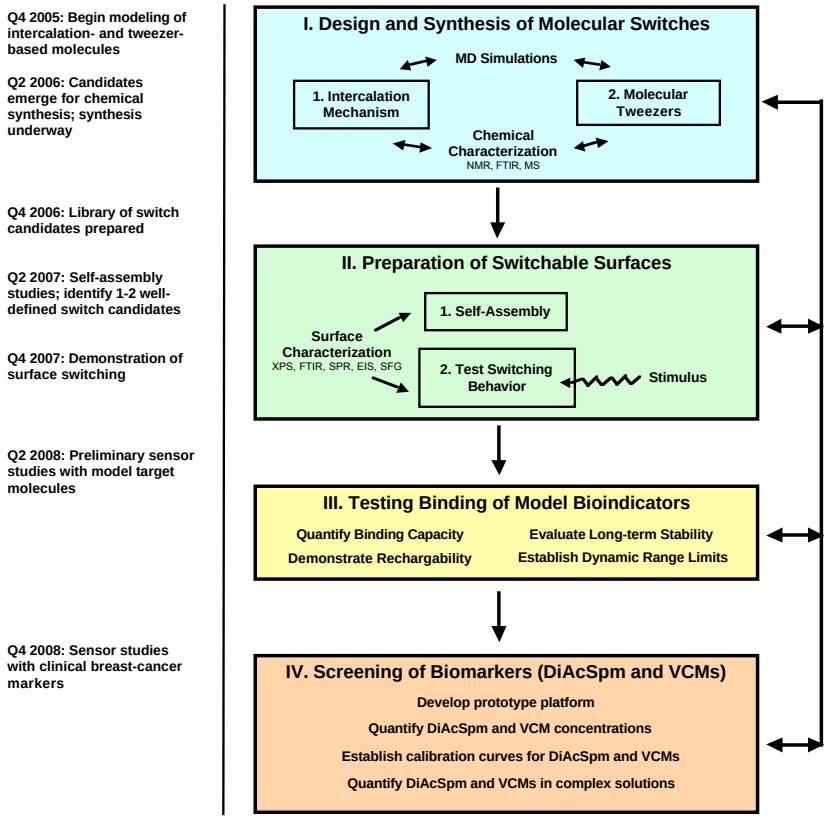

Scheme 1: *Originally proposed outline of the proposed activities towards "smart surfaces" technology.*

studies. However, these efforts are very expensive and must be of a collaborative nature. We will leverage the data obtained in this study to obtain NIH funding for follow-up activities. The following section describes the detailed methods proposed to realize our four objectives.

WORK DONE TOWARDS SPECIFIC AIM #1 (YEARS 1 AND 2):

DESIGN AND SYNTHESIS OF MOLECULAR SWITCHES WITH SELECTIVE BINDING PROPERTIES FOR BIOINDICATORS.

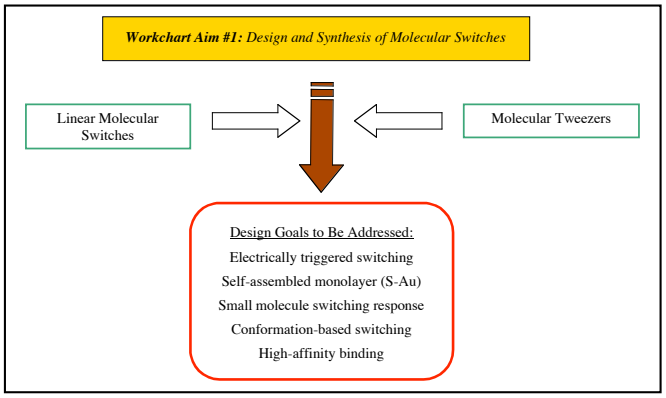

Synthesis of Linear Molecular Switches.

Initially, low-density self-assembled monolayers (LDSAMs) of 16-chlorotrityl-mercaptohexadecanoic acid (CT-MHA) and 16-chlorotrityl-mercaptoundecanoic acid (CT-MUA) were syntheisized with the intent to prepare self-assembled monolayers of linear molecular switches on gold and silver electrodes. Figure 2 outlines the synthetic method for preparing regular SAMs of MHA and MUA as well as the indirect assembly method for preparing LDSAMs as detailed in a recent publication.[1] The indirect method was designed to circumvent the tendency of alkanethiolates to form tightly-packed assemblies resembling two-dimensional crystals.[2,3] The approach involves a multi-step process of conjugating MHA or MUA to bulky, space-filling chlorotrityl (CT) groups to form CT-MHA or CT-MUA esters. The subsequent assembly of CT-MHA or CT-MUA monolayers on gold or silver is followed by cleavage of the bulky CT groups, resulting in LDSAMs of MHA and MUA that are chemically identical to regular SAMs, but differ from the latter in the molecular spacing between the chains.

The synthesis of 16-chlorotrityl-mercaptohexadecanoic acid (CT-MHA) has been reported previously[4] and has now been extended to other variants (MUA). The synthesis of 16-chlorotrityl-mercaptoundecanoic acid (CT-MUA) was performed using a protocol that was similar to that of CT-MHA. The first step involves protection of the thiol tail of MUA with a dimethoxytrityl (DMT) group to form the thioether MUA-DMT. Next, 1.09 g MUA were reacted with 1.76 g DMT-Cl and 0.84 mL of triethylamine in 50 mL of 5:4:1 tetrahydrofuran : acetic acid : water, at room temperature, under argon atmosphere, for 14 hr. MUA-DMT was isolated and purified by silica column chromatography (3:1:1 hexane : ethyl ether : THF) yielding 1.3 g of a yellow/amber oil product.

The second step involves protection of the carboxyl head group of MUA-DMT with a chlorotrityl (CT) group to form the ester/thioether CT-MUA-DMT. Next, 1.3 g of purified MUA-DMT were reacted with 0.91 g of CT-Cl and 0.91 mL

of DIPEA in 50 mL methylene chloride, at room temperature, under argon atmosphere, for 14 hr. CT-MUA-DMT was isolated and purified by silica column chromatography (3:1 hexane : ethyl ether) yielding 0.68 g of a clear oil product. The third step involves de-protection of the DMT group from the thiol tail of MUA to form the ester CT-MUA. 0.68 g of purified CT-MUA-DMT was dissolved in 20 mL of 3:1 THF : methanol and 2 mL 1 M sodium acetate, to which was added a solution of 340 mg silver nitrate in 4 mL of 5:1 methanol : water. The mixture was stirred for 1 hr at room temperature. Precipitate was removed by centrifugation at 4000 × g for 5 minutes, followed by resuspension of the pellet in 15 mL of 3:1 THF : methanol, re-centrifugation at 4000 × g for 5 minutes, and combination of the two supernatants. A solution of 308 g of dithioerythritol (DTE) in 3 mL of 1 M sodium acetate was then added, and the mixture was stirred for 5 hr at room temperature. Precipitate was removed by centrifugation at 4000 × g for 5 minutes, followed by resuspension of the pellet in 15 mL of 3:1 THF : methanol, re-centrifugation at 4000 × g for 5 minutes, and combination of the two supernatants. CT-MUA was isolated and purified by silica column chromatography (50 mL of 3:1 hexane : ethyl ether, followed by 1:1 hexane : ethyl ether), yielding 0.22 g of a clear oil product. CT-MUA (and CT-MHA) was aliquoted and stored at -20° C until used.

Synthesis of molecular tweezers.

On a basis of a rational modeling approach we have identified promising initial structures for molecular tweezers and have worked towards a successful implementation of their synthesis. While initial synthesis efforts were challenging, we were able to establish a successful route recently (manuscript in preparation). While we are hopeful that this route can generate sufficient amounts of materials (gram scale) for our studies, we have so far only isolated analytical amounts of the end product. Further work will be directed towards repetition and refinement of the initial work to generate sufficient materials for the monolayer work proposed in Aimw #2 and #3.
Detaills of the synthesis are outlined below.

Cholic tetraol **2**: To a solution of cholic acid (16.4g, 97%) in anhydrous THF (300 mL) was carefully added $LiAlH_4$ (8.6 g, 95%). The resulting suspension was stirred at 50 °C under nitrogen for 24 hrs. After cooling in ice bath, the excess $LiAlH_4$ was quenched by careful addition of dilute HCl. 3 M HCl (600 mL) was added and the THF was then removed. After filtration, the solid crude product was washed with water and recrystallized from ethanol to give white crystals (14.5 g, 91%).

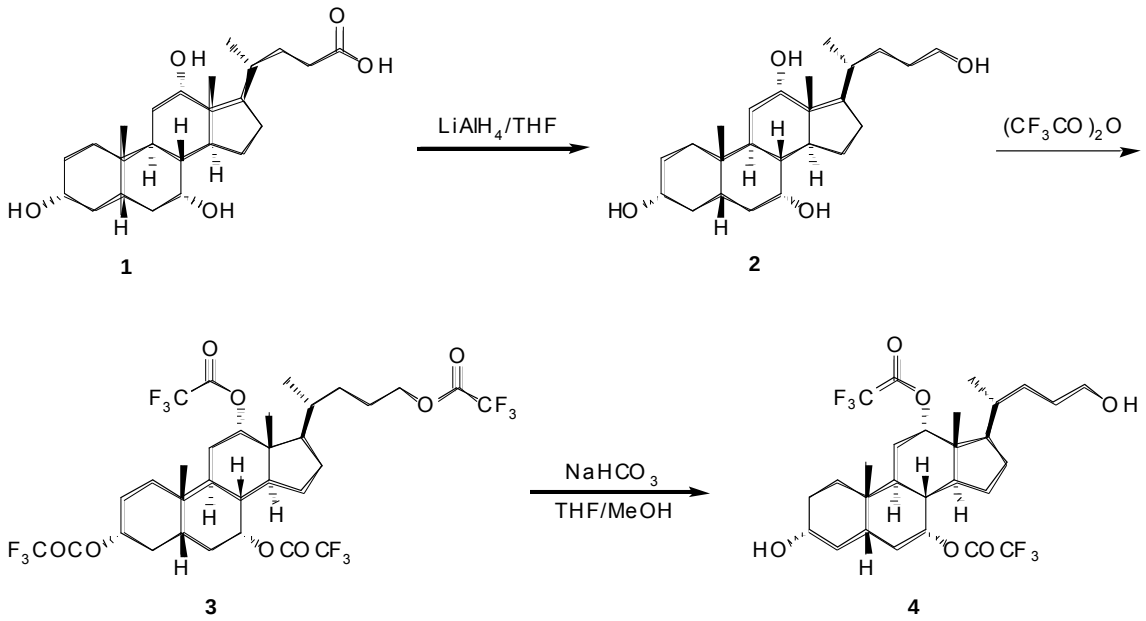

1 2 3 4

Cholic tetra-trifluoroacetate **3**: To a 250 mL round bottom flask cooled in ice bath charged with cholic tetraol **2** (9.1g) was added trifluoroacetic anhydride (60 mL) dropwise under nitrogen. After the addition, the solution was stirred at room temperature overnight. The volatile compounds were then removed under vacuum to give a colorless oil which was used without further purification.

Cholic di-trifluoroacetate **4:** To a cholic tetra-trifluoroacetate **3** solution in anhydrous THF (40 mL) was added anhydrous methanol (200 mL) and sodium bicarbonate (10.0 g) and the resulting mixture was kept in refrigerator at 4 °C for 6 days.

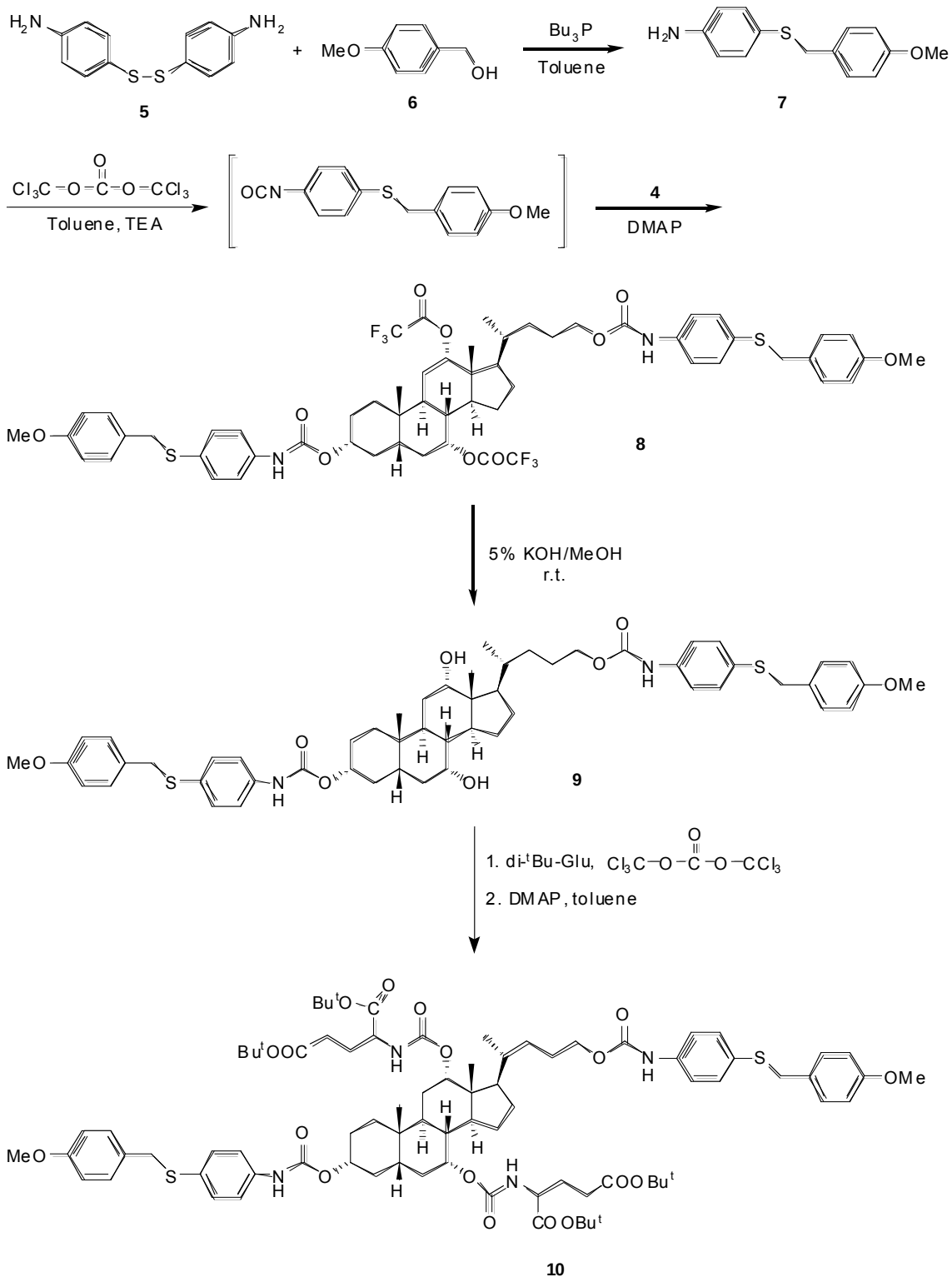

5 6 7 8 9 10

The reaction mixture was poured into ice water (500 mL) and extracted with ether (3 x 250 mL). The combined extracts was washed with brine (2 x 300

mL) and dried over Na_2SO_4. After filtration and removal of solvent, the pale yellow oil was purified on silica gel using hexanes/ethyl acetate (7/3, v/v) as eluent to give the product as a colorless solid.

Protected 4-aminophenyl thiol **7**: A solution of 4-aminophenyl disulfide **5** (5.3 g) and 4-methoxybenzyl alcohol **6** (2.2 mL) in anhydrous toluene (120 mL) was degassed by two freeze-pump-thaw cycles, followed by addition of tributylphosphine (5.0 mL) under argon and two more freeze-pump-thaw cycles. The mixture was then stirred at 70 °C under argon for 24 hrs. After cooling to room temperature, the reaction mixture was diluted with diethyl ether (200 mL), washed with 5 wt% aqueous NaOH (2 x 150 mL) and brine (2 x 150 mL), and dried over Na_2SO_4. After filtration and removal of solvents, the crude product was purified on silica gel using hexanes/ethyl acetate (7/3) as eluent to give the product as pale yellow crystals (3.9 g).

Cholic di-carbamate **8**: To a solution of protected 4-aminophenyl thiol **7** (3.5 g) in anhydrous toluene (60 mL) was added bis(trichloromethyl) carbonate (1.75 g). The resulting solution was refluxed under argon for three hours and then cooled to room temperature. Cholic di-trifluoroacetate **4** (3.8 g) was added into this cooled solution under argon purge and the solution was stirred at 60 °C under argon overnight. The reaction mixture was then cooled to room temperature, diluted with diether ether (300 mL), washed with 2 M HCl (3 x 50 mL) and brine (2 x 100 mL), and dried over Na_2SO_4. After filtration and removal of solvents, the residue was purified on silica gel using hexanes/EtOAc (65/35, v/v) as eluent to give the product as a pale yellow solid (4.8 g).

Cholic diol **9**: To a solution of NaOH (5.0 g) in methanol (150 mL) was added a solution of cholic di-carbamate **8** (5.4 g) in THF (30 mL). The resulting solution was stirred for 12 hours at room temperature, followed by the addition of 10 mL acetic acid. The solution was then poured into 400 mL of water and extracted with diethyl ether (3 x 250 mL). The combined ether layer was dried over Na_2SO_4. Filtration and removal of solvent gave crude product as a light brown oil which was purified on silica gel using hexanes/EtOAc (3/2, v/v) to give the product as white solid (4.2 g).

Cholic tetracarbamate **10**: To a solution of L-Glutamic acid di-*tert*-butyl ester hydrochloride (1.52 g) in anhydrous toluene (10 mL) cooled at – 80 °C was added triethylamine (2.1 mL) and a bis(trichloromethyl) carbonate (530 mg) solution in anhydrous toluene (4 mL) under nitrogen. The solution was allowed to slowly warm up to room temperature and stirred at RT for 4 hours. A cholic diol **9** (750 mg) solution in anhydrous toluene (10 mL) and anhydrous pyridine (4.5 mL) were then added into the reaction mixture using a syringe and the mixture was refluxed for 36 hours under nitrogen. After cooling to RT, the solution was diluted by diethyl ether (150 mL), washed with 2 M HCl (2 x 100 mL) and brine (2 x 100 mL), and dried over Na_2SO_4. After filtration and removal of solvents, the residue was purified on silca gel using CH_2Cl_2/ether (95/5, v/v) as eluent to give the

product as a light brown oil (140 mg). Subsequently, the thiol protection group was removed and the resulting disulfide derivative was confirmed on the basis of H-NMR and mass spectrometry.

WORK DONE TOWARDS SPECIFIC AIM #2 (YEARS):

PREPARATION AND CHARACTERIZATION OF SMART SCREENING PLATFORMS FOR MODEL BIOINDICATORS.

Self-assembly of monolayers has been conducted so far with linear switches only and has been recently reported. The self-assembly of molecular tweezers will follow the approach described herein and the lessons learnt from the characterization of linear switches will equally apply to molecular tweezers.

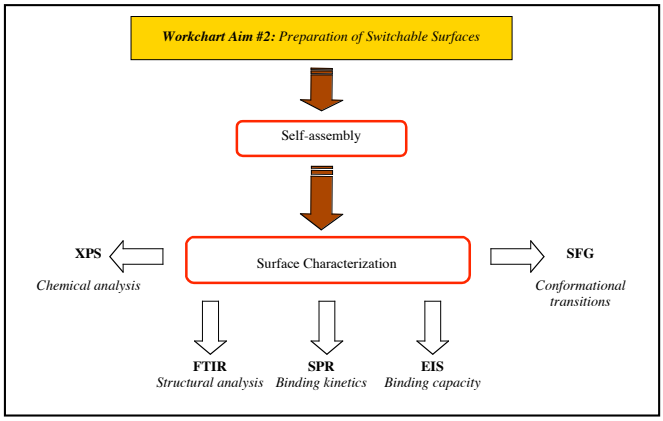

Monolayers of mercaptohexadecanoic acid and mercaptoundecanoic acid were assembled on both, gold and silver electrodes. When conducting electrochemical impedance spectroscopy under physiological conditions, these monolayers exhibit significant changes in their electrochemical barrier properties upon application of electrical DC potentials below +400 mV with respect to a standard calomel electrode. We further found the impedance switching to be reversible under physiological conditions. Moreover, the impedance can be fine-tuned by changing the magnitude of the applied electrical potential. Before and during impedance switching at pH 7.4 in aqueous buffer solutions, the low-density monolayers showed good stability according to grazing angle infrared spectroscopy data.

Further details of the synthesis and characterization via FTIR and impedance spectroscopy have been reported in a recent publication and have been included as attachment.

In an extension of these initial studies, we have self-assembled the resulting molecular tweezers, i.e. the disulfide derivative described under Aim #1, on gold electrodes and confirmed the presence of a well defined monolayer by a combination of FTIR spectroscopy and electrochemical impedance spectroscopy.

In independent work, we further examined the storage stability of monolayers made of linear molecular switches for several weeks. Extended stability is an important criterion for selection of suitable signal transduction systems. **A**

manuscript describing the stability has been published in Langmuir in 2007 and is included as attachment.

Microfabrication methods have been used to produce substrates appropriate for monolayer analysis techniques such as electrochemical impedance spectroscopy. These substrates consisted of a 4500 Å SiO_2 insulating layer, a 100 Å titanium adhesive layer, and a 1000 Å gold active layer. The electrical contacting zone allows connection of an electrical lead to the monolayer zone (via the conductive strip). The monolayer zone is of a defined surface area (2.5 cm^2), for controlled measurement of electrochemical parameters that scale with surface area. Root mean square roughness of gold surfaces has been determined by atomic force microscopy to be <2 nm, providing an ultra-flat surface for monolayer assembly. The gold substrate have been prepared by rinsing with copious amounts of absolute ethanol, deionized water, and absolute ethanol. Substrates have been dried under a stream of nitrogen. The monolayer have been formed by immersing the gold substrate into a solution of the precursor following well-characterized protocols.[5,6,7] After rinsing away unadsorbed molecules with ethanol/water/ethanol and drying under nitrogen, the quality of the monolayers have been assessed by a combination of surface-sensitive analytical methods including grazing angle FTIR, X-ray photoelectron spectroscopy, contact angle measurements, ellipsometry, cyclic voltammetry, and electrochemical impedance spectroscopy, and sum frequency generation spectroscopy. **The results of this study yielded in a paper published in Langmuir, which is included as attachment**.

Low-density SAMs represent a technology platform, which have the potential to provide the capability to analyze metabolic breast cancer markers in urine or markers of oxidative stress in breath in the form of an easy-to-use device. The markers that we are targeting are hydrophobic molecules. The unique structure of our low-density self-assembled monolayers provides a nanoporous structure that can potentially capture such hydrophobic target molecules, causing measurable changes in surface properties. To initially elucidate this promise, we conducted intercalation studies of model metabolites into low-density monolayers and probed their functional and structural changes by means of electrochemical impedance spectroscopy and FTIR spectroscopy. Especially, electrochemical impedance spectroscopy can draw subtle distinctions between relatively subtle differences in monolayer structure, tailgroup functionality, and chain length. At lower frequencies (<1000 Hz), the contribution of the impedance due to monolayer capacitance dominates that of the electrolyte solution resistance, and vice versa at high frequencies (>1000 hz). High density monolayers exhibit greater impedance than low density monolayers, due to increased coverage of the electrode area and reduced surface area for current transfer. Methyl-terminated monolayers show greater impedance than carboxyl-terminated monolayers, due to greater hydrophobicity and reduced penetration of charge-carrying solution ions. C16 chain length monolayers show greater impedance than C11 chain length monolayers, due to greater crystallinity and

ordering of the hydrophobic aliphatic chains, which likewise provides a greater insulative barrier.

The effect that intercalation has on monolayer impedance is shown in Figures 4, 5, and 6. Low density monolayers were incubated in 1 mM solutions of either stearic acid or octadecyl rhodamine in 65:35 ethanol:water overnight. Stearic acid is used as a model molecule for a volatile breath metabolite. Figure 4 shows the results for incubation of a low-density SAM of MHA in stearic acid solution, Figure 5 shows the results for incubation of a low-density SAM of MHA in octadecyl rhodamine solution, and Figure 6 shows the results for incubation of a low-density SAM of MUA (shorter chain length) in stearic acid solution. High-density and low-density SAMs stored overnight in ethanol are included as controls. Incubation in the analyte solution in each case increases the Nyquist plot modulus (line height) and phase angle (line steepness). This indicates intercalation of molecules into the monolayers due to blockage of electrode area by the fatty acids and a transition from the looser structure of the low density monolayers to a more highly ordered structure characteristic of high density monolayers. High density monolayer controls show the highest impedance, low density monolayer controls show the lowest impedance, and intercalated monolayers show an intermediate impedance.

If the impedance of high-density SAMs is also changed after incubation in analyte solutions, then it could be concluded that non-intercalative interactions are responsible for the observed shifts in monolayer permeability. However, Figures 7 and 8 suggest that incubation of high-density SAMs in stearic acid solution does not alter their measured impedance. Figure 7 shows the results for incubation of a high-density SAM of MHA in stearic acid solution, and Figure 8 shows the results for incubation of a high-density SAM of MUA in stearic acid solution. The tightly-packed structure of high-density SAMs does not allow the penetration of analyte molecules exhibited by the low-density systems.

Intercalation of analyte molecules into low-density SAMs should lead to increased restriction of chain conformations, leading to a shift from a more fluid structure to a more tightly-packed structure. Figure 9 shows IR spectra comparing high density and low density reference monolayers versus a low-density monolayer with incubated in stearic acid. Intercalation of stearic acid within the low-density monolayer results in asymmetric and symmetric -CH_2- stretch peaks that are shifted towards the characteristic wavenumbers of high density monolayers and away from those of low density monolayers. This indicates that intercalation causes a low-density SAM to assume a more tightly packed structure as a result of increased occupation of the intersticial spaces in the monolayer.

In order to better understand the kinetics of the intercalation process, we performed a time-course study on the intercalation of stearic acid in a low-density MHA SAM. Figure 10 shows that impedance increases steadily with time until about 7 h. Equilibrium thus takes a significant amount of time to be reached—a time scale similar to that for the organization of the alkyl chains during self-assembly of a high density SAM. The conformational freedom inherent in the low

density monolayer system may dictate such extended equilibration times for full intercalation of analyte molecules.

We next addressed the influence of solvent on the intercalation process. Figure 11 shows the affect of applied positive potential of +400 mV on monolayer impedance phase angle for a low-density SAM. The deviation of the phase angle at low-frequencies is indicative of the increase in electrochemical permeability of the SAM as a result of the applied potential. This effect is not experienced by a low-density MHA monolayer that is incubated in MHA solution in order to backfill the intersticial spaces, shown in Figure 12. In this case, there is much less conformational freedom to allow for changes in structure for a tightly packed monolayer. These data are shown as reference to illustrate the influence that the external solvent has on analyte intercalation. Figures 13-15 show the response to applied potential of low-density SAMs incubated in 1 mM stearic acid solutions prepared with different solvents. The results shown in Figure 13 were for 1 mM stearic acid in ethanol. The results shown in Figure 14 were for 1 mM stearic acid in 2:1 ethanol:water. The results shown in Figure 15 were for 1 mM stearic acid in 1:1 ethanol:water. We see that as the solvent becomes more polar, there is less responsiveness to applied potential, indicating greater levels of intercalation. This is understandable because there should be a greater driving force for transfer of the hydrophobic tails of the analyte molecules out of a polar solvent and into the low-density SAMs.

Figures

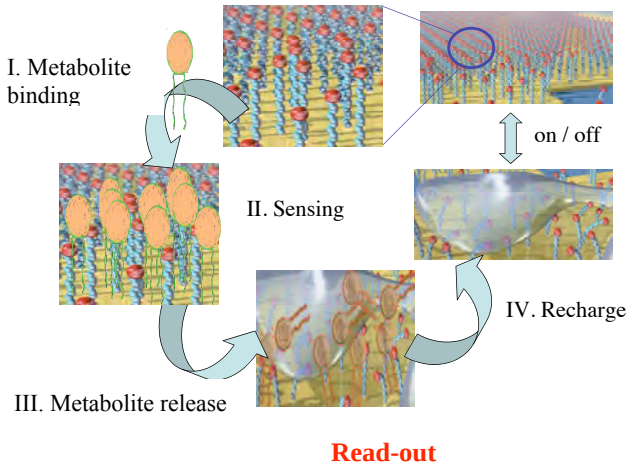

Figure 1: Illustration of the sensing concept.

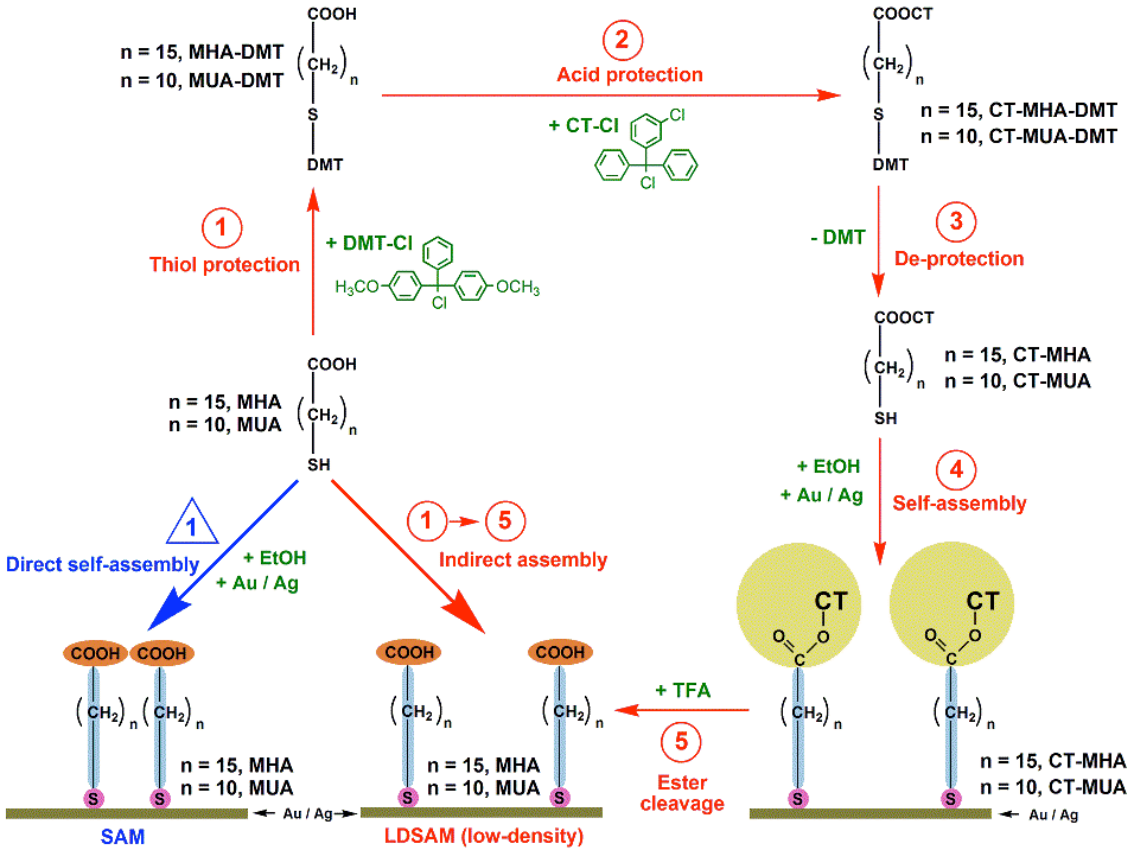

Figure 2. Preparation methods for traditional SAMs and LDSAMs (from Peng et al., *Langmuir* 2007, included as attachment).

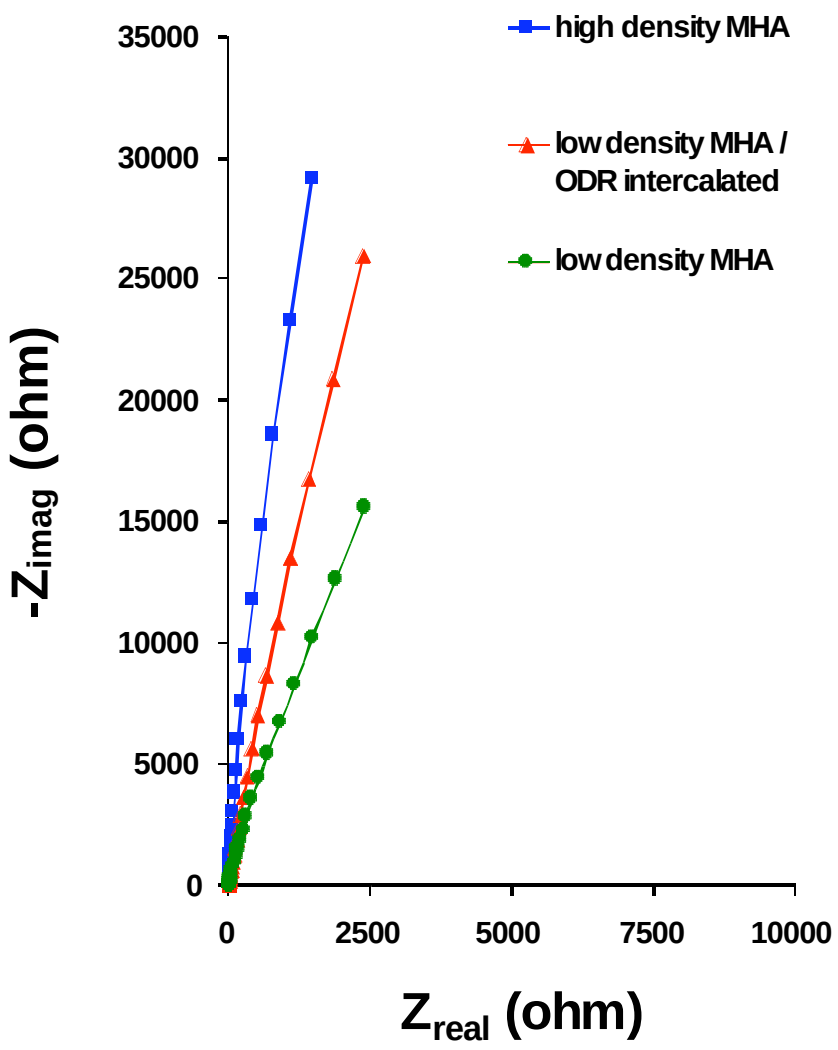

Figure 3. Nyquist impedance plots of MHA monolayers: high-density, low-density, and low-density incubated in octadecyl rhodamine.

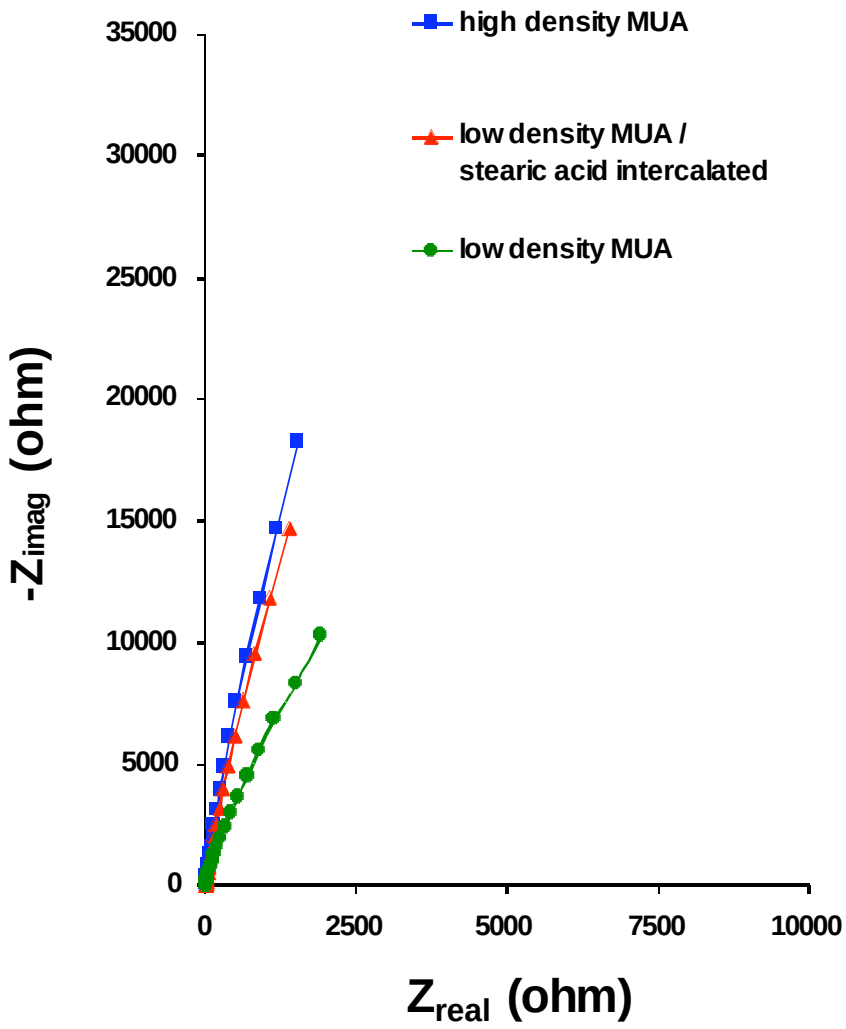

Figure 4. Nyquist impedance plots of MUA monolayers: high-density, low-density, and low-density incubated in stearic acid.

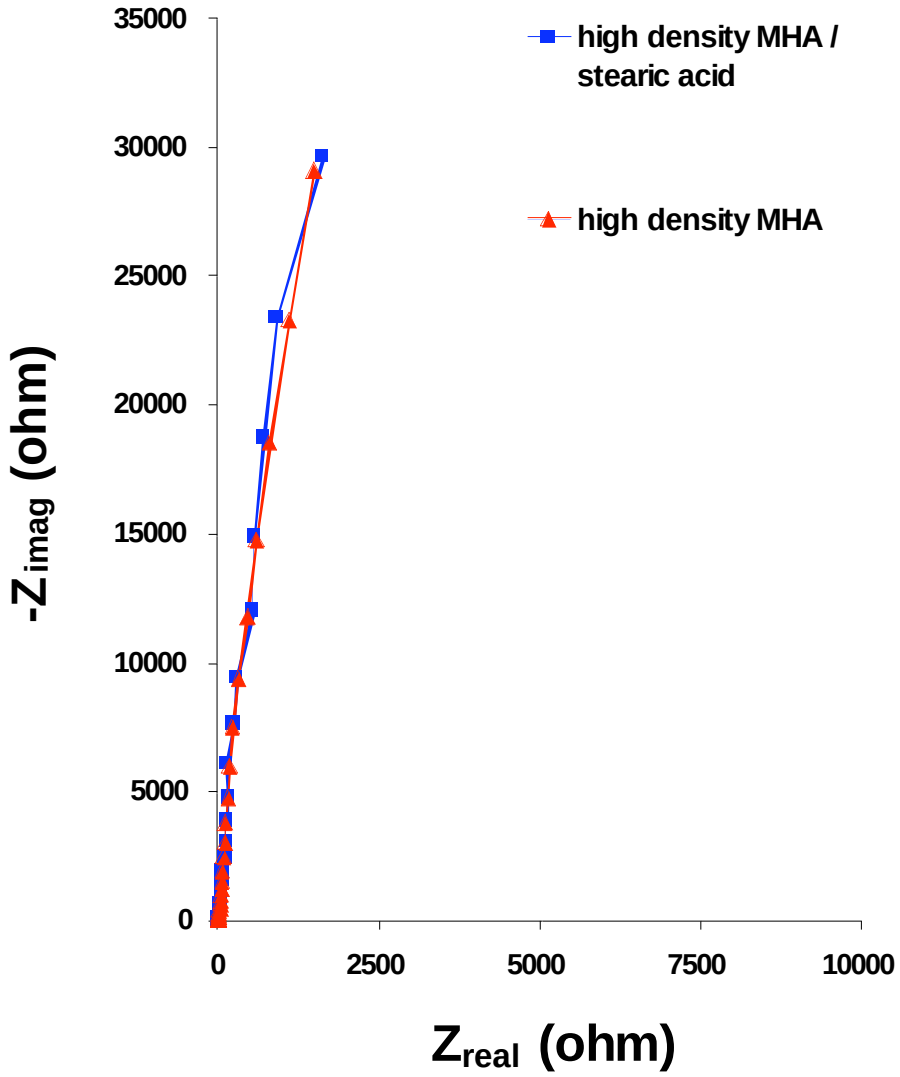

Figure 5. Nyquist impedance plots of MHA monolayers: high density and high density incubated in stearic acid.

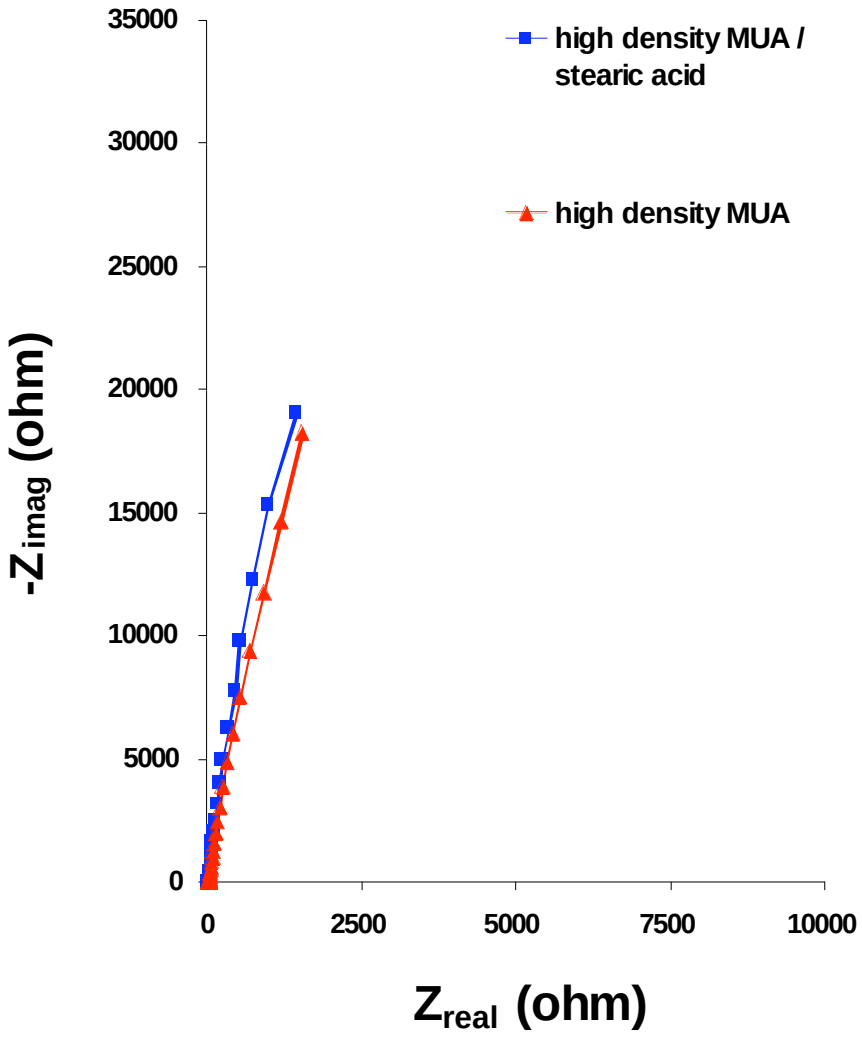

Figure 6. Nyquist impedance plots of MUA monolayers: high density and high density incubated in stearic acid.

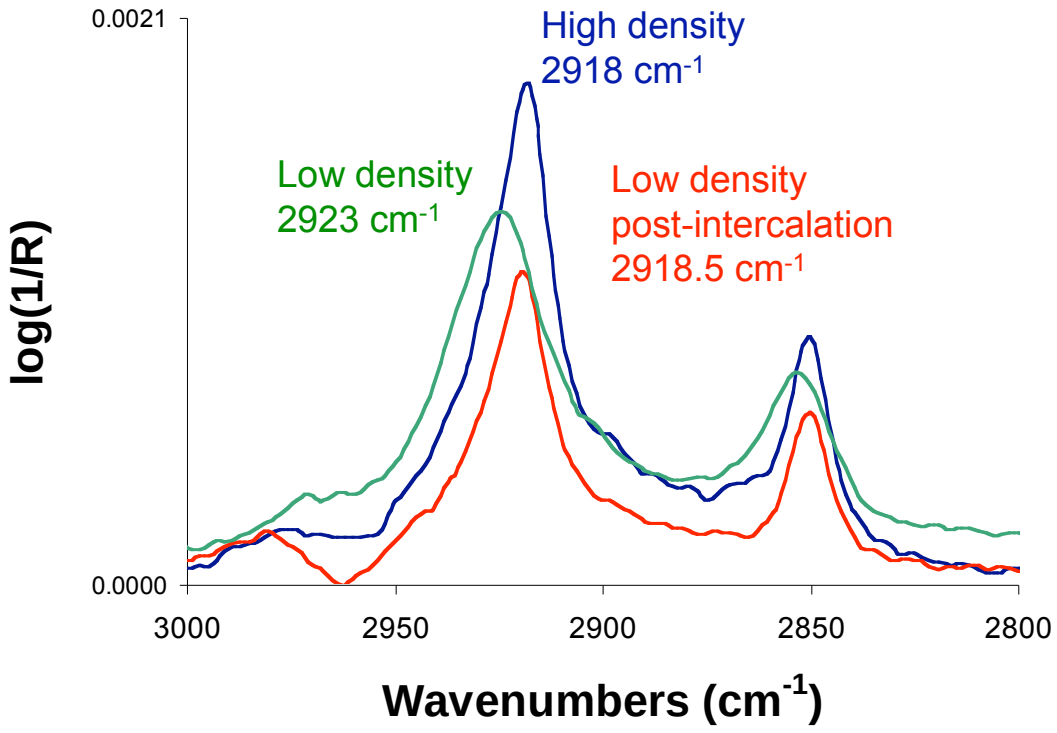

Figure 7. FTIR spectra demonstrating effect of intercalation on monolayer structure.

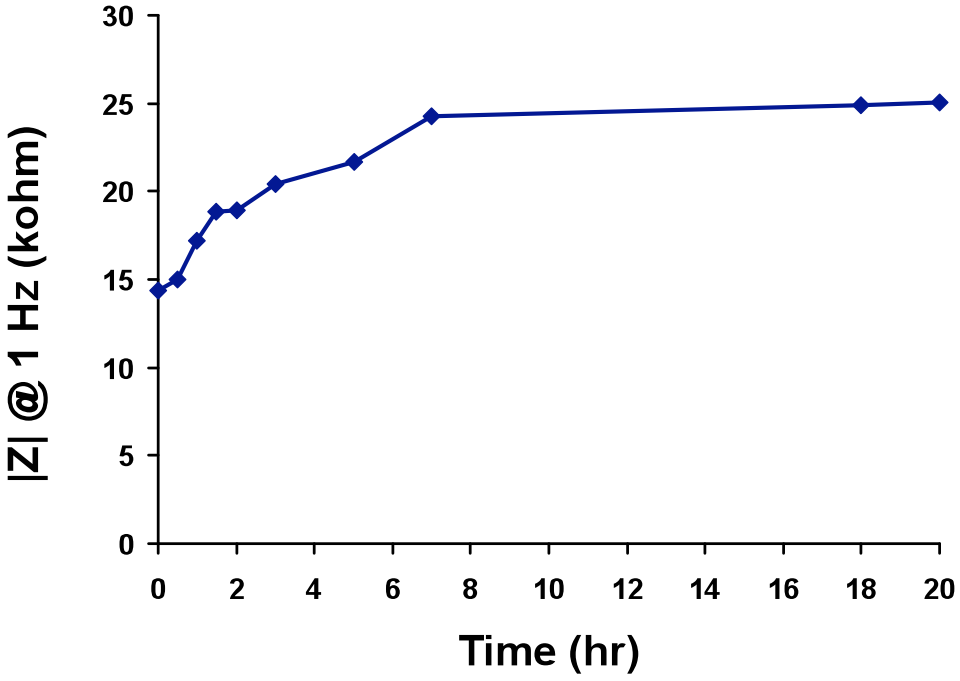

Figure 8. Time-course evaluation of intercalation of low-density MHA in 1 mM stearic acid.

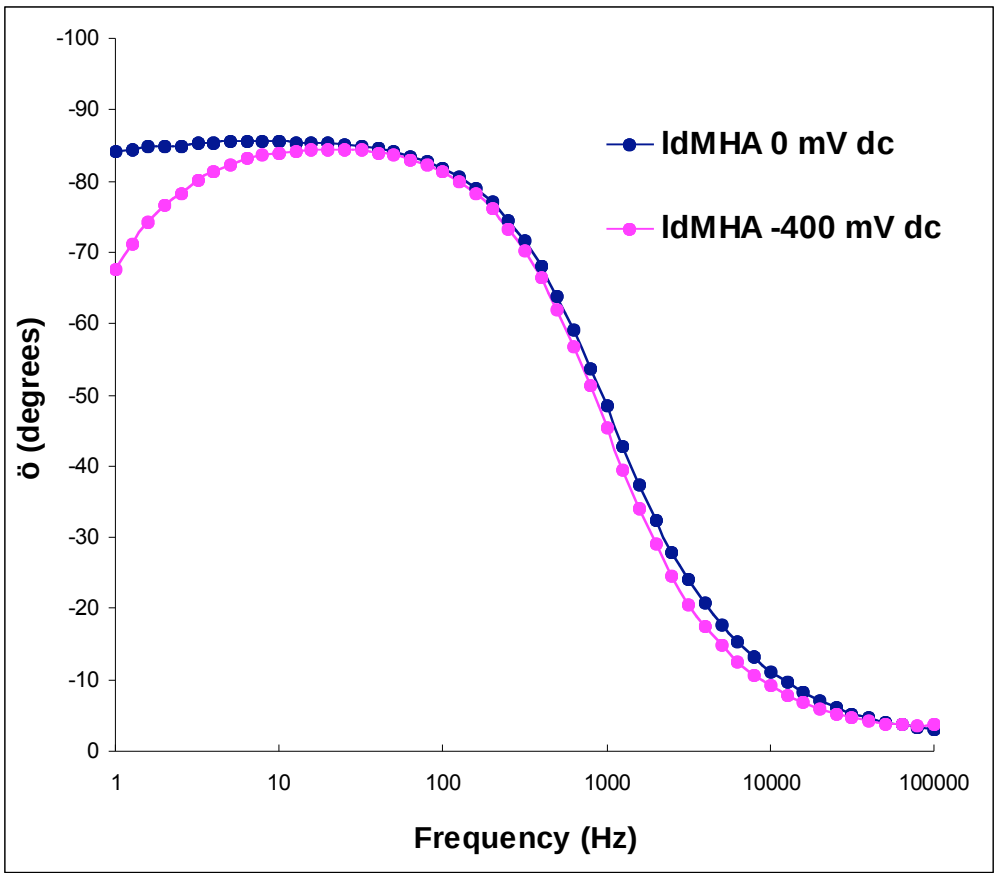

Figure 9. Effect of applied potential on impedance phase angle of low-density MHA.

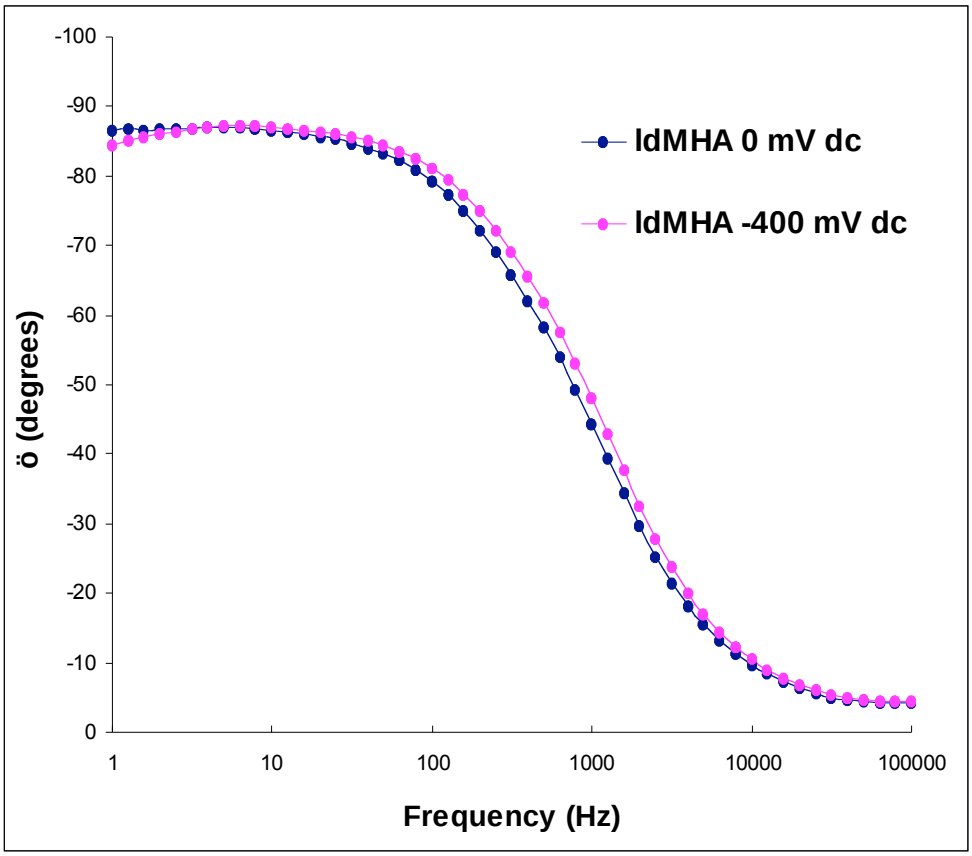

Figure 10. Effect of applied potential on impedance phase angle of low-density MHA backfilled with MHA.

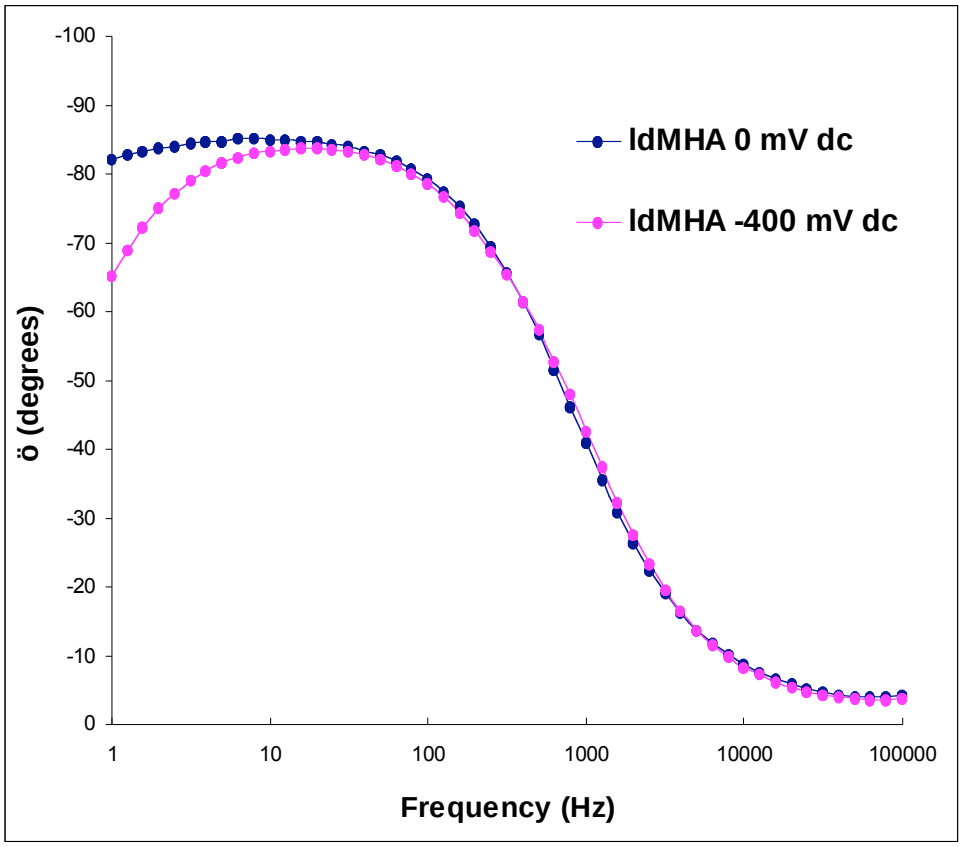

Figure 11. Effect of applied potential on impedance phase angle of low-density MHA incubated in 1 mM stearic acid dissolved in ethanol.

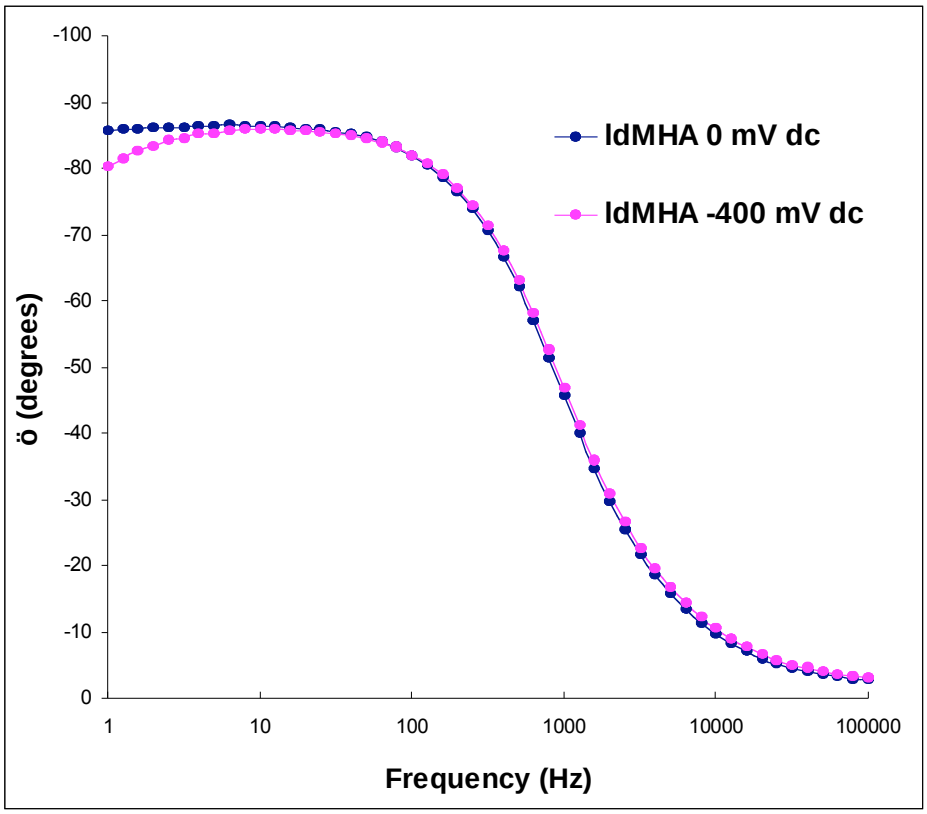

Figure 12. Effect of applied potential on impedance phase angle of low-density MHA incubated in 1 mM stearic acid dissolved in 2:1 ethanol:water.

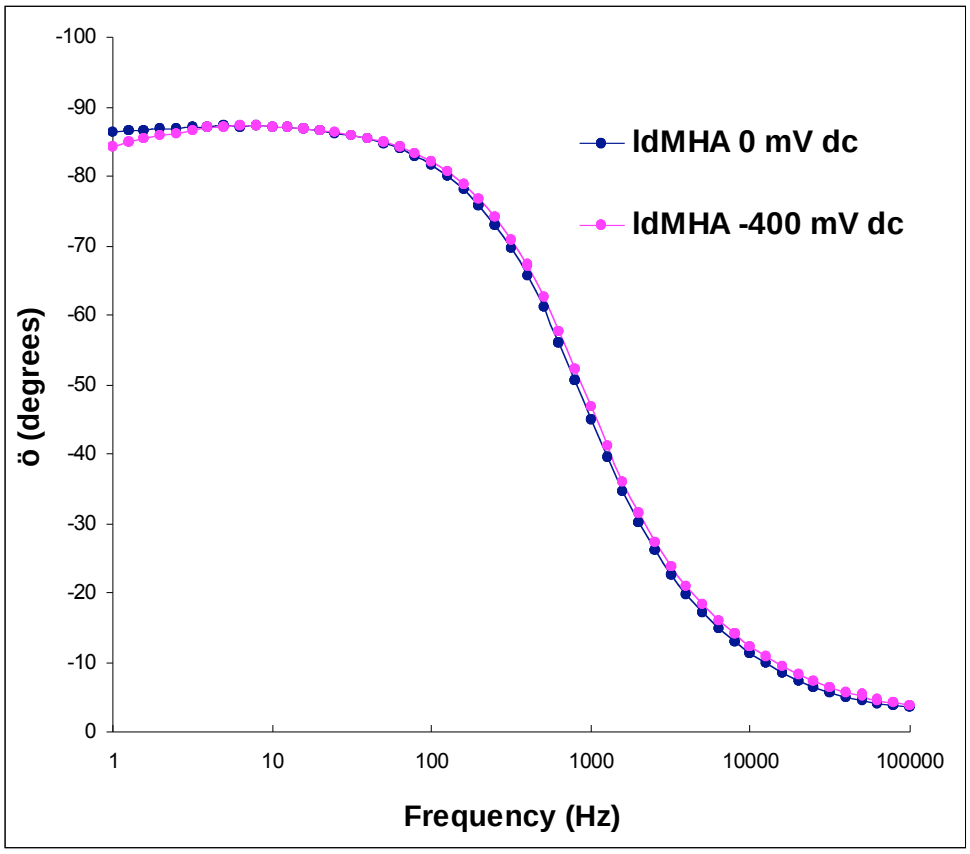

Figure 13. Effect of applied potential on impedance phase angle of low-density MHA incubated in 1 mM stearic acid dissolved in 1:1 ethanol:water.

C. KEY RESEARCH ACCOMPLISHMENTS

- Two different types of linear molecular switches have been identified, synthesized, characterized and sufficient quantities have been prepared for further studies. These molecules will be used as signal transduction units in future breast cancer detection devices.

- One type of molecular switch has been designed by a rationale approach and has subsequently synthesized in a multi-step synthesis. Analytical amounts have been already prepared and the characterization of the molecular tweezers and some of the molecular precursors has been mostly accomplished. However, the material synthesized in the first approach is still not sufficient for assembly in monolayers and the synthesis will be repeated to ensure sufficient materials.

- Low-density monolayers have been prepared on the basis of the linear molecular switches and the resulting monolayers have been fully characterized by FTIR, XPS, and ellipsometry.

- Silver has been established as an alternative electrode material to gold, which has the promise of cost benefits during integration and translational deployment.

- Switching of two monolayers has been demonstrated on the basis of impedance spectroscopy. The fact that switching correlates with a change in impedance is a critical feature of the system because it allows for convenient monitoring of the surfaces AND detection of analytes in the later phase of the project.

- Monolayers were demonstrated to not only undergo binary switching, but the be tunable by a transient application of small electrical potentials. Another important property, when considering use of linear molecular switches as signal transduction systems for breast cancer analysis.

- The storage stability of self-assembled monolayers of linear molecular switches has been demonstrated over a period of 4 weeks. Storage stability is an important criterion for translational deployment.

- Microstructuring methods have been developed that can be used for patterning of electrodes with areas of low- and high-density.

- Initial intercalation experiments on low-density monolayers have been conducted with model metabolites and support fundamental feasibility of the concept.

- Intercalation of fatty acids (stearic and palmitic acid) and octadecyl rhodamine within low-density monolayers has been demonstrated by electrochemical impedance spectroscopy, infrared spectroscopy, and surface plasmon resonance spectroscopy. A time-course study of intercalation shows that a steady increase of impedance accompanies intercalation of stearic acid until about 7 hours, when equilibrium is reached. The influence of external solvent on intercalation was also assessed, with more polar solvents promoting greater levels of intercalation.

D. REPORTABLE OUTCOMES

1) Work sponsored under this proposal (Aim #1 and #2) has resulted in a first and second **full paper**, which appeared in 2007 in a special issue of Langmuir, which described major contributions in the area of smart materials. The paper is included as attachment. The publication had graduate and undergraduate student co-author.

D.K. Peng, J. Lahann, *Langmuir* **2007,** *23*, 10184-10189.

D.K. Peng, S.T. Yu, D.J. Alberts, J. Lahann, Switching the Electrochemical Impedance of Low-Density Self Assembled Monolayers, *Langmuir* **2007***, 23*, 297-304 (**invited paper**).

2) Work sponsored under this proposal (Aim #2) has resulted in submission of a third **paper** to Nano Letters. The paper is included as attachment. The publication has graduate and undergraduate student co-authors.

D.K. Peng, A.A. Ahmadi, J. Lahann, Spatial nd Temporal Remodeling of Synthetic Surfaces, *Nano Letters* **2008**, (submitted).

3)A **perspective article** on smart systems has been accepted to ACS Nano.

M. Yoshida, J. Lahann, Smart Nanomaterials, *ACS Nano* **2008**, (in press, **invited Perspective**).

4)Four Conference presentations.

D. Peng, J. Lahann, "Binding of Hydrophobic Analytes Using Electrically-Responsive Self-Assembled Monolayers," AIChE Annual Meeting, San Francisco, CA **2006**.

D. Peng, J. Lahann, "Molecular Intercalation in Switchable Self-Assembled Monolayers," AIChE Annual Meeting, Cincinnati, OH **2005**.

D. Peng, J. Lahann, "Lipid Intercalation in Switchable Self-Assembled Monolayers," AIChE Annual Meeting, Austin, TX **2004**.

D. Peng; J. Lahann, Switchable Surfaces Based on Low-Density Self-Assembled Monolayers, MRS Spring Meeting, San Francisco, CA, **2008**.

D. CONCLUSION

During the first two years of this three-year program we have made considerable progress. We have finished work proposed under Aim #1 and Aim #2. We further made considerable progress towards Aim #3. The work with linear molecular switches has been already completed and we have established the tools and methods to finalize the work with molecular tweezers, as soon as sufficient quantities have been synthesized. In spite of the high-risk character of the project, the progress is in line with the initially proposed timeline. Interaction of surfaces even with model metabolites turned out to be challenging. This has slowed down the overall progress and it is unclear, if we will be able to start work with real metabolites sufficiently early to obtain substantial data within this project. More work will need to be focused on the switchability of the intercalation mechanism. We plan to assess the effect of applied potential on the ability of our surfaces to selectively intercalate target analytes, as well as the ability of the surfaces to expel captured analytes through potential-induced conformational transitions. Demonstrating this will be critical for selecting the next steps towards developing a screening platform.

Nevertheless, we already published **2 papers, 1 perspective, and 1 review article under this grant and a third, major paper is submitted to Nano Letters.** All in all, we feel, we have made very good progress under this project.

E. REFERENCES

[1] D.K. Peng, S.T. Yu, D.J. Alberts, J. Lahann, Switching the Electrochemical Impedance of Low-Density Self Assembled Monolayers, *Langmuir* **2007**, 23, 297-304.

[2] Love, J.C.; Estroff, L.A.; Kriebel, J.K.; Nuzzo. R.G.; Whitesides G.M. *Chem. Rev.* **2005**, *105*, 1103-1169.

[3] a) Schreiber, F. *J. Phys.: Condens. Matter* **2004**, *16*, R881-R900; b) Schwartz, D.K. *Annu. Rev. Phys. Chem.* **2001**, *52*, 107-137; c) Ulman, A. *Chem. Rev.* **1996**, *96*, 1533-1554.

[4] Lahann, J.; Mitragotri, S.; Tran, T.N.; Kaido, H.; Sundaram, J.; Choi, I.S.; Hoffer, S.; Somorjai, G.A.; Langer, R. *Science* **2003**, *299*, 371-373.

[5] R. G. Nuzzo, D. L. Allara, "Adsorption of Bifunctional Organic Disulfides on Gold Surfaces," *Journal of the American Chemical Society*, **105**, 4481, 1983.

[6] A. Ulman, "Formation and Structure of Self-Assembled Monolayers," *Chemical Reviews*, **96**, 1533, 1996.

[7] D. K. Schwartz, "Mechanisms and Kinetics of Self-Assembled Monolayer Formation," *Annual Review of Physical Chemistry*, **52**, 107, 2001.

Spatial and Temporal Remodeling of Synthetic Surfaces

David K. Peng, Allen A. Ahmadi, and Joerg Lahann*

Department of Chemical Engineering, University of Michigan, Ann Arbor, Michigan 48109

RECEIVED DATE ; E-mail: lahann@umich.edu

The ability to undergo spatial and temporal remodeling is one of the ubiquitous features of nature. In fact, essentially any biological structure undergoes defined molecular interactions and lateral mobility over controlled time domains. Nature uses rather fluent nanostructures including integrin clusters in focal adhesion sides for modulation of many crucial biological events. To engineer synthetic analogues of such complex biointerfaces, impartment of lateral mobility will be a key challenge, although some progess has already been made with lipid bilayers.

Self-assembled monolayers (SAMs) of organothiolates on coin metals have been widely studied because of the flexibility and consistency with which they can produce well-defined structures with diverse surface chemistries.[1] In contrast to lipid bilayers, SAMs of organothiolates are generally thought to lack fluidity of the constituents, although lateral motion has been previously observed for a single thiolate molecule embedded in a high-density SAM.[18] In fact, a well-established characteristic of the most widely studied SAM systems—alkanethiolates on gold—is the relatively high degree of order and positional constraint exhibited by their constituent molecules as a result of the spontaneous self-assembly process. Although this tightly-packed structure is important for certain applications (*e.g.*, electrical insulators, chemical etch resists), increasing attention is being given to SAMs designed with low density configurations and increased steric freedom, allowing for functions such as active conformational transitions[2-4] and the tuning of surface properties including friction,[5] electron transfer,[6] protein adsorption,[7-9] and surfactant interactions.[10-12]

Past studies on high-density systems generally observe that increasing temperature initially results in increased disorder amongst the flexible alkyl chains of the monolayer, followed by thermally-induced desorption of the thiolate from the surface, with the energetic thresholds for each stage differing depending on the specific monolayer system. The effect of elevated temperature on traditional, high-density SAMs has been examined since the initial discoveries[13] and for a wide variety of SAM systems thereafter,[14-17] but low-density systems have not yet been characterized as thoroughly.

Herein, we have studied the thermally-induced, lateral mobility of low-density SAMs and examined the role of interactions between neighboring low- and high-density regions that are otherwise chemically identical. If the surface density of the alkanethiolates varies anisotropically, continuous lateral diffusion of thiolates may occur within the plane of the gold surface until steady-state equilibrium with an average surface density is reached. Our synthetic approach takes advantage of microcontact printing to generate surfaces with well-defined, micropatterned regions of low-density SAM residing in a background of high-density SAM. We then expose these surfaces to elevated temperature for a defined time period, after which we use a combination of surface analytical methods including ellipsometry, infrared spectroscopy, and electrochemical impedance spectroscopy to analyze the resulting effects on film thickness, conformational structure, and electrochemical permeability. In order to assess the influence of inter-chain interaction energy on thermal responsiveness, two sets of surfaces with different chain lengths were studied.

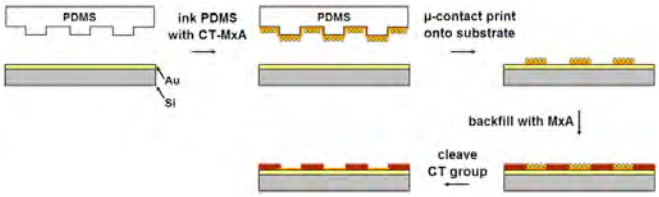

Figure 1. Schematic illustration of the procedure for patterning regions of low-density SAM in a background of high-density SAM.

The procedure for preparing micropatterned SAMs is summarized in Figure 1. In brief, a PDMS stamp with an arrayed pattern of 35 x 35 μm squares was UV-ozone treated, inked with a 1 mM ethanolic solution of a low-density SAM precursor, *i.e.*, the chlorotrityl (CT) ester of either mercaptohexadecanodoic acid (MHA, 16-carbon [C16] length) or mercaptoundecanoic acid (MUA, 11-carbor [C11] length).[2,3] The inked PDMS was then stamped onto a gold surface for 30 s and the unexposed regions were subsequently backfilled with the high-density monolayer by immersing the substrate for 30 min in a 1 mM ethanolic solution of either mercaptohexadecanodoic acid or mercaptoundecanoic acid. The backfilling molecules' chain length was selected to match that of the precursor. The substrate was repeatedly washed with ethanol and immersed in a 1:1 solution of trifluoroacetic acid and ethanol for 2 min to cleave the acid labile chlorotrityl ester from the low-density precursor molecules. Storing the substrates at room temperature for periods up to and beyond 1 week did not influence the observed pattern. This procedure consistently yielded surfaces of low-density SAM square-shaped regions in a high density SAM background, either at the C16 or C11 chain length. Next, samples were incubated for 5 hours at 298 K, 333 K, 373 K, or 423 K.

In order to assess monolayer thickness, imaging ellipsometry was performed using a Nanofilm EP3 nulling ellipsometer with a wavelength of 532 nm, angle of incidence of 60°, and polarizer range of 4°, with 10 image scans per sample for both ellipsometric delta and psi. Figure 2 shows imaging ellipsometry delta maps and delta profiles of C16 and C11 density-patterned SAMs after 5 hr exposure at each temperature level. Because the chemical identity of both regions is identical, the observed contrast reflects differences in film thickness caused by differences in packing

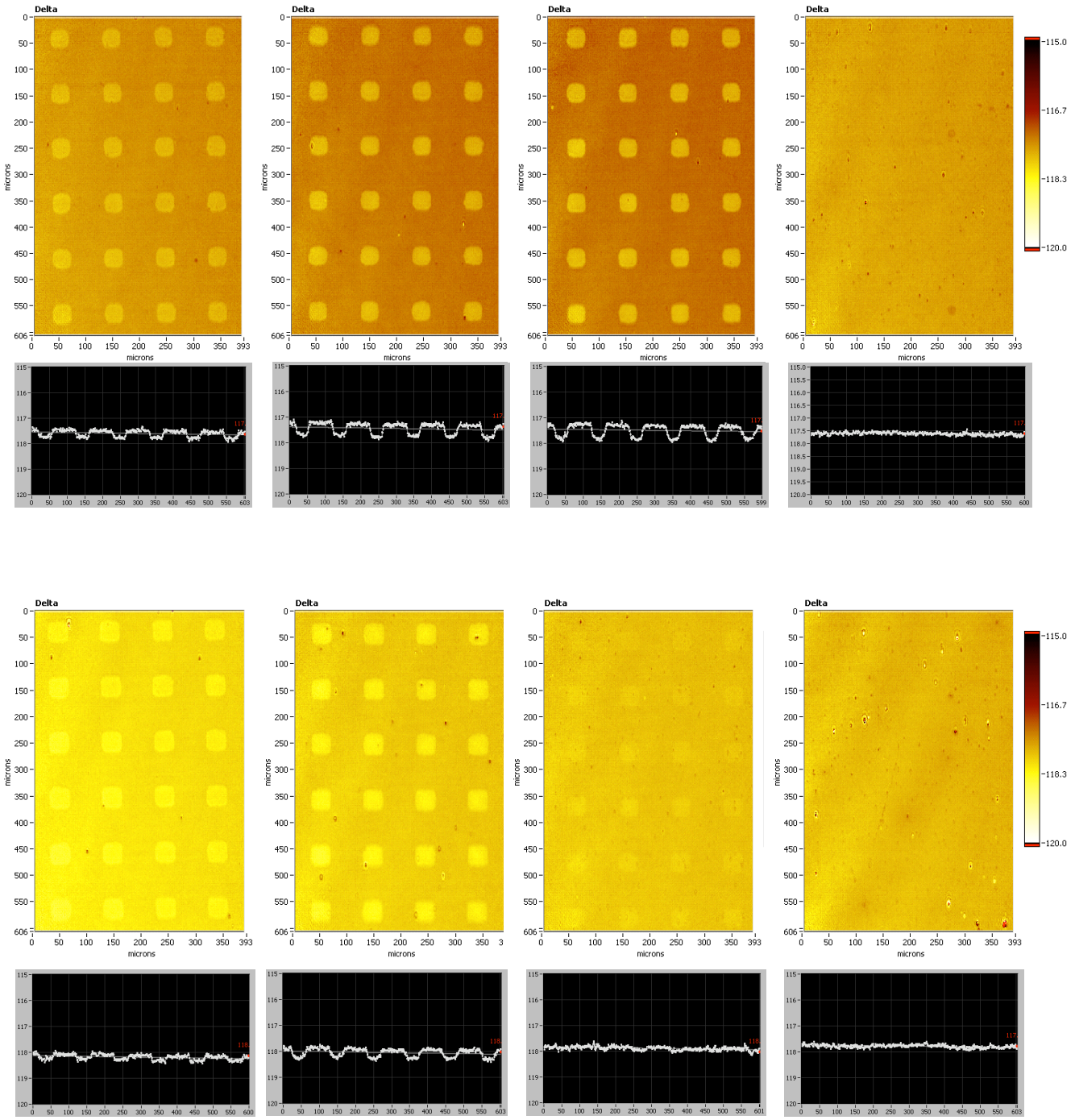

Figure 2. Imaging ellipsometry delta maps and delta profiles of micropatterned SAMs after 5hr exposure to elevated temperature (a) C16 length, 298 K (b) C16 length, 333 K, (c) C16 length, 373 K, and (d) C16 length, 423 K (e) C11 length, 298 K, (f) C11 length, 333 K, (g) C11 length, 373 K, and (h) C11 length, 423 K. Delta profiles represent delta values along a vertical line drawn across one column of square patterns.

density between the square and background regions. Qualitatively, the high-density regions show greater thickness than the loosely-packed low-density regions. For the C16 samples [Figure 2, (a) - (d)], a thickness pattern is visible for surfaces kept at 298 K, 333 K, and 373 K, but for the sample kept at 423 K, the pattern is no longer visible. For the C11 samples [Figure 2, (e) – (h)], the thickness pattern is visible for surfaces kept at 298 K and 333 K, but is faded for the sample kept at 373 K, and is invisible for at 423 K.

Ellipsometric delta and psi data can also be used to actually quantify film thicknesses if appropriate modeling parameters are available. Here we used n = 1.45, k = 0 to model the monolayer film plus air atmosphere and n = 0.4632, k = 2.3171 for the gold film. Results of the thickness analysis are shown in Figure 3 as the average of 3 samples. For the C16 samples shown in Figure 3a, the thickness of the high-density background increased from 298 K (1.62 nm) to 333 K (1.82 nm) and further to 373 K (1.85 nm). However, additional increase in temperature resulted in a decrease in thickness to 423 K (1.40 nm). In contrast, the low-density

squares in Figure 3a did not show significant thickness differences for the samples kept at 298 K (1.23 nm), 333 K (1.16 nm), and 373 K (1.26 nm), but showed increased thickness at 423 K (1.40 nm). These changes in film thickness correspond to altered SAM densities on the surfaces at different temperatures. At lower temperatures, the high-density SAMs assume lower tilt angles with increasing temperature and therefore show lower film thicknesses. The low-density SAMs are already disordered and show therefore little change in thickness with moderate temperature increase.

At 423 K, however, the situation is changed drastically. Now, a threshold temperature is reached, and the decrease in nanofilm thickness may, at least in principle, be attributed to either desorption of free MHA from the high-density monolayer or lateral diffusion of alkanethiolates into adjacent low-density regions. However, desorption of MHA should occur for the low-density monolayers at a rate equal or even higher than the rate of the high-density monolayers. Since this is not the case, desorption can be ruled out. Instead, the decrease in apparent thickness observed for the high-density regions is accompanied by an actual increase in the film thickness of low-density regions. Therfore, the enhanced thickness of the low-density regions after increasing the temperature from 373 K to 423 K indicates a net increase in MHA density of the low-density regions. The leveling effect – decreased density in former high-density areas; increased densities in former low-density areas - may be attributed to a net diffusion of alkanethiolates from high-density regions into the low-density areas at elevated temperatures. The fact that the surface losses the initial pattern and shows an average thickness suggests that after 5 hr at 423 K, the diffusion process has come to a steady-state equilibrium, such that the thickness of both the background and square-pattern regions is the same, with the entire surface homogeneously distributed with MHA.

In the case of MUA samples shown in Figure 3b, similar trends are observed. Initially, the high-density background regions show a continuous increase in apparent thickness from 298 K (0.97 nm) to 333 K (1.18 nm), and again to 373 K (1.22 nm). Similar to the MHA samples, however, a subsequent decrease in thickness occurred between 373 K (1.22 nm) and 423 K (0.97 nm). The low-density region experienced an increase in thickness from 298 K (0.66 nm) to 333 K (0.78 nm) and 373 K (1.12 nm). At higher temperature, a decrease in thickness from 373 K (1.12 nm) to 423 K (0.97 nm) was witnessed. At 423 K, no significant difference in the trends observed for the high-density SAMs of MHA and MUA were observed. In contrast, the increase in thickness of the low-density monolayers at 373 K indicates a lower temperature barrier for lateral diffusion in case of the shorter thiolates. At 423 K, the lack of observable contrast between the high- and low-density regions, as well as the decrease in thickness for both regions compared to samples incubated at 373 K, both suggest steady-state diffusion and further points towards an earlier onset of desorption of MUA from the surface.

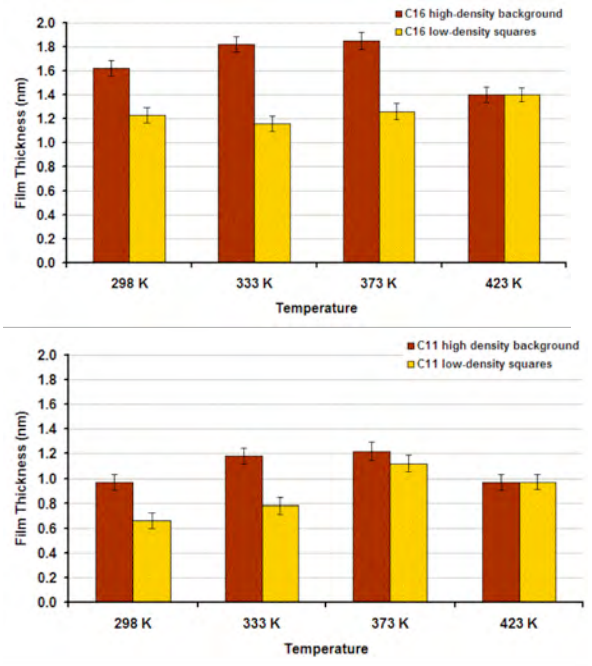

Figure 3. Ellipsometric thickness of (a) MHA (C16) and (b) MUA (C11) micropatterned SAMs with high-density (brown) and low-density (yellow) regions.

In order to elucidate whether the leveling effects in nanofilm thickness observed at elevated temperatures are caused by chemical reactions, such as oxidation of the thiol groups, X-ray photoelectron spectroscopy (XPS) was performed on C16 samples before and after incubation at 423 K for 5 hrs using an Axis Ultra (Kratos Analyticals, UK) instrument equipped with a monochromatized AlKα X-ray source. Electrons were collected with a pass energy of 20 keV for C_{1s} and O_{1s} and 40 keV for S_{2p}. Spectra were normalized with respect to aliphatic carbon at 285.0 eV, and components were modeled with a Marquardt fitting algorithm. Figure S1 shows that spectra before heat treatment (a-c) are qualitatively similar to spectra after heat treatment (d-f). Quantification of the XPS data, shown in Table 1, reveals the ratio of carbon to oxygen remains very close to the theoretical value for an MHA molecule, indicating continuous maintenance of chemical integrity. Table 1 further summarizes the quantitative analysis of the high-resolution C_{1s} XPS spectra. The experimental data are in close agreement with the theoretically determined composition; both before and after heat treatment.

To further support the chemical analysis based on XPS, Fourier transform infrared (FTIR) spectra were obtained in order to assess the effect of patterning and temperature on the conformational structure of the SAMs. Analysis was performed using a Thermo Nicolet 6700 spectrometer with an 85° grazing angle attachment and 128 scans per sample at 4 cm^{-1} resolution. Figure S2 shows the resulting spectra, which represent an average over the entire patterned surface, including both low- and high-density regions. C16 samples are shown in Figure S2.a, and C11 samples are shown in Figure S2.b. Spectra for unpatterned high- and low-density SAMs at room temperature are included as reference (black and grey lines, respectively). Comparing the reference samples, we see the low-density asymmetric and symmetric C-H stretching bands are red-shifted relative to the high-density bands—an effect resulting from the increased fluidity of the low-density alkyl chains. For the micropatterned samples, the C16 sample at 298 K shows peaks at 2918.5 cm^{-1} and 2850.3 cm^{-1}, while the C11 sample at 298 K shows peaks at 2919.7 cm^{-1} and 2850.1 cm^{-1}. These bands are modestly red-shifted relative to the unpatterned high-density C16 and C11 samples. Band broadening is also evident, particularly for the C11 sample at 298 K. Although distinct peaks for high- and low-density regions were not observed in this case, the intermediately located and broadened absorption bands of the patterned samples suggest an aggregate level of fluidity and structure consistent with the ellipsometric data above. As temperature is increased, the bands for the C16 patterned samples do not shift significantly until 423

K (with bands at 333K and 373K looking essentially identical to those at 273K); at 423K, they are shifted further than the low-density C16 reference sample. The C11 samples, meanwhile, begin to shift at 373 K (bands at 333 K looking essentially identical to those at 273 K), and at 423 K, they are shifted further than the low-density C11 reference sample. These data indicate structural stability of the C16 patterned samples for 5 hr up to at least 373 K, as well as increased thermal sensitivity of the C11 samples relative to the longer and more energetically stable C16 samples.

The changes in structure and conformation induced by elevated temperature also influence the electrochemical properties of the patterned SAMs. Low-density SAMs exhibit greater ionic permeability and therefore lower resistance and capacitance than high-density SAMs.[3,4] Electrochemical impedance spectroscopy (EIS) is a sensitive method for measuring these properties.[19,20]

Patterning and elevated temperature were thus observed to have a consistent trend of effects on MHA and MUA SAMs with respect to film thickness as measured by ellipsometry, conformational structure as measured by FTIR spectroscopy, and electrochemical barrier properties as measured by EIS. Elevated temperature appears to cause migration of thiolates from high-density regions to low density regions. This effect depends both on temperature and on SAM chain length, suggesting interplay between the energetics of the gold-thiol interaction and inter-chain van-der-Waals interactions. Independent of the lateral migration effect, micropatterned SAMs of low-density MHA and MUA show good thermal stability at temperatures up to 373 K and 333 K, respectively, which may have positive implications for potential technological applications.

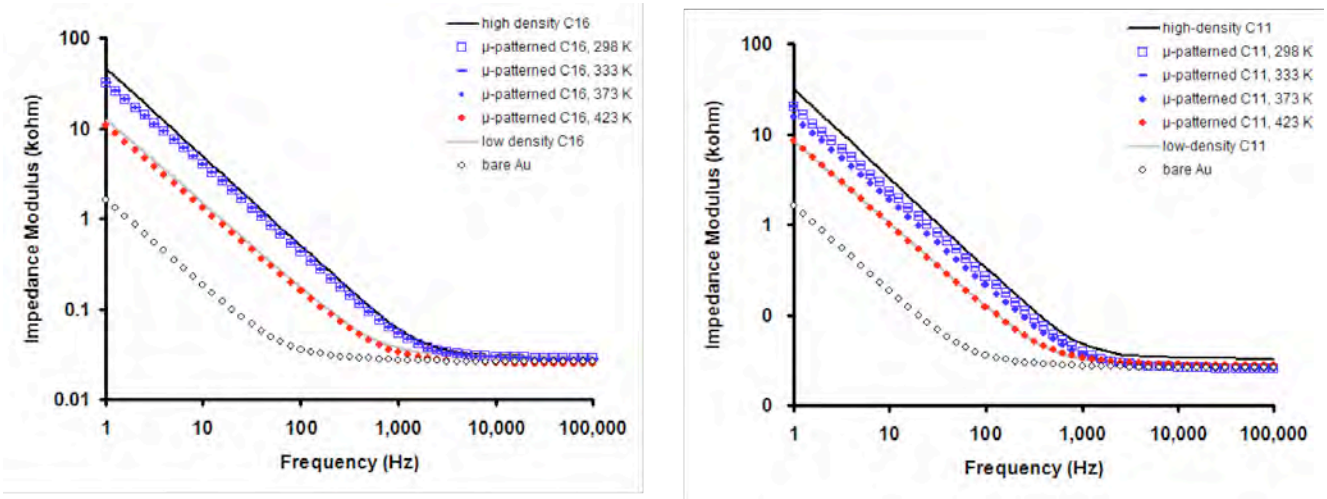

Figure 4. Ellipsometric thickness modeling of (a) C16 and (b) C11 micropatterned SAMs.

Figure 4 shows EIS results for the patterned samples as well as unpatterned high- and low-density SAM and bare gold reference samples. Analysis was performed using a Gamry PCI4/300 potentiostat, EIS300 software module, and standard 3-electrode electrochemical cell (saturated calomel reference electrode, platinum mesh counter electrode, and N_2-purged phosphate buffered saline electrolyte). The applied potential had an AC amplitude of 10 mV r.m.s., frequency range of 1 Hz to 10^5 Hz, and DC bias of 0 mV w.r.t. SCE, and the current response was recorded at ten points per decade in frequency. The results corroborate the FTIR results, with micropatterned samples showing greater permeability (lower impedance) than high density samples, as a result of the presence of the "leaky" low-density patterned regions. For C16 samples (Figure 6a), no significant difference in impedance was observed for samples kept at 298 K, 333 K, and 373 K, but the sample kept at 423 K had an impedance trace close to that of the low-density C16 reference sample. For C11 samples (Figure 6b), no significant difference in impedance was observed for samples kept at 298 K and 333 K, but the sample kept at 373 K had a marginally lower impedance trace, and the sample kept at 423 K had a impedance trace very close to that of the low-density C11 reference sample. The maintenance of robust electrochemical barrier properties is thus observed for C16 patterned SAMs for 5 hr up to at least 373 K, while C11 patterned SAMs show a lower thermal threshold for losses in integrity.

Acknowledgement. This project was funded by grants from the National Institutes of Health (5 R21 EB005732-02) and the Department of Defense (Idea Award, W81XWH-06-1-0271), as well as a graduate fellowship for D.K.P. from the National Institutes of Health / University of Michigan Cellular Biotechnology Training Program.

References

(1) Love, J.C.; Estroff, L.A.; Kriebel, J.K.; Nuzzo. R.G.; Whitesides G.M. *Chem. Rev.* **2005**, *105*, 1103-1169.
(2) Lahann, J.; Mitragotri, S.; Tran, T.N.; Kaido, H.; Sundaram, J.; Choi, I.S.; Hoffer, S.; Somorjai, G.A.; Langer, R. *Science* **2003**, *299*, 371-373.
(3) Peng, D.K.; Yu, S.T.; Alberts, D.J.; Lahann, J. *Langmuir* **2007**, *23*, 297-304.
(4) Peng, D.K.; Lahann, J. *Langmuir* **2007**, *23*, 10184-10189.
(5) Lee, S.; Shon, Y.S.; Colorado R.; Guenard, R.L.; Lee, T.R.; Perry, S.S. *Langmuir* **2000**, *16*, 2220-2224.
(6) Shao, H.B.; Yu, H.Z.; Zhao, J.W.; Zhang, H.L.; Liu, Z.F. *Chem Lett* **1997**, 749-750.
(7) Choi, E.J.; Foster M.D.; Daly, S.; Tilton, R.; Przybycien, T.; Majkrzak, C.F.; Witte, P.; Menzel, H. *Langmuir* **2003**, *19*, 5464-5474.
(8) Liu, Y.; Mu, L.; Liu, B.; Zhang, S.; Yang, P.; Kong, J. *Chemical Communications* **2004**, *10*, 1194-1195.
(9) Petrash, S.; Cregger, T.; Zhao, B.; Pokidysheva, E.; Foster, M.D.; Brittain, W.J.; Sevastianov, V.; Majkrzak, C.F. *Langmuir* **2001,** *17*, 7645-7651.
(10) Arduengo, A.J.; Moran, J.R.; Rodriguez-Parada, J.; Ward, M.D. *J. Am. Chem. Soc.* **1990**, *112*, 6153-6154.

(11) Bao, H.F.; Peng, Z.Q.; Wang, E.K.; Dong, S.J. *Langmuir* **2004**, *20*, 10992-10997.
(12) Peng, Z.Q.; Dong, S.J. *Langmuir* **2001**, *17*, 4904-4909.
(13) Bain, C.D.; Troughton, E.B.; Tao, Y.T.; Whitesides, G.M. *J Am. Chem. Soc.* **1989**, *111*, 321-335.
(14) Zhang, Z.S.; Wilson, O.M.; Efremov, M.Y.; Olson, E.A.; Braun, P.V.; Senaratne, W.; Ober, C.K.; Zhang, M.; Allen, L.H. *Applied Physics Letters* **2004**, *84*, 5198-5200.
(15) Schreiber, F. *Progress in Surface Science* **2000**, *65*, 151-256.
(16) Nuzzo, R.G.; Korenic, E.M.; Dubois, L.H. *J. Chem. Phys.* **1990**, *93*, 767-773.
(17) Fenter, P.; Eisenberger, P.; Liang, K.S. *Physical Review Letters* **1993**, *70*, 2447-2450.
(18) Wakamatsu, S.; Fujii, S.; Akiba, U.; Fujihira, M. *Nanotechnology* **2003**, *14*, 258-263.
(19) Boubour, E.; Lennox, R.B. *Langmuir* **2000**, *16*, 4222-4228.
(20) Boubour, E.; Lennox, R.B. *Langmuir* **2000**, *16*, 7464-7470.

Supplemental Materials

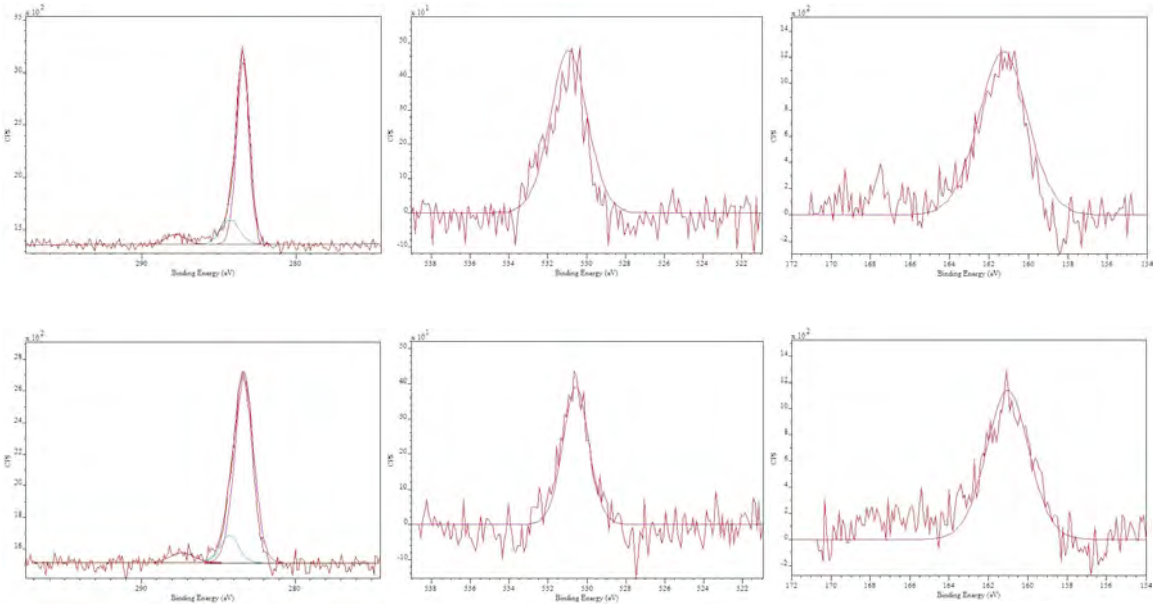

Figure 4. X-ray photoelectron spectra of micropatterned SAMs. Before 5 hr exposure to 423 K: (a) C 1s, (b) O 1s, (c) S 2p. After 5 hr exposure to 423 K: (d) C 1s, (e) O 1s, (f) S 2p.

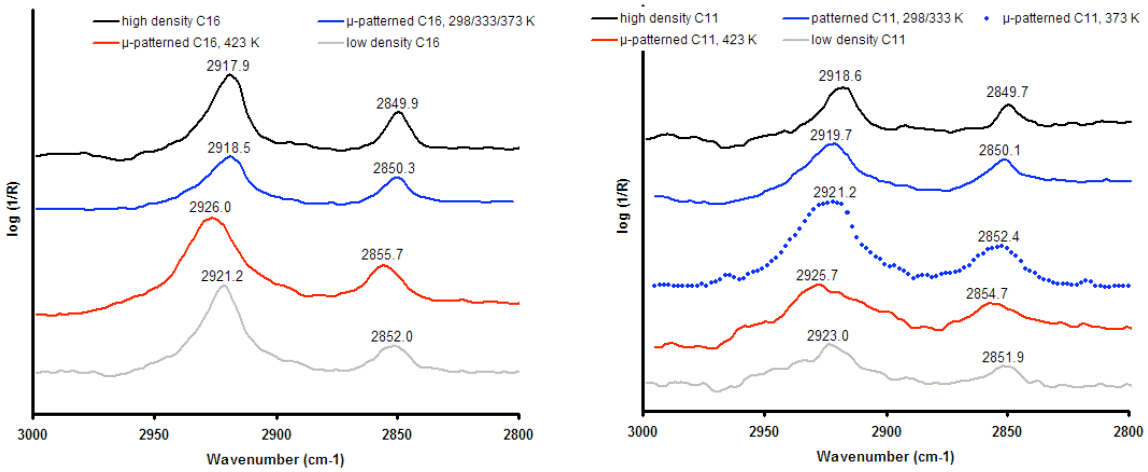

Figure 5. FTIR of (a) C16 and (b) C11 micropatterned SAMs

Table 1.

	Theoretical	Patterned SAM		Patterned SAM After 5 hr @ 423 K	
	%	Area	%	Area	%
C 1s	88.9%	1501	86.9%	2166	89.2%
O 1s	11.1%	534	13.0%	957	10.8%

Table 2.

	Theoretical	Patterned SAM		Patterned SAM After 5 hr @ 423 K	
		Area	%	Area	%
$C\text{-}H_2$	82%	1869	79%	1839	83%
C-S, $C\text{-}CO_2H$	12%	354	15%	258	12%
CO_2H	6%	144	6%	117	5%

PERSPECTIVE

Smart Nanomaterials

Mutsumi Yoshida and Joerg Lahann*

Departments of Chemical Engineering, Materials Science and Engineering, and Macromolecular Science and Engineering, 2300 Hayward Street, University of Michigan, Ann Arbor, Michigan 48109

On-demand switchable materials, such as surfaces that can alter their optical appearance, are ubiquitous in nature. For instance, cuttlefish, a subclass of cephalopods, are experts of camouflage, as they change their body patterns and colors depending on their surrounding environment *via* a visually driven, neurally controlled chromatophore apparatus (Figure 1).[1] Chromatophores contain pigment granules that can be differentially dispersed throughout the cell; when the granules are concentrated in the center of the cell, the cell appears light in color, whereas when the granules are scattered throughout the cell, it appears dark.[2] Granules are transported rapidly along the cytoskeletal network by motor proteins, and it is this speed by which these granules are transported that enables a quick change in body color. There are many other cases where nature uses time-control very effectively in switching critical properties. Although most synthetic materials still lack such switchability, new synthetic tools and enhanced fundamental understanding have brought such "smart" materials within reach of the materials research community. By definition, smart materials are materials that can respond to external stimuli or their environment.[3,4] Recent examples of smart materials include self-healing polymers that release healing agents upon structural damage,[5,6] electronic paper displays, whose ink appears or disappears depending on electrical charge,[7] and meta-materials that serve as an "invisibility cloak" to make objects invisible at a particular wavelength.[8,9] Analogous to the camouflage behavior of cuttlefish, gels that change color in response to external stimuli such as temperature, pressure, humidity, and salt concentration have been fabricated in the laboratory.[10] By altering the thickness of a thin film composed of alternating layers of two self-assembling polymers, polystyrene and poly(2-vinyl-pyridine), the refractive index of the layer is changed, thereby altering the visible color of the gel. Applications for these gels include colorimetric sensors that detect changes in external conditions, as well as display devices.[10] Given the wide range of uses in nature, smart materials may have a wide range of potential applications in medicine, and many of them, including thermoresponsive hydrogels,[11] switchable surfaces,[12] and photoresponsive materials,[13] have already been explored in this capacity. Another prominent motivation of the quest for synthetic materials with dynamically controlled properties is their potential use as dynamic blueprints in time-resolved

Although most synthetic materials still lack switchability, new synthetic tools and enhanced fundamental understanding have brought such 'smart' materials within reach of the materials research community.

Despite this encouraging progress, the implementation of switchable properties will continue to be one of the central obstacles in nanomaterials science in the decades to come. Ultimately, imparting dynamic properties to nanomaterials will result in systems where the materials themselves will be the actual active device. In this issue of *ACS Nano*, Balazs and coworkers describe numerical simulations to predict the switching properties of a smart membrane material.[14] The membrane comprises lipid bilayers in conjunction

ABSTRACT "Smart" materials—materials that respond to a stimulus or their environment to produce a dynamic and reversible change in critical properties—have enabled progress in many areas, including display technologies, drug delivery, and self-healing materials for coating applications, among others. Many of the current examples of smart materials are biomimetic, since nature employs and depends on dynamic and rapid switching for critical functions such as vision, camouflage, and ion channel regulation. Despite progress in designing smart materials and surfaces, much work is still needed in this area to increase their implementation in useful applications. In this Perspective, the challenges and outlook in this area are highlighted, including the work of Balazs and co-workers found in this issue of *ACS Nano*.

See the accompanying Article by Balazs *et al.* on page XXXX.

*Address correspondence to lahann@umich.edu

Received for review May 31, 2008 and accepted May 31, 2008.

10.1021/nn800332g CCC: $40.75

Figure 1. Camouflage of a cuttlefish that mimics its environment, in this case a checkerboard.[1] Republished with permission from ref . Copyright 2006 Elsevier.

with amphiphilic Janus particles. In contrast to conventional lipid bilayers, lipid ~~bilayer~~ membranes embedded with Janus particles bearing hydrophilic and hydrophobic moieties form stable pores upon perforation by mechanical force opening ~~of~~ the pore, exposing their hydrophilic portion to the solvent. As the mechanical force is reduced, particles that lined the pores migrate toward each other until they form stable clusters. Thus, the pore never completely closes and remains as a stable hole due to the self-assembled cluster of particles. If re-exposed to the initial stimulus, the pore can reopen, which is in clear contrast to lipid bilayers without anisotropic particles. As a consequence, the composite membrane can ~~form stable pores that~~ open and close on demand. In this way, ~~the~~ smart property has been imparted to the membrane, resulting in stimuli-responsive pores that can be opened and closed controllably and reversibly. It can be expected that ~~smart~~ membranes such as the example that Balazs and co-workers present can selectively control transport of materials and may find potential use in self-healing materials, nanofluidics, and drug delivery (Figure 2).

Fundamentally, the system studied by Balazs and co-workers is intriguing in that it combines an oriented interface, the lipid bilayer, with anisotropic particles. Thus far, activities toward smart materials have exploited two lines of design (Figure 3). The first approach is the design of surface coatings or bulk materials that undergo reversible molecular transitions depending on the presence or absence of a stimulus. Stimuli include changes in pH, salt content, temperature, the presence of a specific analyte, electrical or magnetic fields, or light. A second approach takes advantage of anisotropic particles that can change surface properties if oriented at an interface in a controlled manner.

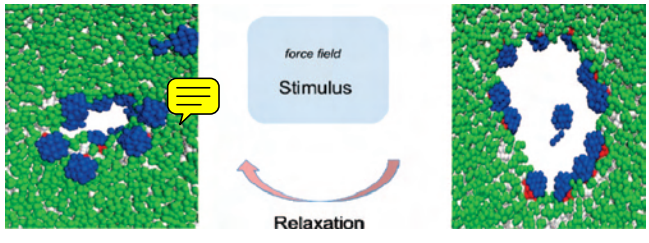

Figure 2. Smart membrane system consisting of anisotropic particles embedded in a lipid bilayer. Adapted from ref . Copyright 2008 American Chemical Society.

Conformation-Based Switching. A number of smart surfaces have been developed that can switch surface properties upon exposure to internal or external stimuli. Well-known examples include stimuli-responsive polymers, such as poly(*N*-isopropyl acrylamide) (pNIPAAm). This thermoresponsive polymer has been widely explored for a variety of biomedical applications including drug delivery (recently reviewed in refs 15–19), modulation of cell adhesion and protein adsorption,[20–22] and cell sheet engineering.[23] Another class of biologically inspired thermoresponsive molecules is based on elastin-like polypeptides (ELPs). These polypeptides contain the valine-proline-glycine-X-glycine motif, where X may be any amino acid other than proline.[24] The molecules are water-soluble at lower temperatures but reversibly aggregate at elevated temperatures. The switching can be induced by changes in temperature, pH, or ionic strength.[25,26] Elastin-like polypeptides have been micropatterned to capture and to release other proteins fused to ELPs *via* hydrophobic interactions upon transition.[27]

In addition to temperature, light can also serve as a stimulus, providing an alternative to actuate the smart properties in applications where temperature changes may not be a viable option. Several chemically triggered systems that change wettability upon light irradiation include azobenzene,[28] pyrimidine,[29] O-carboxymethylated ~~calix[4]resorcinarene~~,[30] or spiropyran[31] groups. More recently, shape-memory polymers that respond to UV light have been reported.[13,32,33] Such polymers are composed of an elastic polymer network and a molecular switch, which determines their permanent shape and forms reversible cross-links upon photostimulus, respectively.[34] This polymer can change from its flat ribbon-like structure to a tight coil, then

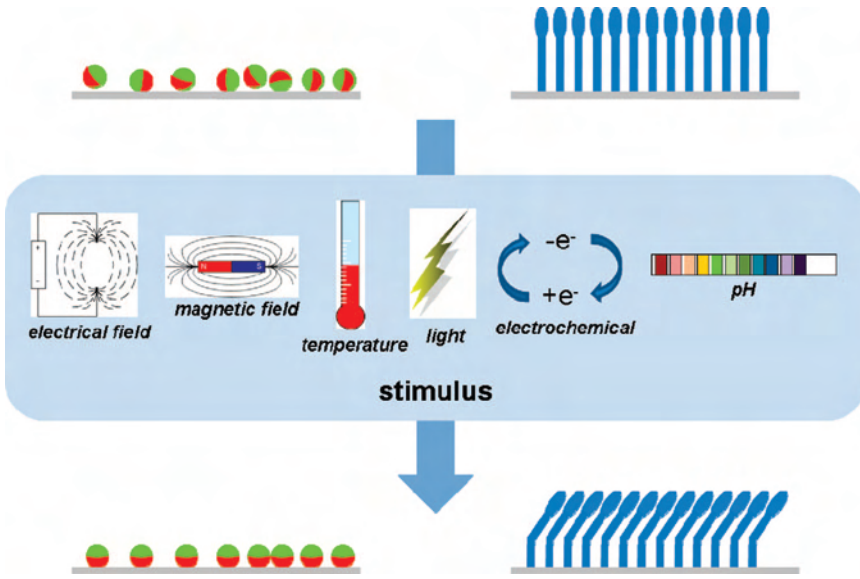

Figure 3. Two potential approaches toward the design of smart materials. The orientation of anisotropic particles (left) as well as the conformation of molecular switches (right) are altered relative to a surface by application of a stimulus. The switching results in different surface properties.

back to a ribbon, in response to light.[13]

Alternatively, electrochemical transformations of self-assembled monolayers (SAMs) have been explored to produce smart substrates. For example, alteration in surface wettability has been shown upon application of electrical potentials in combination with SAMs of alkanethiolates on gold.[35] In this system, a decrease in contact angle of >80° to 0° was observed. In another approach, conformational switching of surface-confined molecules was used to control interfacial properties dynamically.[36] Similarly, control of molecule concentration spatially and temporally by taking advantage of surfactant desorption has been reported.[37] By using electrodes, surfactants bearing redox-active groups were alternated between surface-active or -inactive forms, changing the surface pressure, enabling control of the position and motion of liquids. In yet another approach, electrical potential was used to trigger conformational transitions of alkanethiols on gold, while maintaining constant environmental parameters (solvent, electrolyte content, pH, temperature, and pressure).[36] A mercaptohexadecanoic acid derivative containing a globular end group was used to form a SAM whose end groups were tightly packed while maintaining uniform spacing at the gold/thiol interface and in between the hydrophobic chains.[36] Following cleavage of the bulky end group, a mercaptohexadecanoic acid SAM of low density resulted, allowing the hydrophobic chains to alter their conformation reversibly in response to changes in the electrical potential. This change in conformational transition led to changes in surface wettability, thereby allowing dynamic control of interfacial properties. Other electrochemically driven switchable surface designs to control surface wettability include gold electrodes coated with monolayers of bipyridinium-containing thiols,[38] rotaxanes, [39] and pseudorotaxanes, which result in surfaces that capture and release aromatic guest molecules.[40]

Anisotropy-Based Switching. While all of these examples exploit structural transitions in molecular systems with appropriate energy balances between two or more states, surfaces that switch based on orientational switching of anisotropic particles at an interface can also be envisioned. Such an approach requires the availability of particles with distinct differences in their appearance depending on from which side they are observed (Figure 4). Synthesis of anisotropic particles goes well beyond efforts established for centro-symmetric particles. Successful methods include the use of a spinning disk,[52,53] self-assembly,[54,55] fusion of pre-existing particles,[56] surface modification with partial masking,[57–60] selective deposition,[61,62] surface modification through partial contact with reactive media,[63–65] microcontact printing,[47,66] and template-assisted self-assembly.[67,68] Other examples include heterodimer nanoparticles,[69] solidified paraffin droplets,[70] and magnetic microbeads.[71] For certain materials, dumbbell-, snowman-, or acorn-like nanoparticles have been developed. Known methods include controlled crystallization from precursor core−shell particles[72,73] and selected surface nucleation.[74–76] In related work, Rainer *et al.* employed polystyrene-*b*-polybutadiene-*b*-poly(methyl methacrylate) and similar polystyrene-*b*-polybutadiene-*b*-poly(methacrylic acid) triblock copolymers for the synthesis of Janus micelles.[77,78] These triblock copolymers have well-defined bulk morphologies due to their unique microphase separations. After following the selective cross-linking reaction of core polybutadiene blocks, dissolution of the bulk materials yielded anisotropic micelles.

Among the most promising processes currently under evaluation for fabrication of anisotropic particles are methods based on the relatively simple manipulation of liquids followed by rapid solidification. In this way, multicompartment particles with nonequilibrium mate-

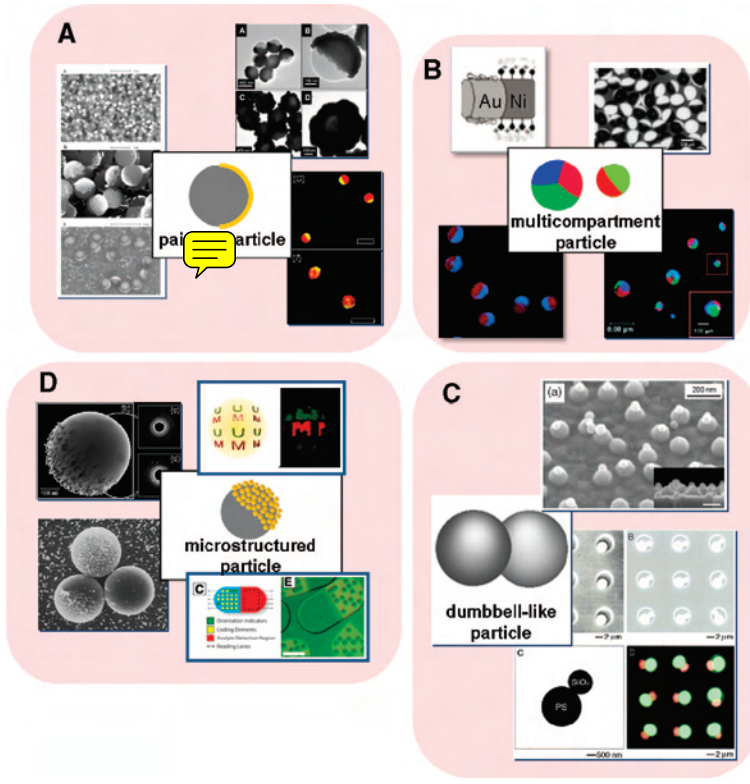

Figure 4. Representative examples of anisotropic particles with potential for anisotropy-based switching. Painted particles include particles that were selectively modified by gel-trapping,[41] metal deposition,[42] or layer-by-layer deposition.[43] Multicompartment particles include bimetallic nanorods[44] and larger microbeads,[45] as well as triphasic[46] and biphasic nanocolloids. Dumbbell-like particles are made by fusion of different types of particles.[47,48] Microstructured particles include particles with controlled topology[49] and lithographically modified particles,[50] as well as encoded particles[51] and those prepared by metal evaporation and chemisorption onto latex particles. Caption assignments are made clockwise starting in the upper left quadrant. Image credits are listed clockwise within each respective quadrant. (A) Republished with permission from ref , 2004 Wiley-VCH Verlag GmbH & Co.; from ref , 2006 Springer; from ref , 2005 American Chemical Society. (B) Republished with permission from ref , 2003 Macmillan Publishers Ltd.; from ref , 2006 Wiley-VCH Verlag GmbH & Co.; from ref , 2006 American Chemical Society. (C) Bhaskar and Lahann, unpublished data; republished with permission from ref , 2004 Wiley-VCH Verlag GmbH & Co.; from ref , 2001 American Chemical Society. (D) Republished with permission from ref , 2008 American Chemical Society; from ref , 2007 The National Academy of Sciences of the United States of America; from ref , 2007 American Association for the Advancement of Science; from ref , 1997 American Chemical Society. The four center images are original.

rials distributions can be fabricated in large quantities. Solidification must occur sufficiently quickly to prevent mixing between temporarily formed compartments. By using flow-focusing technology,[79–81] microdroplets containing chromophore molecules and biomolecules in separate phases have been generated and cured by appropriate cross-linking mechanisms.[82–84] Larger biphasic and multiphasic particles with diameters of 50−150 μm and narrow size distributions were prepared using microfluidics.

Other examples include the fabrication of microparticles using hydrodynamic jets,[85–87] or elctrohydrodynamic cojetting.[88] A prominent strategy toward anisotropic micro- and nanoparticles uses electrohydrodynamic cojetting.[46,88] In this method, the interface between the two jetting solutions is sustained during jet fragmentation and size reduction. In principle, such novel particle geometries enable independent control of key parameters, such as chemical composition, surface functionalization,

What sets today's synthetic materials apart from biological materials is the ability to undergo defined changes in key properties over time.

biological loading, shape, and size for each compartment, thereby effectively mimicking the architecture of biological cells. This approach toward designer nanoparticles leads to unique capabilities that enable the design of particles with multiple and distinct surface patterns or nanocompartments. Because of its intrinsic simplicity and generality, the electrohydrodynamic cojetting process can be applied to a wide range of specialty and nonspecialty materials including many FDA-approved materials.[89,90] The fact that each compartment can be designed independently from the other compartments affords anisotropic particles with multiple, orthogonal materials functions. In particular, electrohydrodynamic cojetting can be employed successfully in cases where the functions of incompatible materials must be engineered in close proximity to one another.

SUMMARY

Major efforts have been undertaken to create increasingly sophisticated materials that start to mimic biological materials with respect to precision, architecture, and functionality. Still, most of today's materials are intrinsically static. In other words, what sets today's synthetic materials apart from biological materials is the ability to undergo defined changes in key properties over time. Combinations of theoretical and experimental methods will sig-

nificantly widen the design parameters available for smart materials. In this regard, the study by Balazs and co-workers is remarkable. Their theoretical results suggest that through simple introduction of anisotropic particles into lipid bilayers, responsive pores could be created, which can open and close on demand. Although their study focuses on reversible switching due to mechanical forces, alternate triggers such as temperature or pH may also be explored for switching. Beyond the smart membrane studied by Balazs and co-workers, materials containing anisotropic particles can be expected to find applications in fundamental studies of cell architecture as well as in biomedical applications, such as drug delivery or molecular imaging. Despite the impressive advances recently made with switchable materials, even our most basic understanding of surface processes involving molecular switches as well as multicompartment particles is still rudimentary, and much work lies ahead in developing synthetic analogues of switchable systems, such as those used for camouflage by the cuttlefish.

REFERENCES AND NOTES

1. Mäthger, L. M.; Barbosa, A.; Miner, S.; Hanlon, R. T. Color Blindness and Contrast Perception in Cuttlefish (Sepia Officinalis) Determined by a Visual Sensorimotor Assay. *Vision Res.* **2006**, *46*, 1746–1753.
2. Wallin M. Nature's Palette. *Biosci. Explained 2002*, *1*, 1−12..
3. Langer, R.; Tirrell, D. A. Designing Materials for Biology and Medicine. *Nature* **2004**, *428*, 487–492.
4. Hoffman, A. S. "Intelligent" Polymers in Medicine and Biotechnology. *Artif Organs* **1995**, *19*, 458–467.
5. White, S. R.; Sottos, N. R.; Geubelle, P. H.; Moore, J. S.; Kessler, M. R.; Sriram, S. R.; Brown, E. N.; Viswanathan, S. Autonomic Healing of Polymer Composites. *Nature* **2001**, *409*, 794–797.
6. Cho, S. H.; Andersson, H. M.; White, S. R.; Sottos, N. R.; Braun, P. V. Polydimethylsiloxane-Based Self-Healing Materials. *Adv. Mater.* **2006**, *18*, 997–1000.
7. Comiskey, B.; Albert, J. D.; Yoshizawa, H.; Jacobson, J. An Electrophoretic Ink for All-Printed Reflective Electronic Displays. *Nature* **1998**, *394*, 235–255.
8. Mullins, J. Now You See Me. . *The New Scientist* **2007**, *193*, 38–41.
9. Schurig, D.; Mock, J. J.; Justice, B. J.; Cummer, S. A.; Pendry, J. B.; Starr, A. F.; Smith, D. R. Metamaterial Electromagnetic Cloak at Microwave Frequencies. *Science* **2006**, *314*, 977–980.
10. Kang, Y.; Walish, J. J.; Gorishnyy, T.; Thomas, E. L. Broad Wavelength Range Chemically Tunable Block Copolymer Photonic Gels. *Nat. Mater.* **2007**, *6*, 957–960.
11. Yang, J.; Yamato, M.; Kohno, C.; Nishimoto, A.; Sekine, H.; Fukai, F.; Okano, T. Cell Sheet Engineering: Recreating Tissues Without Biodegradable Scaffolds. *Biomaterials* **2005**, *26*, 6415–6422.
12. Lahann, J.; Langer, R. Smart Materials With Dynamically Controllable Surfaces. *MRS Bull.* **2005**, *30*, 185–188.
13. Lendlein, A.; Jiang, H.; Jünger, O.; Langer, R. Light-Induced Shape-Memory Polymers. *Nature* **2005**, *434*, 879–882.
14. Alexeev, A.; Uspal, W. E.; Balazs, A. C. Harnessing Janus Nanoparticles to Create Controllable Pores in Membranes. *ACS Nano* **2008**, *2*.
15. Kavanagh, C. A.; Rochev, Y. A.; Gallagher, W. M.; Dawson, K. A.; Keenan, A. K. Local Drug Delivery in Restenosis Injury: Thermoresponsive Co-Polymers as Potential Drug Delivery Systems. *Pharmacol. Ther.* **2004**, *102*, 1–15.
16. Kikuchi, A.; Okano, T. Pulsatile Drug Release Control Using Hydrogels. *Adv. Drug Deliv. Rev.* **2002**, *54*, 53–77.
17. Kost, J.; Langer, R. Responsive Polymeric Delivery Systems. *Adv. Drug Deliv. Rev.* **2001**, *46*, 125–148.
18. Chilkoti, A.; Dreher, M. R.; Meyer, D. E.; Raucher, D. Targeted Drug Delivery by Thermally Responsive Polymers. *Adv. Drug Deliv. Rev.* **2002**, *54*, 613–630.
19. Soppimath, K. S.; Aminabhavi, T. M.; Dave, A. M.; Kumbar, S. G.; Rudzinski, W. E. Stimulus-Responsive "Smart" Hydrogels as Novel Drug Delivery Systems. *Drug Dev. Ind. Pharm.* **2002**, *28*, 957–974.
20. Yamato, M.; Kwon, O. H.; Hirose, M.; Kikuchi, A.; Okano, T. Novel Patterned Cell Coculture Utilizing Thermally Responsive Grafted Polymer Surfaces. *J. Biomed. Mater. Res.* **2001**, *55*, 137–140.
21. Yamato, M.; Konno, C.; Koike, S.; Isoi, Y.; Shimizu, T.; Kikuchi, A.; Makino, K.; Okano, T. Nanofabrication for Micropatterned Cell Arrays by Combining Electron Beam-Irradiated Polymer Grafting and Localized Laser Ablation. *J. Biomed. Mater. Res. A* **2003**, *67*, 1065–1071.
22. Yamato, M.; Konno, C.; Utsumi, M.; Kikuchi, A.; Okano, T. Thermally Responsive Polymer-Grafted Surfaces Facilitate Patterned Cell Seeding and Co-Culture. *Biomaterials* **2002**, *23*, 561–567.
23. Yamato, M.; Okano, T. Cell Sheet Engineering. *Mater Today* **2004**, *7*, 42–47.
24. Urry, D. W.; Luan, C. H.; Parker, T. M.; Gowda, D. C.; Prasad, K. U.; Reid, M. C.; Safavy, A. Temperature of Polypeptide Inverse Temperature Transition Depends on Mean Residue Hydrophobicity. *J. Am. Chem. Soc.* **1991**, *113*, 4346–4348.
25. Urry, D. W. Physical Chemistry of Biological Free Energy Transduction As Demonstrated by Elastic Protein-Based Polymers. *J Phys. Chem. B* **1997**, *101*, 11007–11028.
26. Hyun, J.; Lee, W-K; Nath, N.; Chilkoti, A.; Zauscher, S. Capture and Release of Proteins on the Nanoscale by Stimuli-Responsive Elastin-Like Polypeptide "Switches". *J. Am. Chem. Soc.* **2004**, *126*, 7330–7335.
27. Nath, N.; Chilkoti, A. Fabrication of a Reversible Protein Array Directly from Cell Lysate Using a Stimuli-Responsive Polypeptide. *Anal. Chem.* **2003**, *75*, 709–715.
28. Shin, J. Y.; Abbott, N. L. Using Light to Control Dynamic Surface Tensions of Aqueous Solutions of Water Soluble Surfactants. *Langmuir* **1999**, *15*, 4404–4410.
29. Abbott, S.; Ralston, J.; Reynolds, G.; Hayes, R. Reversible Wettability of Photoresponsive Pyrimidine-Coated Surfaces. *Langmuir* **1999**, *15*, 8923–8928.
30. Ichimura, K.; Oh, S-K; Nakagawa, M. Light-Driven Motion of Liquids on a Photoresponsive Surface. *Science* **2000**, *288*, 1624–1626.
31. Bunker, B. C.; Kim, B. I.; Houston, J. E.; Rosario, R.; Garcia, A. A.; Hayes, M.; Gust, D.; Picraux, S. T. Direct Observation of Photoswitching in Tethered Spiropyrans Using the Interfacial Force Microscope. *Nano Lett.* **2003**, *3*, 1723–1727.
32. Yu, Y.; Ikeda, T. Photodeformable Polymers: A New Kind of Promising Smart Material for Micro- and Nano-Applications. *Macromol. Chem. Phys.* **2005**, *206*, 1705–1708.
33. Jiang, H.; Kelch, S.; Lendlein, A. Polymers Move in Response to Light. *Adv. Mater.* **2006**, *18*, 1471–1475.
34. Yoshida, M.; Langer, R.; Lendlein, A.; Lahann, J. From Advanced Biomedical Coatings to Multi-Functionalized Biomaterials. *Polym. Rev.* **2006**, *46*, 347–375.
35. Abbott, N. L.; Gorman, C. B.; Whitesides, G. M. Active Control of Wetting Using Applied Electrical Potentials and Self- Assembled Monolayers. *Langmuir* **1995**, *11*, 16–18.
36. Lahann, J.; Mitragotri, S.; Tran, T. N.; Kaido, H.; Sundaram, J.; Choi, I. S.; Hoffer, S.; Somorjai, G. A.; Langer, R. A Reversibly Switching Surface. *Science* **2003**, *299*, 371–374.

37. Gallardo, B. S.; Gupta, V. K.; Eagerton, F. D.; Jong, L. I.; Craig, V. S.; Shah, R. R.; Abbott, N. L. Electrochemical Principles for Active Control of Liquids on Submillimeter Scales. *Science* **1999**, *283*, 57–60.
38. Wang, X.; Kharitonov, A. B.; Katz, E.; Willner, I. Potential-Controlled Molecular Machinery of Bipyridinium Monolayer-Functionalized Surfaces: An Electrochemical and Contact Angle Analysis. *Chem. Commun.* **2003**, *9*, 1542–1543.
39. Katz, E.; Lioubashevsky, O.; Willner, I. Electromechanics of a Redox-Active Rotaxane in a Monolayer Assembly on an Electrode. *J. Am. Chem. Soc.* **2004**, *126*, 15520–15532.
40. Bunker, B. C.; Huber, D. L.; Kushmerick, J. G.; Dunbar, T.; Kelly, M.; Matzeke, C.; Cao, J. G.; Jeppesen, J. O.; Perkins, J.; Flood, A. H.; Stoddart, J. F. Switching Surface Chemistry with Supramolecular Machines. *Langmuir* **2007**, *23*, 31–34.
41. Paunov, V. N.; Cayre, O. J. Supraparticles and "Janus" Particles Fabricated by Replication of Particle Monolayers at Liquid Surfaces Using a Gel Trapping Technique. *Adv. Mater.* **2004**, *16*, 788–791.
42. Suzuki, D.; Kawaguchi, H. Janus Particles with a Functional Gold Surface for Control of Surface Plasmon Resonance. *Colloid Polym. Sci.* **2006**, *284*, 1471–1476.
43. Li, Z. F.; Lee, D. Y.; Rubner, M. F.; Cohen, R. E. Layer-by-layer Assembled Janus Microcapsules. *Macromolecules* **2005**, *38*, 7876–7879.
44. Salem, A. K.; Searson, P. C.; Leong, K. W. Multifunctional Nanorods for Gene Delivery. *Nat. Mater.* **2003**, *2*, 668–671.
45. Nisisako, T.; Torii, T.; Takahashi, T.; Takizawa, Y. Synthesis of Monodisperse Bicolored Janus Particles with Electrical Anisotropy Using a Microfluidic Co-Flow System. *Adv. Mater.* **2006**, *18*, 1152–1156.
46. Roh, K. H.; Martin, D. C.; Lahann, J. Triphasic Nanocolloids. *J. Am. Chem. Soc.* **2006**, *128*, 6796–6797.
47. Koo, H. Y.; Yi, D. K.; Yoo, S. J.; Kim, D-Y. A Snowman-Like Array of Colloidal Dimers for Antireflecting Surfaces. *Adv. Mater.* **2004**, *16*, 274–277.
48. Yin, Y.; Lu, Y.; Xia, Y. A Self-Assembly Approach to the Formation of Asymmetric Dimers from Monodispersed Spherical Colloids. *J. Am. Chem. Soc.* **2001**, *123*, 771–772.
49. Ho, C.-C.; Chen, W.-S.; Shie, T.-Y.; Lin, J.-N.; Kuo, C. Novel Fabrication of Janus Particles from the Surfaces of Electrospun Polymer Fibers. *Langmuir* **2008**, *24*, 5663–5666.
50. Chen, H. Y.; Rouillard, J. M.; Gulari, E.; Lahann, J. Colloids with High-Definition Surface Structures. *Proc. Natl. Acad. Sci. U.S.A.* **2007**, *104*, 11173–11178.
51. Pregibon, D. C.; Toner, M.; Doyle, P. S. Multifunctional Encoded Particles for High-Throughput Biomolecule Analysis. *Science* **2007**, *315*, 1393–1396.
52. Electronic Reusable Paper; http://www2.parc.com/hsl/projects/gyricon/.
53. Sheridon, N. K. ; Richley, E. A. ; Mikkelsen, J. C. ; Tsuda, D. ; Crowley, J. M. ; Oraha, K. A. ; Howard, M. E. ; Rodkin, M. A. ; R. Swidler, R. S. *Proc. IDRC, SID/IEEE***1997**.
54. Kubowicz, S.; Baussard, J. F.; Lutz, J. F.; Thunemann, A. F.; von Berlepsch, H.; Laschewsky, A. Multicompartment Micelles Formed by Self-Assembly of Linear ABC Triblock Copolymers in Aqueous Medium. *Angew. Chem., Int. Ed.* **2005**, *44*, 5262–5265.
55. Li, Z.; Kesselman, E.; Talmon, Y.; Hillmyer, M. A.; Lodge, T. P. Multicompartment Micelles from ABC Miktoarm Stars in Water. *Science* **2004**, *306*, 98–101.
56. Kim, S-H; Yi, G-R; Kim, K. H.; Yang, S-M. Photocurable Pickering Emulsion for Colloidal Particles with Structural Complexity. *Langmuir* **2008**, *24*, 2365–2371.
57. Bao, Z. N.; Chen, L.; Weldon, M.; Chandross, E.; Cherniavskaya, O.; Dai, Y.; Tok, J. B. H. Toward Controllable Self-Assembly of Microstructures: Selective Functionalization and Fabrication of Patterned Spheres. *Chem. Mater.* **2002**, *14*, 24–26.
58. Paunov, V. N. Novel Method for Determining the Three-Phase Contact Angle of Colloid Particles Adsorbed at Air-Water and Oil-Water Interfaces. *Langmuir* **2003**, *19*, 7970–7976.
59. Paunov, V. N.; Cayre, O. J. Supraparticles and "Janus" Particles Fabricated by Replication of Particle Monolayers at Liquid Surfaces Using a Gel Trapping Technique. *Adv. Mater.* **2004**, *16*, 788–791.
60. Casagrande, C.; Fabre, P.; Raphael, E.; Veyssie, M. Janus Beads: Realization and Behavior at Water Oil Interfaces. *Europhys. Lett.* **1989**, *9*, 251–255.
61. Hugonnot, E.; Carles, A.; Delville, M. H.; Panizza, P.; Delville, J. P. "Smart" Surface Dissymmetrization of Microparticles Driven by Laser Photochemical Deposition. *Langmuir* **2003**, *19*, 226–229.
62. Takei, H.; Shimizu, N. Gradient Sensitive Microscopic Probes Prepared by Gold Evaporation and Chemisorption on Latex Spheres. *Langmuir* **1997**, *13*, 1865–1868.
63. Nakahama, K.; Kawaguchi, H.; Fujimoto, K. A Novel Preparation of Nonsymmetrical Microspheres Using the Langmuir−Blodgett Technique. *Langmuir* **2000**, *16*, 7882–7886.
64. Petit, L.; Sellier, E.; Duguet, E.; Ravaine, S.; Mingotaud, C. Dissymmetric Silica Nanospheres: A First Step to Difunctionalized Nanomaterials. *J. Mater. Chem.* **2000**, *10*, 253–254.
65. Petit, L.; Manaud, J. P.; Mingotaud, C.; Ravaine, S.; Duguet, E. Sub-Micrometer Silica Spheres Dissym-Metrically Decorated with Gold Nanoclusters. *Mater. Lett.* **2001**, *51*, 478–484.
66. Cayre, O.; Paunov, V. N.; Velev, O. D. Fabrication of Dipolar Colloid Particles by Microcontact Printing. *Chem. Commun.* **2003**, 2296–2297.
67. Nagle, L.; Fitzmaurice, D. Templated Nanowire Assembly on the Surface of a Patterned Nanosphere. *Adv. Mater.* **2003**, *15*, 933–935.
68. Yin, Y. D.; Lu, Y.; Xia, Y. N. A Self-Assembly Approach to the Formation of Asymmetric Dimers from Monodispersed Spherical Colloids. *J. Am. Chem. Soc.* **2001**, *123*, 771–772.
69. Gu, H. W.; Yang, Z. M.; Gao, J. H.; Chang, C. K.; Xu, B. Heterodimers of Nanoparticles: Formation at a Liquid-Liquid Interface and Particle-Specific Surface Modification by Functional Molecules. *J. Am. Chem. Soc.* **2005**, *127*, 34–35.
70. Hong, L.; Jiang, S.; Granick, S. Simple Method to Produce Janus Colloidal Particles in Large Quantity. *Langmuir* **2006**, *22*, 9495–9499.
71. Lattuada, M.; Hatton, T. A. Preparation and Controlled Self-Assembly of Janus Magnetic Nanoparticles. *J. Am. Chem. Soc.* **2007**, *129*, 12878–12889.
72. Giersig, M.; Ung, T.; Liz-Marzan, L. M.; Mulvaney, P. Direct Observation of Chemical Reactions in Silica-Coated Gold and Silver Nanoparticles. *Adv. Mater.* **1997**, *9*, 570–575.
73. Gu, H. W.; Zheng, R. K.; Zhang, X. X.; Xu, B. Facile One-Pot Synthesis of Bifunctional Heterodimers of Nanoparticles: A Conjugate of Quantum Dot and Magnetic Nanoparticles. *J. Am. Chem. Soc.* **2004**, *126*, 5664–5665.
74. Reculusa, S.; Poncet-Legrand, C.; Ravaine, S.; Mingotaud, C.; Duguet, E.; Bourgeat-Lami, E. Syntheses of Raspberrylike Silica/Polystyrene Materials. *Chem. Mater.* **2002**, *14*, 2354–2359.
75. Teranishi, T.; Inoue, Y.; Nakaya, M.; Oumi, Y.; Sano, T. Nanoacorns: Anisotropically Phase-Segregated CoPd Sulfide Nanoparticles. *J. Am. Chem. Soc.* **2004**, *126*, 9914–9915.
76. Yu, H.; Chen, M.; Rice, P. M.; Wang, S. X.; White, R. L.; Sun, S. H. Dumbbell-Like Bifunctional Au-Fe3O4 Nanoparticles. *Nano Lett.* **2005**, *5*, 379–382.
77. Erhardt, R.; Boker, A.; Zettl, H.; Kaya, H.; Pyckhout-Hintzen, W.; Krausch,

G.; Abetz, V.; Mueller, A. H. E. Janus Micelles. *Macromolecules* **2001**, *34*, 1069–1075.
78. Erhardt, R.; Zhang, M. F.; Boker, A.; Zettl, H.; Abetz, C.; Frederik, P.; Krausch, G.; Abetz, V.; Muller, A. H. E. Amphiphilic Janus Micelles with Polystyrene and Poly(Methacrylic Acid) Hemispheres. *J. Am. Chem. Soc.* **2003**, *125*, 3260–3267.
79. Utada, A. S.; Lorenceau, E.; Link, D. R.; Kaplan, P. D.; Stone, H. A.; Weitz, D. A. Monodisperse Double Emulsions Generated from a Microcapillary Device. *Science* **2005**, *308*, 537–541.
80. Xu, S. Q.; Nie, Z. H.; Seo, M.; Lewis, P.; Kumacheva, E.; Stone, H. A.; Garstecki, P.; Weibel, D. B.; Gitlin, I.; Whitesides, G. M. Generation of Monodisperse Particles by Using Microfluidics: Control Over Size, Shape, and Composition. *Angew. Chem., Int. Ed.* **2005**, *44*, 724–728.
81. Martin-Banderas, L.; Flores-Mosquera, M.; Riesco-Chueca, P.; Rodriguez-Gil, A.; Cebolla, A.; Chavez, S.; Ganan-Calvo, A. M. Flow Focusing: A Versatile Technology to Produce Size-Controlled and Specific-Morphology Microparticles. *Small* **2005**, *1*, 688–692.
82. Nisisako, T.; Torii, T.; Higuchi, T. Novel Microreactors for Functional Polymer Beads. *Chem. Eng. J.* **2004**, *101*, 23–29.
83. Nie, Z. H.; Li, W.; Seo, M.; Xu, S. Q.; Kumacheva, E. Janus and Ternary Particles Generated by Microfluidic Synthesis: Design, Synthesis, and Self-Assembly. *J. Am. Chem. Soc.* **2006**, *128*, 9408–9412.
84. Shepherd, R. F.; Conrad, J. C.; Rhodes, S. K.; Link, D. R.; Marquez, M.; Weitz, D. A.; Lewis, J. A. Microfluidic Assembly of Homogeneous and Janus Colloid-Filled Hydrogel Granules. *Langmuir* **2006**, *22*, 8618–8622.
85. Kim, J. W.; Larson, R. J.; Weitz, D. A. Uniform Nonspherical Colloidal Particles with Tunable Shapes. *Adv. Mater.* **2007**, *19*, 2005–2009.
86. Utada, A. S.; Lorenceau, E.; Link, D. R.; Kaplan, P. D.; Stone, H. A.; Weitz, D. A. Monodisperse Double Emulsions Generated from a Microcapillary Device. *Science* **2005**, *308*, 537–541.
87. Xu, S.; Nie, Z.; Seo, M.; Lewis, P.; Kumacheva, E.; Stone, H. A.; Garstecki, P.; Weibel, D. B.; Gitlin, I.; Whitesides, G. M. Generation of Monodisperse Particles by Using Microfluidics: Control Over Size, Shape, and Composition. *Angew. Chem., Int. Ed.* **2005**, *44*, 724–728.
88. Roh, K. H.; Martin, D. C.; Lahann, J. Biphasic Janus Particles with Nanoscale Anisotropy. *Nat. Mater.* **2005**, *4*, 759–763.
89. Roh, K. H.; Yoshida, M.; Lahann, J. Water-Stable Biphasic Nanocolloids with Potential Use as Anisotropic Imaging Probes. *Langmuir* **2007**, *23*, 5683–5688.
90. Yoshida, M.; Roh, K. H.; Lahann, J. Short-Term Biocompatibility of Biphasic Nanocolloids with Potential Use as Anisotropic Imaging Probes. *Biomaterials* **2007**, *28*, 2446–2456.

Switching the Electrochemical Impedance of Low-Density Self-Assembled Monolayers†

David K. Peng, Sandy T. Yu, David J. Alberts, and Joerg Lahann*

Department of Chemical Engineering, University of Michigan, 2300 Hayward Street, Ann Arbor, Michigan 48105

Received June 12, 2006. In Final Form: August 16, 2006

Because the active remodeling of biointerfaces is a paramount feature of nature, it is very likely that future, advanced biomaterials will be required to mimic at least certain aspects of the dynamic properties of natural interfaces. This need has fueled a quest for model surfaces that can undergo reversible switching upon application of external stimuli. Herein, we report the synthesis and characterization of a model system for studying reversibly switching surfaces based on low-density monolayers of mercaptohexadecanoic acid and mercaptoundecanoic acid. These monolayers were assembled on both gold and silver electrodes. When conducting electrochemical impedance spectroscopy under physiological conditions, these monolayers exhibit significant changes in their electrochemical barrier properties upon application of electrical DC potentials below +400 mV with respect to a standard calomel electrode. We further found the impedance switching to be reversible under physiological conditions. Moreover, the impedance can be fine-tuned by changing the magnitude of the applied electrical potential. Before and during impedance switching at pH 7.4 in aqueous buffer solutions, the low-density monolayers showed good stability according to grazing angle infrared spectroscopy data. We anticipate low-density monolayers to be potentially useful model surfaces when designing active biointerfaces for cell-based studies or rechargeable biosensors.

Introduction

Although great progress has been made over the past decade in the development of passive cell substrates for biomedical applications,[1−5] future research will need to address the intrinsically static character of such artificial substrates and the functional limitations encountered due to the lack of active, dynamic biomaterial properties.[5,6] At the cell−extracellular matrix (ECM) interface, both cell receptors and ECM proteins undergo rapid, dynamic remodeling.[7−10] This active remodeling of the biointerface is a critical feature of natural ECM, and the design of next-generation biomaterials must account for the dynamic aspects of these interfaces. The need for substrates that can dynamically regulate biological functions such as cell adhesion, proliferation, and differentiation has recently led to a variety of "smart material" designs in which control of biomaterial properties is stimulated by changes in temperature or pH or via light-induced or electrochemical modifications.[11−23] Herein, we report studies on a new class of smart materials—low-density self-assembled monolayers, or LDSAMs—which can undergo reversible conformational transitions that dynamically change the macroscopic surface properties of the monolayers.[23,24] Unlike traditional self-assembled monolayers (SAMs), which assemble in tightly packed arrangements, LDSAMs show increased conformational freedom of their constituent alkanethiolate molecules, which allows LDSAMs to exhibit unique, reversible responsiveness to the application of electrical potential.[23]

Although a range of surface analysis methods are available for characterization of switchable surfaces—including infrared spectroscopy, X-ray photoelectron spectroscopy (XPS), surface plasmon spectroscopy, ellipsometry, sum frequency generation spectroscopy, and cyclic voltammetry (CV)—electrochemical impedance spectroscopy (EIS) has become an increasingly important tool for SAM analysis. This trend is seen mainly because of the precise surface-sensitive analytical information that electrochemical methods provide and because of the small (∼10 mV) sinusoidal probe voltages that are used in EIS, which make it a less perturbing method than CV.

Studies of the electrical properties of SAMs by EIS can be divided into those that examine electronic conduction through SAMs using redox-active probes and those that follow the ionic conduction through SAMs using solution ions in the absence of redox probes. The majority of the EIS studies on SAMs reported in the literature have been conducted using redox probes, which has enabled studies of a variety of important characteristics of SAMs.[25−36] For instance, studies have examined the growth

† Part of the Stimuli-Responsive Materials: Polymers, Colloids, and Multicomponent Systems special issue.

* To whom correspondence should be addressed. E-mail: lahann@umich.edu.

(1) Stevens, M. M.; George, J. H. *Science* **2005**, *310*, 1135−1138.
(2) Lutolf, M. P.; Hubbell, J. A. *Nat. Biotechnol.* **2005**, *23*, 47−55.
(3) Vogel, V.; Baneyx, G. *Annu. Rev. Biomed. Eng.* **2003**, *5*, 441−63.
(4) Mrksich, M. *Curr. Opin. Chem. Biol.* **2002**, *6*, 794−797.
(5) Lahann, J.; Langer, R. *MRS Bull.* **2005**, *30*, 185−188.
(6) Stupp, S. I.; Donners, J. J. J. M.; Li, L. S.; Mata. A. *MRS Bull.* **2005**, *30*, 864−873.
(7) Holmbeck, K.; Szabova, L. *Birth Defects Res. C Embryo Today* **2006**, *78*, 11−23.
(8) Midwood, K. S.; Williams, L. V.; Schwarzbauer, J. E. *Int. J. Biochem. Cell Biol.* **2004**, *36*, 1031−1037.
(9) Brown, L. *Am. J. Physiol. Heart Circ. Physiol.* **2005**, *289*, H973−974.
(10) Davis, G. E.; Senger, D. R. *Circ. Res.* **2005**, *97*, 1093−1107.
(11) de las Heras Alarcon C.; Pennadam, S.; Alexander, C. *Chem Soc. Rev.* **2005**, *34*, 276−285.
(12) Kikuchi, A.; Okano, T. *J. Controlled Release* **2005**, *101*, 69−84.
(13) Tsuda, Y.; Kikuchi, A.; Yamato, M.; Sakurai, Y.; Umezu, M.; Okano, T. *J. Biomed. Mater. Res. A* **2004**, *69*, 70−78.
(14) Riskin, M.; Basnar, B.; Chegel, V. I.; Katz, E.; Willner, I.; Shi, F.; Zhang, X. *J. Am. Chem. Soc.* **2006**, *128*, 1253−1260.
(15) Wang, X.; Kharitonov, A.; Katz, E.; Willner, I. *Chem. Commun.* **2003**, *9*, 1542−1543.
(16) Jeong, B.; Gutowska, A. *Trends Biotechnol.* **2002**, *20*, 305−311.
(17) Russell, T. P. *Science* **2002**, *297*, 964−967.
(18) Liu, Y.; Mu, L.; Liu, B. H.; Zhang, S.; Yang, P. Y.; Kong, J. L. *Chem. Commun.* **2004,** *10*, 1194−1195.
(19) Abbott, S.; Ralston, J.; Reynolds, G.; Hayes, R. *Langmuir* **1999**, *15*, 8923−8928.
(20) Ichimura, K.; Oh, S. K.; Nakagawa, M. *Science* **2000**, *288*, 1624−1626.
(21) Abbott, N. L.; Gorman, C. B.; Whitesides, G. M. *Langmuir* **1995**, *11*, 16−18.
(22) Chi, Y. S.; Lee J. K.; Lee, S. G.; Choi, I. S. *Langmuir* **2004**, *20*, 3024−3027.
(23) Lahann, J.; Mitragotri, S.; Tran, T. N.; Kaido, H.; Sundaram, J.; Choi, I. S.; Hoffer, S.; Somorjai, G. A.; Langer, R. *Science* **2003**, *299*, 371−373.
(24) Katz, E.; Lioubashevsky, O.; Willner, I. *J. Am. Chem. Soc.* **2004**, *126*, 15520−15532.

10.1021/la061677o CCC: $37.00
Published on Web 10/26/2006

properties of dodecaneselenol,[26] octadecanethiol,[27] and naphthalene disulfide[28] monolayers, determining the relative time scales for monolayer adsorption and reorganization/crystallization; electron-transfer kinetics have been examined for dodecanethiol[29] and 4′-hydroxy-4-mercaptobiphenyl[30,31] monolayers; and monolayer pinhole size and separation have been studied for octadecanethiol monolayers.[32] Redox probe studies have also examined the passivation of a gold surface by 2-mercapto-3-*n*-octylthiophene,[33] the fractional coverage of octadecanethiol molecules,[34] and the change in the electrical "apparent thickness" of alkanethiol monolayers.[35]

In solutions without redox couples, ionic permeability through the monolayers plays the dominant role in the conduction of current. This phenomenon has been used to study acid−base reactions for mercaptohexadecanoic acid (MHA) and mercaptododecylamine monolayers,[37] the ionic insulating properties of alkanethiol monolayers of different chain lengths,[38,39] the effect of applied potential on alkanethiol monolayer structure,[40] the potential-induced desorption of monolayers,[41] and the insulating properties of adsorbed protein layers on alkanethiol monolayers.[42] The studies of Boubour and Lennox[39−41] in particular have presented a number of observations that suggest the usefulness of redox-inactive EIS for studying ionic permeability of low-density monolayers. First, well-packed SAMs, which exhibit strong barriers to ionic penetration, typically display low-frequency (1 Hz < f < 1000 Hz) phase angles approaching 90° (the theoretical phase angle for an ideal capacitor). In contrast, SAMs that display low-frequency phase angles below 87° show current leakage at pinholes and grain boundaries. Second, only in the medium-to-high-frequency range (100 Hz and up) does a change in electrolyte composition (e.g., salt concentration) affect the impedance trace. Third, upon the application of DC potential greater than a certain critical potential, the monolayer structure is perturbed and ionic permeability increases significantly, as long as potential-induced desorption can be excluded.

Despite the usefulness of redox probes for the determination of monolayer properties, practical concerns, particularly when pursuing biological or biomedical applications, will require far different environments from those seen in a typical electrochemical cell containing soluble hexaferrocyanide/hexaferricyanide. For this reason, the EIS measurements taken during these studies were performed in phosphate-buffered saline (PBS), an inert, redox-inactive, and physiologically relevant electrolyte solution. Our findings show that this analytical setup can be used to make accurate distinctions between different SAM types that are structurally very similar, and the aforementioned studies also provide a precedent for the study of purely ionic conductance through SAMs in the absence of redox couples.[39−41]

Although the physicochemical properties of a range of different SAMs have been studied extensively,[25,43−46] these studies have been limited to traditional dense SAMs, which do not exhibit tunable responsiveness to dynamic stimuli. Here we extend this method to LDSAMs assembled on gold and silver.

Experimental Section

Materials. MHA, mercaptoundecanoic acid (MUA), hexadecanethiol (HDT), undecanethiol (UDT), dimethoxytrityl chloride (DMT-Cl), triethylamine (TEA), diisopropylethylamine (DIPEA), absolute ethanol, and PBS were purchased from Sigma Aldrich (St. Louis, MO). Chlorotrityl chloride (CT-Cl) was purchased from TCI America (Portland, OR). Chemicals were used as received. Deionized water was produced using a Barnstead International (Dubuque, IA) E-pure system. Prime grade silicon wafers were purchased from Silicon Valley Microelectronics (Santa Clara, CA). Gold, silver, and titanium (99.99+%) were purchased from Alfa Aesar (Ward Hill, MA).

Synthesis of 16-Chlorotrityl-mercaptohexadecanoic Acid (CT-MHA) and 16-Chlorotrityl-mercaptoundecanoic Acid (CT-MUA). The synthesis of 16-chlorotrityl-mercaptohexadecanoic acid (CT-MHA) has been reported previously.[23] The synthesis of 16-chlorotrityl-mercaptoundecanoic acid (CT-MUA) was performed using a protocol that was similar to that of CT-MHA. The first step involves protection of the thiol tail of MUA with a dimethoxytrityl (DMT) group to form the thioether MUA-DMT. Next, 1.09 g of MUA was reacted with 1.76 g of DMT-Cl and 0.84 mL of triethylamine in 50 mL of 5:4:1 tetrahydrofuran/acetic acid/water, at room temperature, under argon atmosphere, for 14 h. MUA-DMT was isolated and purified by silica column chromatography (3:1:1 hexane/ethyl ether/THF) yielding 1.3 g of a yellow/amber oil product. The second step involves protection of the carboxyl headgroup of MUA-DMT with a chlorotrityl (CT) group to form the ester/thioether CT-MUA-DMT. Next, 1.3 g of purified MUA-DMT was reacted with 0.91 g of CT-Cl and 0.91 mL of DIPEA in 50 mL methylene chloride at room temperature under argon atmosphere for 14 h. CT-MUA-DMT was isolated and purified by silica column chromatography (3:1 hexane/ethyl ether) yielding 0.68 g of a clear oil product. The third step involves deprotection of the DMT group from the thiol tail of MUA to form the ester CT-MUA. Purified CT-MUA-DMT (0.68 g) was dissolved in 20 mL of 3:1 THF/methanol and 2 mL of 1 M sodium acetate to which was added a solution of 340 mg of silver nitrate in 4 mL of 5:1 methanol/water. The mixture was stirred for 1 h at room temperature. Precipitate was removed by centrifugation at 4000*g* for 5 min, followed by resuspension of the pellet in 15 mL of 3:1 THF/methanol, recentrifugation at 4000*g* for 5 min, and combination of the two supernatants. A solution of 308 g of dithioerythritol (DTE) in 3 mL of 1 M sodium acetate was then added, and the mixture was stirred for 5 h at room temperature. Precipitate was removed by centrifugation at 4000*g* for 5 min, followed by resuspension of the pellet in 15 mL of 3:1 THF/methanol, recentrifugation at 4000*g* for 5 min, and combination of the two supernatants. CT-MUA was isolated and purified by silica column chromatography (50 mL of 3:1 hexane/ethyl ether, followed by 1:1 hexane/ethyl ether), yielding 0.22 g of a clear oil product. CT-MUA (and CT-MHA) was aliquoted and stored at −20° C until used. [MUA-DMT] ^{1}H NMR (300 MHz, $CDCl_3$) δ 1.17−1.39 (m), 1.57−1.69 (m), 1.81−1.88 (m), 2.12−2.17 (t), 2.31−2.38 (t); 2.67−2.72 (t), 3.79 (s), 6.78−6.85 (m),

(25) Love, J. C.; Estroff, L. A.; Kriebel, J. K.; Nuzzo. R. G.; Whitesides G. M. *Chem. Rev.* **2005**, *105*, 1103−1169.
(26) Protsailo, L. V.; Fawcett, W. R.; Russell, D.; Meyer, R. L. *Langmuir* **2002**, *18*, 9342−9349.
(27) Diao, P.; Jiang, D.; Cui, X.; Gu, D.; Tong, R.; Zhong, B. *J. Electroanal. Chem.* **1999**, *464*, 61−67.
(28) Bandyopadhyay, K.; Vijayamohanan, K.; Shekhawat, G. S.; Gupta, R. P. *J. Electroanal. Chem.* **1998**, 447, *1*, 11−16.
(29) Xing, Y. F.; O′Shea, S. J.; Li, S. F. Y. *J. Electroanal. Chem.* **2003**, *542*, 7−11.
(30) Janek, R. P.; Fawcett, W. R.; Ulman, A. *Langmuir* **1998**, *14*, 3011−3018.
(31) Janek, R. P.; Fawcett, W. R.; Ulman, A. *J. Phys. Chem. B* **1997,** *101*, 8550−8558.
(32) Diao, P.; Guo, M.; Tong, R. *J. Electroanal. Chem.* **2001**, *495*, 98−105.
(33) Peng, Z.; Dong, S. *Langmuir* **2001**, *17*, 4904−4909.
(34) Diao, P.; Guo, M.; Jiang, D.; Jia, Z.; Cui, X.; Gu, D.; Tong, R.; Zhong, B. *J. Electroanal. Chem.* **2000**, *480*, 59−63.
(35) Cui, X.; Jiang, D.; Diao, P.; Li, J.; Tong, R.; Wang, X. *J. Electroanal. Chem.* **1999**, *470*, 1, 9−13.
(36) Widrig, C. A.; Chung, C.; Porter, M. D. *J. Electroanal. Chem.* **1991**, *310*, 335−359.
(37) Schweiss, R.; Werner, C.; Knoll, W. *J. Electroanal. Chem.* **2003**, *540*, 145−151.
(38) Protsailo, L. V.; Fawcett, W. R. *Langmuir* **2002**, *18*, 8933−8941.
(39) Boubour, E.; Lennox, R. B. *Langmuir* **2000**, *16*, 4222−4228.
(40) Boubour, E.; Lennox, R. B. *J. Phys. Chem. B* **2000**, *104*, 9004−9010.
(41) Boubour, E.; Lennox, R. B. *Langmuir* **2000**, *16*, 7464−7470.
(42) Bordi, F.; Prato, M.; Cavalleri, O.; Cametti, C.; Canepa, M.; Gliozzi, A. *J. Phys. Chem. B* **2004**, *108*, 20263−20272.
(43) Schreiber, F. *J. Phys.: Condens. Matter* **2004**, *16*, R881−R900.
(44) Schwartz, D. K. *Annu. Rev. Phys. Chem.* **2001**, *52*, 107−137.
(45) Ulman, A. *Chem. Rev.* **1996**, *96*, 1533−1554.
(46) Dubois, L. H. *Annu. Rev. Phys. Chem.* **1992**, *43*, 437−463.

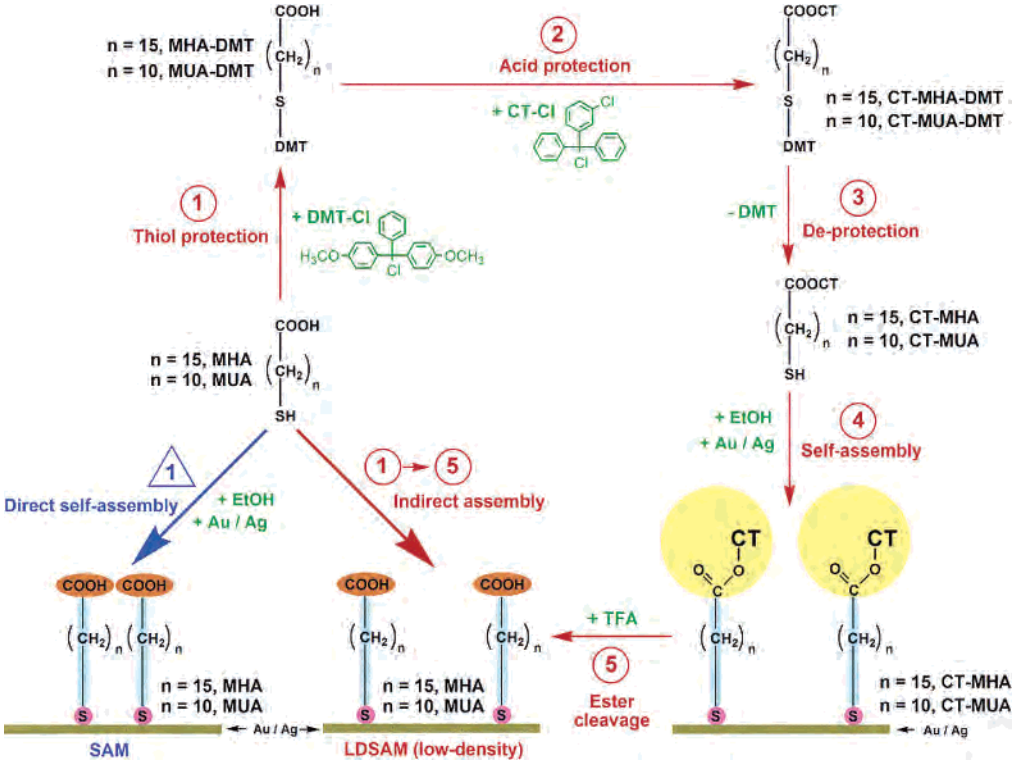

Figure 1. Preparation methods for traditional SAMs and LDSAMs. The formation of LDSAMs involves an indirect strategy via the CT ester, which consists of a bulky spacer group.

7.15−7.40 (m); ^{13}C NMR (100 MHz, $CDCl_3$) δ 29.25, 29.40, 55.44, 113.23, 113.40, 127.99, 128.09, 129.08, 129.36, 129.64, 130.90, 132.35. [CT-MUA-DMT] ^{1}H NMR (300 MHz, $CDCl_3$) δ 1.17−1.29 (m), 1.62−1.69 (m), 1.79−1.88 (m) 2.12−2.17 (t), 2.31−2.37 (m), 2.66−2.71 (t) 3.34 (s), 3.74−3.80 (m), 3.90 (s), 3.95−3.99 (m) 6.69−6.85 (m) 6.94−6.99 (m) 7.08−7.60 (m) 7.74−7.86 (m); ^{13}C NMR (75 MHz, $CDCl_3$) δ 24.92, 25.83, 28.67, 29.18, 29.38, 29.55, 34.20, 39.52, 55.45, 55.74, 55.99, 68.19, 82.82, 113.25, 113.39, 113.80, 115.01, 116.24, 126.63, 127.61, 127.98, 128.23, 128.43, 129.34, 129.65, 129.99, 130.90, 131.58, 131.72, 132.16, 132.84, 137.77, 143.93, 145.75, 179.63. [CT-MUA] ^{1}H NMR (300 MHz, $CDCl_3$) δ 1.10−1.35 (m), 1.56−1.68 (m), 1.95−2.00 (t), 2.31−2.36 (t), 7.17−7.35 (m), 7.43−7.46 (m); ^{13}C NMR (75 MHz, $CDCl_3$) δ 24.92, 25.83, 28.67, 29.18, 29.38, 29.55, 34.20, 39.52, 52.68, 55.45, 55.74, 55.99, 68.19, 82.82, 113.25, 113.39, 113.80, 115.006, 116.243, 126.632, 127.611, 127.98, 128.23, 128.43, 129.34, 129.65, 129.99, 130.90, 131.58, 131.72, 132.16, 132.84, 137.77, 143.93, 145.75, 179.63. Electrospray mass spectrometry gave a mass-to-charge ratio of 517.1948 for the CT-MUA $[M + Na]^+$ adduct, consistent with a theoretical molar mass of 517.1944 g/mol calculated for the nondimerized product.

Substrate and SAM Preparation. Substrates were prepared using prime grade silicon wafers upon which were deposited a 4500 Å SiO_2 insulating layer, a 100 Å titanium adhesive layer, and a 1000 Å gold or silver outer layer. Photolithographic techniques were used to produce patterned devices with a defined 2.2 cm^2 surface area for monolayer assembly and a separate electrical contacting patch; these patterned devices were used for electrochemical impedance spectroscopy measurements, the results of which scale with surface area. Surface roughness of the substrates was <2 nm rms by atomic force microscopy. Substrates were rinsed with a sequence of absolute ethanol, deionized water, and absolute ethanol, then dried under a stream of N_2 prior to SAM preparation.

SAMs were prepared by immersion of the target region of the substrates in 1 mM ethanolic solutions of adsorbate for 48 h at room temperature. After incubation, samples were rinsed with a sequence of absolute ethanol, deionized water, and absolute ethanol, then dried under a stream of N_2.

LDSAMs were prepared by incubation of CT-MHA or CT-MUA monolayer samples in 50% trifluoroacetic acid in ethanol for 2 min, which results in cleavage of the acid-labile ester bonds between the chlorotrityl groups and the immobilized alkanethiolates. Following cleavage, the samples were rinsed with a sequence of absolute ethanol, deionized water, and absolute ethanol, then dried in a stream of N_2.

Instrumentation: EIS and FTIR Spectroscopy. EIS was performed using a standard three-electrode electrochemical cell (SAM sample as working electrode, saturated standard calomel electrode [SCE] as reference electrode, and platinum mesh as counter electrode) with N_2-purged PBS as electrolyte solution. A Gamry PCI4/300 potentiostat with EIS300 software module was used to take EIS measurements. The applied potential had an AC amplitude of 10 mV rms and a frequency range from 1 to 10^5 Hz, with DC bias potentials varying between 0 and +400 mV with respect to (wrt) SCE. The amplitude and phase angle of the current response were recorded at 10 points per decade in frequency.

Fourier transform infrared (FTIR) spectroscopy was performed using a liquid-nitrogen-cooled Thermo Nicolet 6700 spectrometer in 85° grazing angle mode with a 16 mm aperture. One hundred twenty eight scans were taken per sample at 4 cm^{-1} resolution.

Results and Discussion

Self-Assembly. In this study, LDSAMs of MHA and MUA prepared on gold and silver electrodes are compared to their traditional dense SAM analogues. Figure 1 outlines the direct self-assembly method for preparing regular SAMs of MHA and MUA, as well as the indirect assembly method for preparing LDSAMs. The indirect method was designed to circumvent the tendency of alkanethiolates to form tightly packed assemblies resembling two-dimensional crystals.[25,43,45] The approach involves a multistep process of conjugating MHA or MUA to bulky, space-filling CT groups to form CT-MHA or CT-MUA esters. The subsequent assembly of CT-MHA or CT-MUA monolayers on gold or silver is followed by cleavage of the

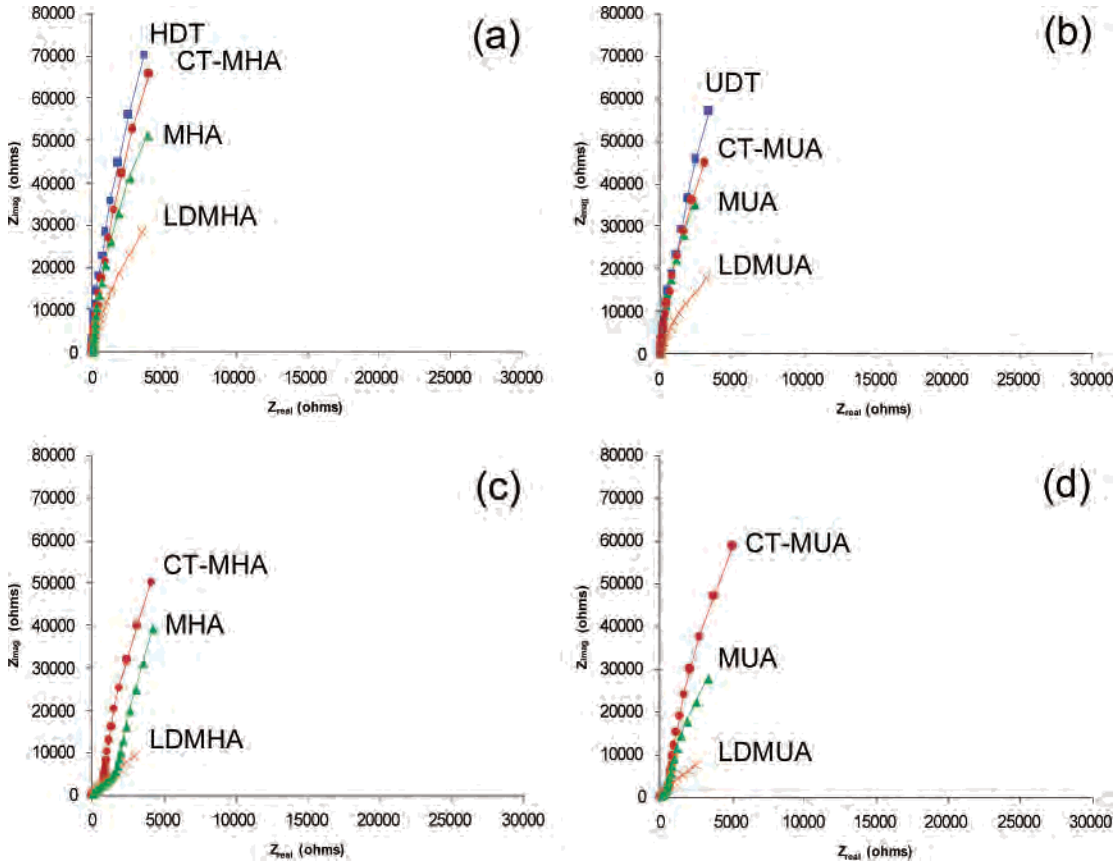

Figure 2. EIS Nyquist plots comparing different monolayer types. (a) C16 SAMs on Au, (b) C11 SAMs on Au, (c) C16 SAMs on Ag, and (d) C11 SAMs on Ag.

bulky CT groups, resulting in LDSAMs of MHA and MUA that are chemically identical to regular SAMs, but differ from the latter in the molecular spacing between the chains. Analysis of the CT-MHA and CT-MUA esters by NMR, mass spectrometry, and FTIR showed agreement of the thiols with the anticipated structures, verified the absence of disulfide dimers, and demonstrated the esters' stability for several months, when stored under inert gas at −20° C.

Electrochemical Impedance Spectroscopy. Figure 2 shows EIS Nyquist plots acquired in PBS buffer (pH 7.4) at 0 mV DC (wrt SCE) for various types of monolayers on gold and silver. When we compare different types of monolayers with the same chain length and on the same substrate, we notice that the highest impedances are seen with the dense CH_3-terminated SAMs (HDT and UDT) followed by the CT-terminated SAMs (CT-MHA and CT-MUA), then the dense COOH-terminated SAMs (MHA and MUA), and finally the LDSAMs (LDMHA and LDMUA). As expected, hydrophobic headgroups and higher packing densities result in greater ionic barrier properties. The greater impedance of the CT-terminated SAMs compared to MHA/MUA can be attributed to the dense packing of the large, hydrophobic CT groups on the surface. Although the impedance of the LDSAMs is low relative to the other monolayers, it is significantly higher than that of bare gold or silver; the impedance modulus at 1 Hz (maximum *y*-axis value) of bare gold and silver is on the order of 1000−2000 Ω (too low to be clearly plotted in Figure 2), which is significantly lower than the most permeable LDSAM of LDMUA on Ag, which has a modulus of 7500 Ω at 1 Hz. This observation suggests the relative homogeneity and continuity of the LDSAMs, with a lack of gross levels of pinhole defects. When we compare the impedance of monolayers with different chain lengths (Figure 2a vs 2b), we typically see higher impedances for the C16-length SAMs than for the corresponding C11-length monolayers. This observation is expected because of the greater resistance to ionic permeation that monolayers with longer chain lengths display.[39] Similarly, monolayers assembled on gold typically showed higher impedances than monolayers assembled on silver (Figure 2a vs 2c). Also noticeable in the Nyquist plots of SAMs on silver are some deviations from linearity in the slope of the data; greater phase angle deviations are seen for the data taken at lower frequencies (closer to the origin). Since solution resistance is the dominant source of impedance at low frequencies, this effect could result from oxidation at the surface of the silver due to trace levels of dissolved oxygen in the PBS solution.

Impedance Switching. The next series of EIS analyses examined the effect of the applied DC potential on monolayer impedances. During these experiments, a series of increasingly positive DC electrical potentials was applied during EIS measurements. Because our LDSAMs have enhanced conformational freedom,[23] we would anticipate the application of positive potential to more easily influence the structure of the monolayers and thus alter their impedance profiles to a greater degree compared to the more sterically hindered dense SAMs.

Nyquist plots of the potential responses of SAMs on gold are shown in Figure 3. The measurements for each type of monolayer were performed consecutively, in order of increasing positive potential, without removing the sample from the electrochemical cell during the experiments. An electrochemical potential of +400 mV wrt SCE was chosen as the upper potential limit to avoid electrochemical oxidation of the thiol or potential-induced monolayer defects.[40] In the case of both (a) the C16- and (b) the C11-length monolayers, the impedance of dense SAMs does not change significantly upon application of potentials up to +400

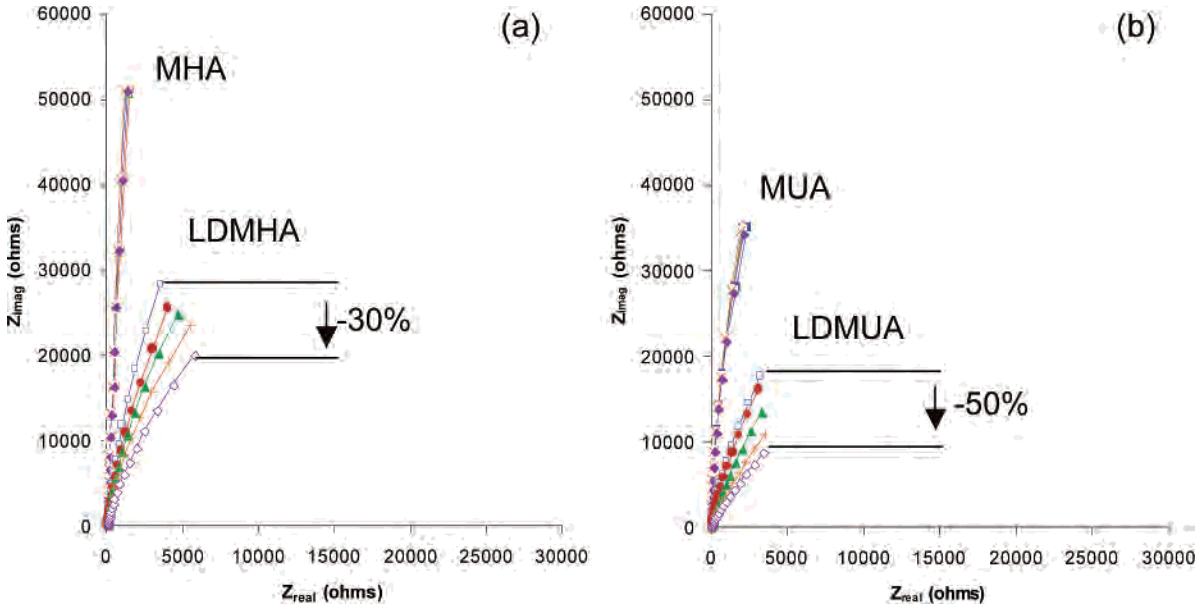

Figure 3. Impedance response of monolayers on Au to a stepwise change in electrical potential between 0 and +400 mV wrt SCE. (a) C16 monolayers and (b) C11 monolayers.

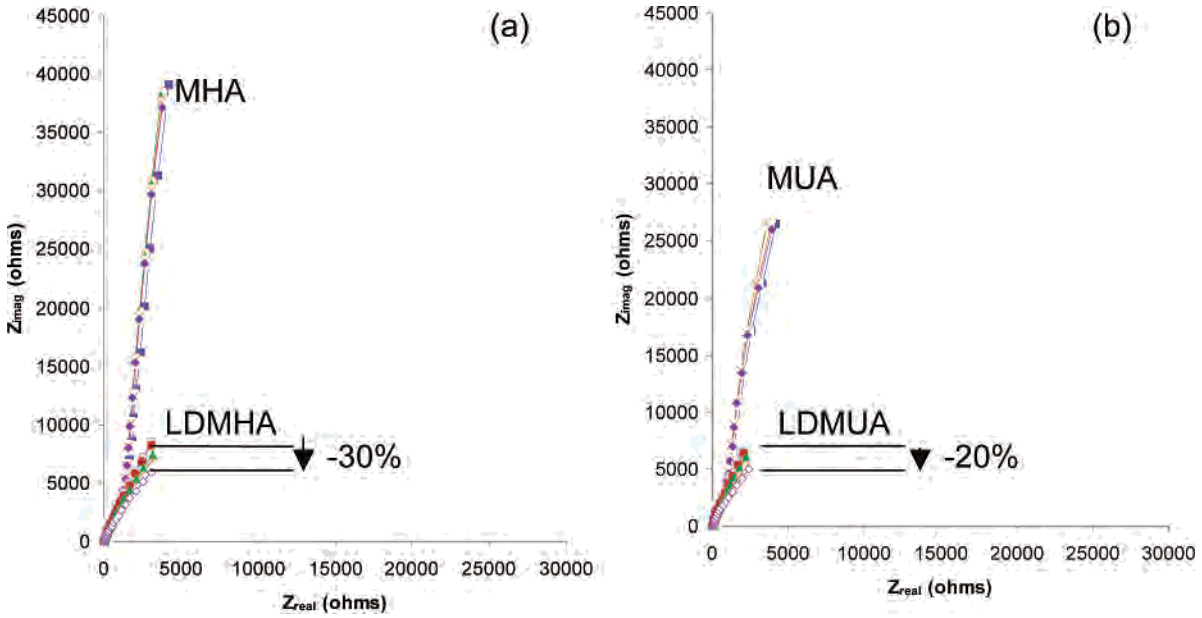

Figure 4. Impedance response of monolayers on Ag to a stepwise change in electrical potential between 0 and +40 mV wrt SCE. (a) C16 monolayers and (b) C11 monolayers.

mV, while the impedance of the LDSAMs decreases stepwise with increasing positive potential, culminating in a decrease in impedance modulus (*y*-axis value) of about 30% for LDMHA at +400 mV and about 50% for LDMUA at +100 mV. LDSAMs of MUA thus showed greater sensitivity to the application of the electrochemical potential than LDSAMs of MHA. These data are in agreement with an increased flexibility of the shorter-chain LDSAMs. The increase of phase angle (trace tilt) seen for LDSAMs at higher potentials also indicates increasingly greater deviations from ideal capacitor behavior and increasing ionic permeability as a result of the conformational transitions induced by the applied potential.

The potential responses of SAMs on silver are shown in Figure 4. In this case, +40 mV wrt SCE was chosen as an upper potential limit because of the increased potential sensitivity of the SAMs on silver (gross deformation of the impedance traces are seen at +60 mV, data not shown). Although the potential response trends were similar to those of SAMs on gold, some differences are apparent. The dense SAMs appear to be somewhat more sensitive to potential than the corresponding monolayers on gold. The effect of applied potential on LDMUA is also relatively small, possibly because of the shorter chain length of this monolayer. The very high level of conformational flexibility that results from this structure may obscure the effect of actively induced conformational transitions.

The results from Figures 3 and 4 generally suggest that the impedance of LDSAMs, unlike that of dense SAMs, can be controlled or tuned across a relatively wide range through the application of small electrical potentials.

After demonstrating the tunability of LDSAMs, we conducted a series of EIS experiments to test the reversibility of the electrical impedance response of LDSAMs—a property which could be useful for technological applications. Previous studies have demonstrated the reversible switching of LDSAMs on gold,

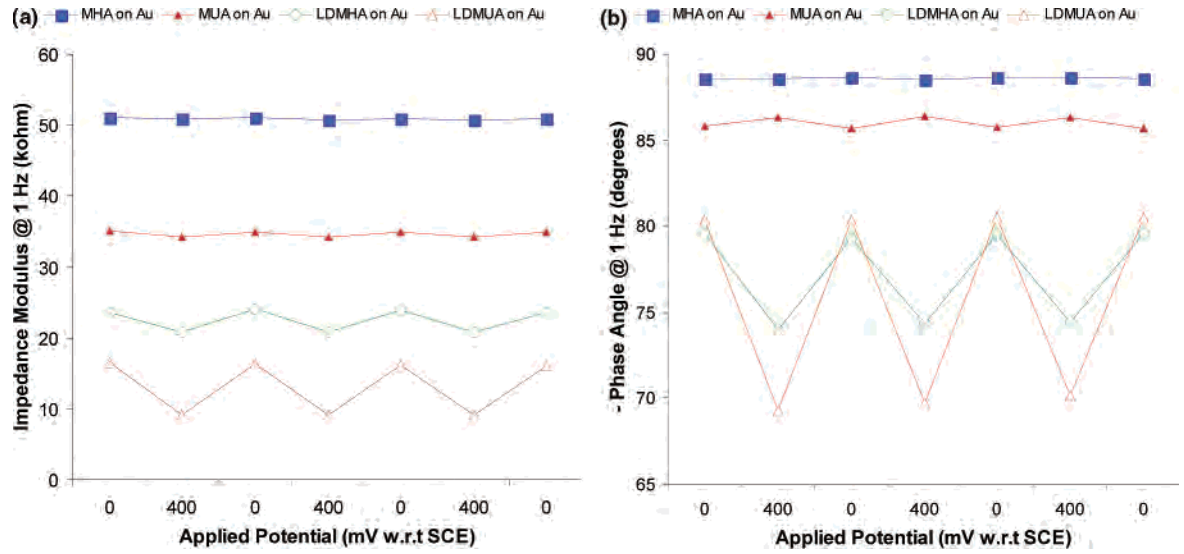

Figure 5. Reversibility of the impedance response for potential switching between 0 and +400 mV wrt SCE for monolayers on Au. (a) Impedance modulus vs frequency and (b) phase angle vs frequency.

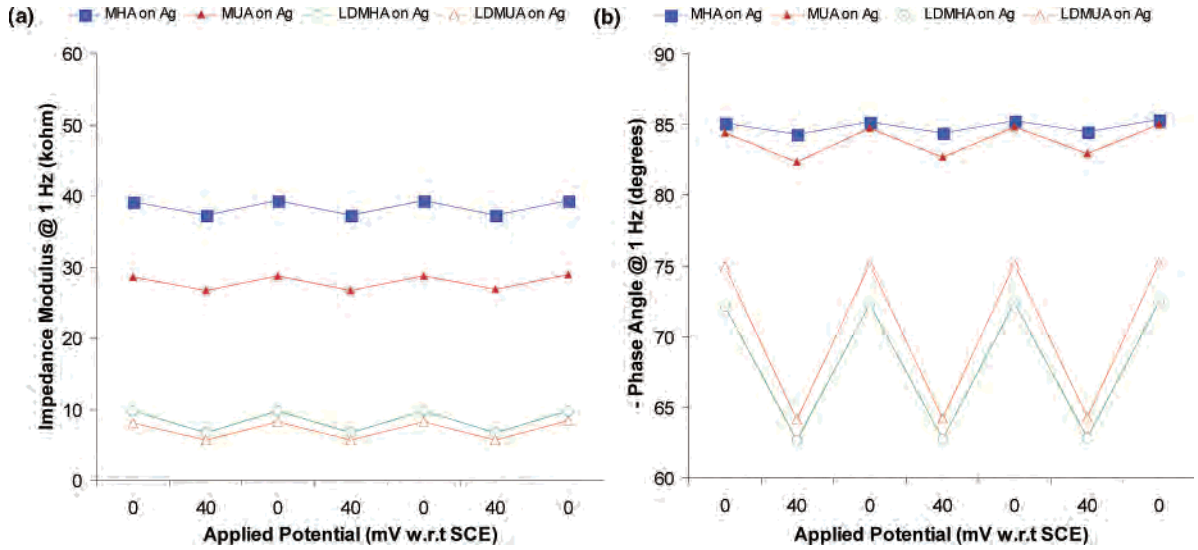

Figure 6. Reversibility of the impedance response for potential switching between 0 and +40 mV wrt SCE for monolayers on Au. (a) Impedance modulus vs frequency and (b) phase angle vs frequency.

conferring dynamic control over surface properties such as wettability.[23] The present experiments address reversible switching of the DC bias potential during EIS analysis between 0 and +400 mV wrt SCE for all Au monolayers (except LDMUA, for which it was between 0 and +100 mV). In contrast, the DC bias potential was switched between 0 and +40 mV wrt SCE for all Ag monolayers. The concurrent EIS analysis provides an assessment of reversible control over ionic conduction through the monolayer.

Figure 5 shows the resulting pattern of impedance moduli and phase angles at 1 Hz from the series of experiments on Au SAMs. Toggling the potential through four switching cycles has the least effect on dense MHA SAMs, whereas MUA SAMs show only a slight response. LDMHAs show a pronounced response, and LDMUAs exhibit the strongest response. The effect is generally similar for impedance modulus and phase angle, although interestingly, with MUA we see a slight inversion effect where the phase angle is marginally higher at +400 mV. The greater responsiveness of the C11 SAMs and the LDSAMs is consistent with our previous observations of the effect of monolayer chain length and density on impedance. Reversibility is very good, with little drift seen in impedance levels over the course of the measurement sequence.

Figure 6 shows the resulting pattern of impedance moduli and phase angles at 1 Hz from the series of experiments on Ag SAMs. Here we see increased potential sensitivity to smaller applied fields but also less dramatic contrast between dense SAMs and LDSAMs. The data show excellent reversibility, again with very little drift of the impedance levels over the course of the experiment.

The data shown in Figures 5 and 6 suggest that conformational flexibility is essential to producing monolayer systems with reversible impedance properties. Although the flexibility conferred by the Ag lattice is clearly sufficient to yield reversibility trends, more distinctly contrasting effects are seen on Au, when comparing LDSAMs with dense SAMs.

Fourier Transform Infrared Spectroscopy. Grazing angle FTIR spectra were recorded for dense SAMs and LDSAMs before and after the EIS reversibility cycling experiments in order to assess the effect of EIS on monolayer integrity and stability. Spectra for Au monolayers are shown in Figure 7, spectra for Ag monolayers are shown in Figure 8, and characteristic

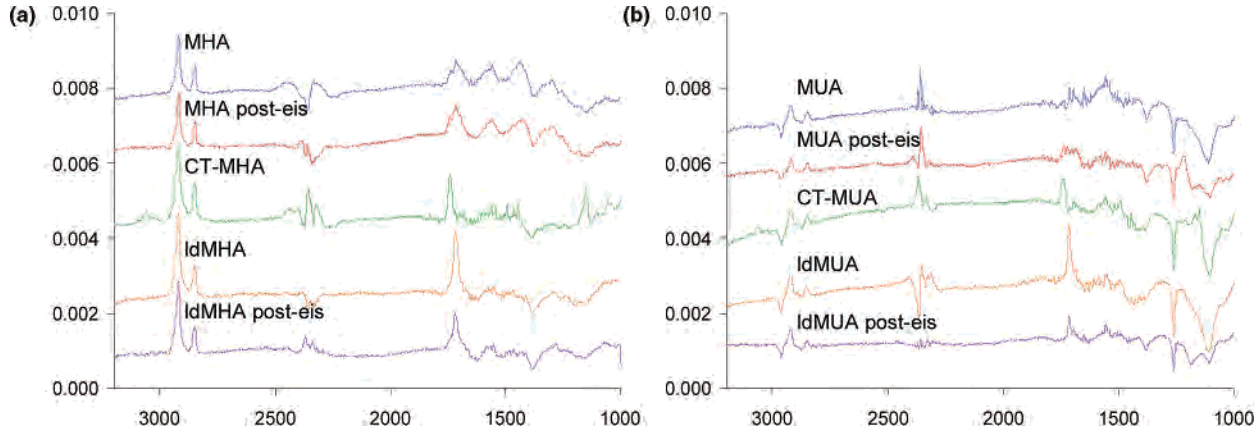

Figure 7. FTIR spectra of several monolayers on Au. (a) C16 monolayers and (b) C11 monolayers.

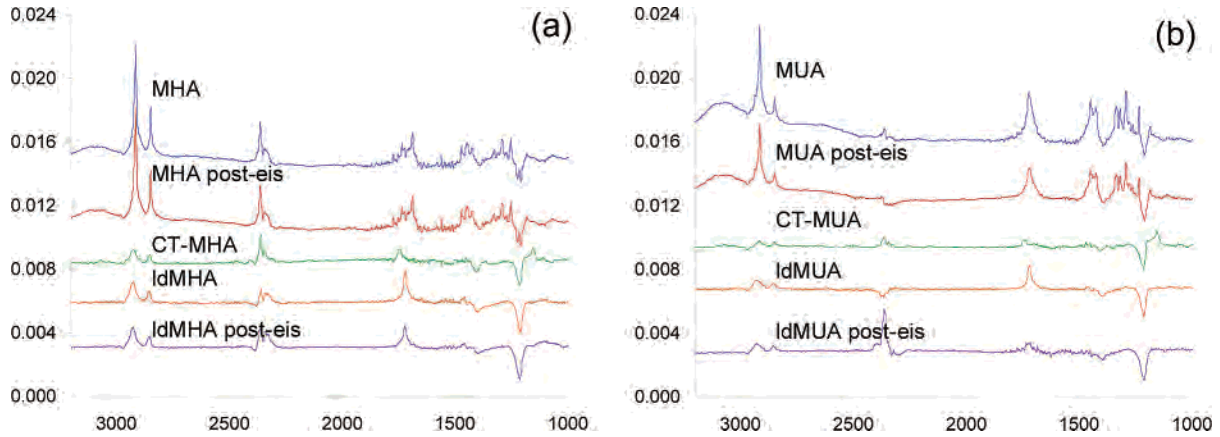

Figure 8. FTIR spectra of several monolayers on Ag. (a) C16 monolayers and (b) C11 monolayers.

Table 1. FTIR Peak Locations for Several Monolayers Assembled on Au and Ag

monolayer	substrate	asym C−H	sym C−H	asym CH_2	sym CH_2	C═O, carbonyl	C−O, ester	C−Cl
MHA	Au	–	–	2919.6	2850.9	1716.2	–	–
MHA-post-EIS	Au	–	–	2919.0	2850.5	1717.7	–	–
CT-NHA	Au	3063.2	3032.6	2921.9	2851.6	–	1743.5	1153.1
LDMHA	Au	–	–	2921.3	2852.0	1720.0	–	–
LDMHA post-EIS	Au	–	–	2920.8	2851.5	1720.1	–	–
MUA	Au	–	–	2922.4	2841.0	1717.5	–	–
MUA-post-EIS	Au	–	–	2921.8	2850.2	1718.1	–	–
CT-MUA	Au	3066.37	3028.8	2922.9	2853.2	–	1743.0	1154.6
LDMUA	Au	–	–	2925.3	2855.3	1718.6	–	–
LDMUA post-EIS	Au	–	–	2923.1	2852.1	1717.8	–	–
MHA	Ag	–	–	2913.9	2846.6	1687.8	–	–
MHA-post-EIS	Ag	–	–	2914.3	2847.2	1686.2	–	–
CT-NHA	Ag			2923.2	2851.0		1741.8	1154.2
LDMHA	Ag	–	–	2925.1	2853.4	1718.4	–	–
LDMHA post-EIS	Ag	–	–	2926.7	2853.7	1720.2	–	–
MUA	Ag	–	–	2913.4	2846.3	1720.7	–	–
MUA-post-EIS	Ag	–	–	2913.3	2846.2	1720.6	–	–
CT-MUA	Ag			2915.0	2847.9	–	1745.7	1153.0
LDMUA	Ag	–	–	2923.9	2854.8	1718.6	–	–
LDMUA post-EIS	Ag	–	–	2928.9	2853.5	1720.8	–	–

peak locations are listed in Table 1. Dense monolayers have characteristic asymmetric and symmetric methylene CH_2 stretches at ∼2920 and ∼2850 cm^{-1}, as well as C═O stretches at ∼1720 cm^{-1}. Chlorotrityl-terminated monolayers show additional peaks at ∼3060 and ∼3030 cm^{-1} (asymmetric and symmetric aromatic C−H stretch) and ∼1150 cm^{-1} (C−Cl stretch), as well as a shift of the C═O stretch from 1720 to ∼1740 cm^{-1} due to the ester bond. Details of the FTIR studies are given in Table 1. After CT group cleavage, LDSAMs show an absence of the previously present aromatic and C−Cl stretches, a C═O shift to the ∼1720 cm^{-1} carbonyl range, and generally minimal shifts in CH_2 stretches, with the exception of LDSAMs of MUA on Ag. LDSAMs show a red-shift in their CH_2 stretches compared to dense MHA and MUA monolayers. This shift reflects the more fluid and less crystalline environment experienced by the methylene groups within low-density monolayers and is also the reason Ag monolayers show a greater red-shift than Au monolayers.

With the exception of a slight shift in the asymmetric CH_2 stretch for LDSAMs of MUA on Ag, there is no difference

between the spectra recorded before and after impedance switching. The data generally suggest that the repeated application of small electrical potentials does not affect the integrity of LDSAMs.

Conclusions

Low-density monolayers of MHA can be prepared via self-assembly of bulky precursor thiols and subsequent cleavage of the spacer.[23] Compared to their dense counterparts, these monolayers show enhanced responsiveness to the application of even small electrical potentials.[23] Although previous studies have focused on LDSAMs assembled on gold,[23] we have now extended this concept to shorter thiols (MUA) self-assembled on gold and to LDSAMs of MHA and MUA on silver substrates. Moreover, we have demonstrated that the application of small electrical potentials can induce switching of the electrochemical barrier properties of these monolayers. EIS conducted in PBS buffer at physiological pH values has proven to be an exquisite method for studying reversible transitions in low-density monolayers. Moreover, the switching of the four LDSAMs (MHA and MUA on Au and Ag) was found to be in clear contrast to the regular SAMs of MHA and MUA that were included in this study as references. In fact, the stepwise application of electrochemical potentials between 0 and +400 mV wrt SCE for Au and between 0 and +40 mV wrt SCE for Ag enabled a fine-tuning of the impedance of LDSAMs. The potential-induced changes in impedance were found to be reversible, as demonstrated by the repeated switching of LDSAMs of MHA and MUA on both gold and silver electrodes. The stability of the LDSAMs during the impedance switching was verified by comparing the grazing angle FTIR spectra of the LDSAMs before and after impedance switching. Within the margins of error, these spectra were identical. LDSAMs show an interesting responsiveness to the application of small electrical potentials. The herein-demonstrated ability to tune and switch their impedance properties may be useful, when considering their potential for biosensors or active biointerfaces for cell-based studies. Much future work is needed before these applications become reality, however.

Acknowledgment. We thank Hsien-Yeh Chen, Onnop Srivannavit, Brian Johnson, and Kenneth Chomistek for help with electrode microfabrication. D.K.P. acknowledges support from a graduate fellowship from the National Institutes of Health through the University of Michigan Cellular Biotechnology Training Program. The project was funded by grants from the National Institutes of Health and an Idea Award of the Department of Defense.

LA061677O

Chemical, Electrochemical, and Structural Stability of Low-Density Self-Assembled Monolayers

David K. Peng and Joerg Lahann*

Department of Chemical Engineering, University of Michigan, 2300 Hayward Street, Ann Arbor, Michigan 48105

Received May 31, 2007

The stability of low-density self-assembled monolayers of mercaptohexadecanoic acid on gold is studied under a variety of storage conditions—air at room temperature, argon at room temperature and 4 °C, and ethanol at room temperature. The structural monotony of the low-density monolayers was assessed by monitoring the alkyl chains of LDSAMs by grazing-angle Fourier transform infrared spectroscopy as a function of time. Independently of the storage conditions, both symmetric and asymmetric methylene stretches at 2923 and 2852 cm^{-1} decreased after 4 weeks to 2919 and 2849 cm^{-1}, respectively. These data suggest an increased ordering of the alkyl chains that is distinctly different from that of conventional high-density monolayers of mercaptohexadecanoic acid included as a reference in this study. As a further extension of this observation, the electrochemical barrier properties of the low-density monolayers were assessed by electrochemical impedance spectroscopy and did not change significantly for any of the storage conditions over a period of 4 weeks. Moreover, X-ray photoelectron spectroscopy was used to assess the chemical changes in the low-density monolayers over time. The chemical composition was essentially unaltered for all storage conditions. Specifically, oxidation of the sulfur headgroup, a common cause of monolayer degradation, was excluded for all test conditions on the basis of XPS analysis. This study confirms excellent storage stability for low-density monolayers under commonly used storage conditions and bridges an important technological gap between these systems and conventional high-density systems.

Introduction

Self-assembled monolayers (SAMs) have been studied extensively because of the ease and flexibility with which they can produce a diverse range of functionalized surfaces.[1−4] Widely characterized SAM systems, such as alkanethiolate monolayers on gold, are typically formed through the spontaneous assembly of their constituent molecules into films with tightly packed, sterically constrained alkyl chains. Several previous studies examined the stability of high-density SAMs. For instance, Schoenfisch et al.[5] and Horn et al.[6] independently examined the stability of alkanethiolate SAMs in air, Flynn et al. investigated the stability of monolayers made of undecanethiol as well as tri(ethylene glycol)-terminated undecanethiol derivatives in biological media,[7] and Willey et al. examined the stability of dodecanethiolate SAMs in air and under the influence of UV light and found limited stability with time.[8]

More recently, low-density SAMs (LDSAMs), which are formed with increased interchain distances, have attracted increasing interest because they display enhanced conformational freedom paired with unique structural characteristics and functions.[9,10] Certain LDSAMs have also been employed as the structural basis of dynamically switchable surfaces.[11] For instance, carboxyl-terminated LDSAMs, such as mercaptohexadecanoic acid monolayers, displayed reversible and controllable switching of surface properties, such as wettability[11] and impedance,[12] upon application of small electrical potentials.

The initial development of switchable LDSAMs has encouraged several related investigations in recent years. For example, the behavior of stimuli-responsive SAMs has been characterized by molecular dynamics simulation,[13] the effects of LDSAMs on protein adsorption[14] and surface friction[15] have been examined, and various LDSAM fabrication methods have been developed, including those employing cyclodextrin inclusion complexes,[14] multidentate chelating alkanethiols,[15] and cleavable fluorocarbons.[16] The promise of fundamental insights into dynamic surface transitions and the technological implications of stimuli-responsive materials have transformed this topic into an active area of research.[17−20]

Although LDSAMs are chemically similar to their high-density counterparts, their increased interstitial spacing may increase their propensity for oxidative degradation, phase segregation, and interfacial restructuring. Before practical applications of LDSAMs can be realized, the influence of extended storage on

* Corresponding author. E-mail: lahann@umich.edu.

(1) Love, J. C.; Estroff, L. A.; Kriebel, J. K.; Nuzzo. R. G.; Whitesides, G. M. *Chem. Rev.* **2005**, *105*, 1103−1169.
(2) Schreiber, F. *J. Phys.: Condens. Matter* **2004**, *16*, R881−R900.
(3) Schwartz, D. K. *Annu. Rev. Phys. Chem.* **2001**, *52*, 107−137.
(4) Ulman, A. *Chem. Rev.* **1996**, *96*, 1533−1554.
(5) Schoenfisch, M. H.; Pemberton, J. E. *J. Am. Chem. Soc.* **1998**, *120*, 4502−4513.
(6) Horn, A. B.; Russell, D. A.; Shorthouse, L. J.; Simpson, R. E. *J. Chem. Soc., Faraday Trans.* **1996**, *92*, 4759−4762.
(7) Flynn, N. T.; Tran, T. N. T.; Cima, M. J.; Langer, R. *Langmuir* **2003**, *19*, 10909−10915.
(8) Willey, T. M.; Vance, A. L.; van Buuren, T.; Bostedt, C.; Terminello, L. J.; Fadley, C. S. *Surf. Sci.* **2005**, *576*, 188−196.
(9) Lahann, J.; Langer R. *MRS Bull.* **2005**, *30*, 185−188.
(10) Choi, I. S.; Chi, Y. S. *Angew. Chem., Int. Ed.* **2006**, *45*, 4894−4897.
(11) Lahann, J.; Mitragotri, S.; Tran, T. N.; Kaido, H.; Sundaram, J.; Choi, I. S.; Hoffer, S.; Somorjai, G. A.; Langer, R. *Science* **2003**, *299*, 371−373.
(12) Peng, D. K.; Yu, S. T.; Alberts, D. J.; Lahann, J. *Langmuir* **2007**, *23*, 297−304.
(13) Vemparala, S.; Kalia, R. K.; Nakano, A.; Vashishta, P. *J. Chem. Phys.* **2004**, *121*, 5427−5433.
(14) Liu, Y.; Mu, L.; Liu, B.; Zhang, S.; Yang, P.; Kong, J. *Chem. Commun.* **2004**, 1194−1195.
(15) Park, J. S.; Vo, A. N.; Barriet, D.; Shon, Y. S.; Lee, T. R. *Langmuir* **2005**, *21*, 2902−2911.
(16) Berron, B.; Jennings, G. K. *Langmuir* **2006**, *22*, 7235−7240.
(17) Winnik, F. M.; Whitten, D. G. *Langmuir* **2007**, *23*, 1−2.
(18) de Las Heras Alarcon, C.; Pennadam, S.; Alexander, C. *Langmuir* **2005**, *34*, 276−285.
(19) Yoshida, M.; Langer, R.; Lendlein, A.; Lahann, J. *Poly. Rev.* **2006**, *4*, 347−375.
(20) Squires, T. M.; Quake, S. R. *Rev. Mod. Phys.* **2005**, *77*, 977−1026.

10.1021/la701607e CCC: $37.00
Published on Web 08/30/2007

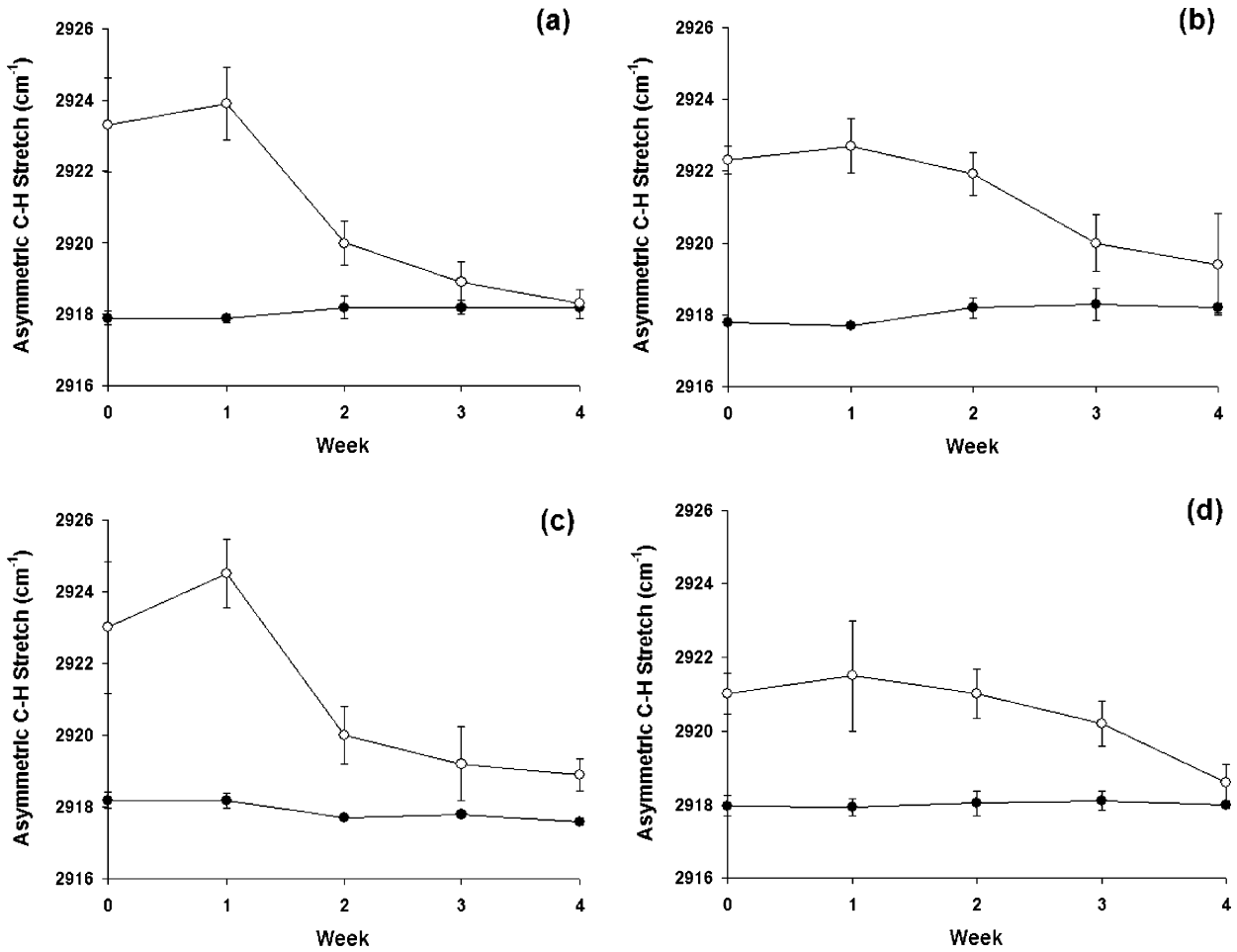

Figure 1. FTIR peak locations for the asymmetric C−H stretch of high-density SAMs (●) and low-density SAMs (○) stored under various conditions: (a) 20 °C under air, (b) 20 °C under argon, (c) 4 °C under argon, and (d) 20 °C under ethanol.

chemical, structural, and electrochemical stability must be fundamentally examined. Thus far, repeated potential-induced switching of carboxyl-terminated LDSAMs in aqueous solution was demonstrated only over several hours.[11] Longer-term stability under different conditions has not yet been assessed in detail and is the focus of this study.

Experimental Section

Materials. Mercaptohexadecanoic acid (MHA), dimethoxytrityl chloride, absolute ethanol, and phosphate-buffered saline (PBS) were purchased from Sigma-Aldrich (St. Louis, MO). Chlorotrityl chloride was purchased from TCI America (Portland, OR). Chemicals were used as received. Deionized water was produced using a Barnstead International (Dubuque, IA) E-pure system. Prime-grade silicon wafers were purchased from Silicon Valley Microelectronics (Santa Clara, CA). Gold and titanium (99.99+%) were purchased from Alfa Aesar (Ward Hill, MA).

Synthesis. As previously reported,[11] 16-chlorotrityl-mercaptohexadecanoic acid (CT-MHA) was synthesized using a three-step protocol involving thiol protection using a dimethoxytrityl group, followed by carboxyl protection using a chlorotrityl group and thiol deprotection to yield CT-MHA.

SAM Preparation. Gold-coated silicon substrates with titanium adhesion layers (100 nm Au, 10 nm Ti) were prepared as previously reported,[12] with a defined 2.2 cm^2 surface area for monolayer assembly and a separate electrical contacting patch for electrochemical measurements. SAMs were prepared by immersion of the target region of the substrates in 1 mM ethanol solutions of adsorbate for 48 h at room temperature. After incubation, samples were rinsed with a sequence of absolute ethanol, deionized water, and absolute ethanol and were dried in a stream of N_2. Low-density SAMs were prepared from the CT-MHA monolayers by incubation for 2 min in 50% trifluoroacetic acid in ethanol, which results in quantitative cleavage of the acid-labile ester bonds and yielded acid-terminated alkanethiolate monolayers. Following cleavage, the samples were rinsed with a sequence of absolute ethanol, deionized water, and absolute ethanol and then dried in a stream of N_2. Three replicate samples were then stored under each of the following conditions: an air atmosphere at room temperature, an argon atmosphere at room temperature, an argon atmosphere at 4 °C, or a N_2-purged ethanol bath with an argon atmosphere. In each case (including the air atmosphere), samples were enclosed within a tightly sealed jar. Three replicate samples of high-density SAMs of MHA were also stored under the same conditions as the control samples.

Instrumentation. Electrochemical impedance spectroscopy (EIS) was performed using a standard three-electrode electrochemical cell (a SAM sample as the working electrode, a saturated standard calomel electrode [SCE] as the reference electrode, and a platinum mesh as the counter electrode) with N_2-purged phosphate-buffered saline as the electrolyte solution. A Gamry PCI4/300 potentiostat with an EIS300 software module was used to take EIS measurements. The applied potential had an ac amplitude of 10 mV rms and a frequency range from 1 to 10^5 Hz, with a dc bias of 0 mV with respect to the SCE. The amplitude and phase angle of the current response were recorded at 10 points per decade in frequency.

X-ray photoelectron spectroscopy (XPS) was performed using an Axis Ultra (Kratos Analyticals, U.K.) instrument equipped with a monochromatized Al Kα X-ray source. Electrons were collected with a pass energy of 20 keV for C 1s and 40 keV for S 2p spectra. Spectra were normalized with respect to aliphatic carbon at 285.0 eV, and components were modeled with a Marquardt fitting algorithm.

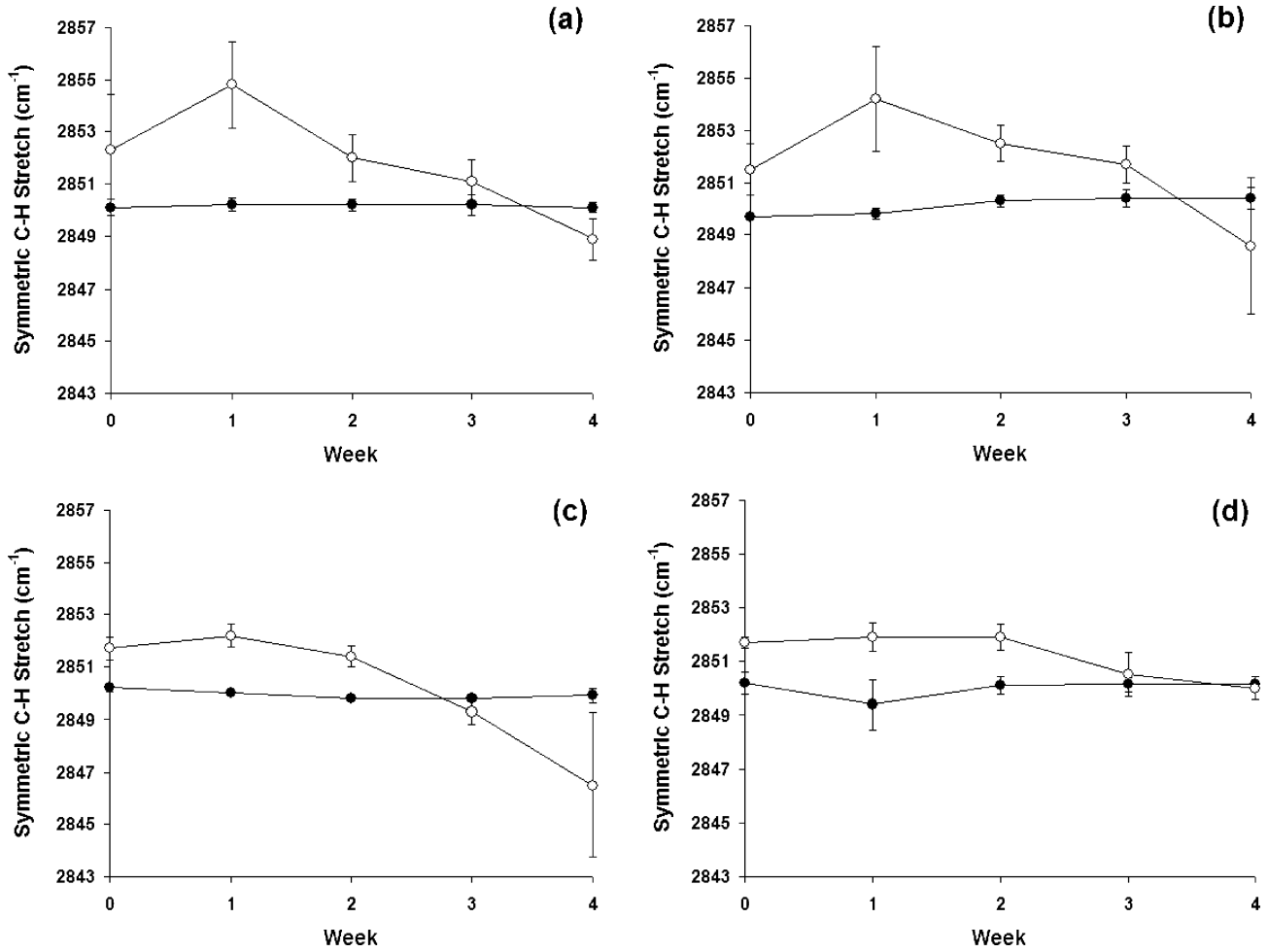

Figure 2. FTIR peak locations for the symmetric C−H stretch of high-density SAMs (●) and low-density SAMs (○) stored under various conditions: (a) 20 °C under air, (b) 20 °C under argon, (c) 4 °C under argon, and (d) 20 °C under ethanol.

Fourier transform infrared (FTIR) spectroscopy was performed using a liquid-nitrogen-cooled Thermo Nicolet 6700 spectrometer in 85° grazing angle mode with a 16 mm aperture. At least 128 scans were taken per sample at 4 cm^{-1} resolution.

Results and Discussion

Prior to monolayer formation, 16-chlorotrityl-mercaptohexadecanoic acid (CT-MHA) was synthesized using a three-step protocol as described previously.[11] Low-density SAMs and conventional SAMs were prepared by the immersion of microfabricated gold electrodes into ethanol solutions of either CT-MHA or MHA for 48 h at room temperature. In the case of the low-density SAMs, samples were immersed for 2 min in a 1:1 mixture of trifluoroacetic acid and ethanol, which resulted in quantitative cleavage of the acid-labile ester bonds. The reaction can be conveniently monitored by grazing-angle FTIR spectroscopy.[11,12]

Monolayers were prepared and stored at room temperature under air, argon, and ethanol as well as at 4 °C under argon. The samples were compared to the corresponding high-density SAMs of MHA, which were stored under identical conditions. The stability of monolayer electrochemical insulating properties was assessed using electrochemical impedance spectroscopy (EIS), and the structural and chemical properties were assessed using Fourier transform infrared (FT-IR) spectroscopy and X-ray photoelectron spectroscopy (XPS), respectively.

Fourier Transform Infrared Spectroscopy. FTIR was performed to assess the effect of storage on the structure of low-density monolayers.[21] High-density SAMs of MHA typically show two characteristic high-frequency IR peaks: an asymmetric C−H stretching peak at ∼2918 cm^{-1} and a symmetric C−H stretching peak at ∼2850 cm^{-1} (peak assignments according to Nuzzo et al.[21]). These stretches are representative of densely packed, crystalline alkyl chains whereas loosely packed alkyl chains typically show asymmetric C−H stretching peaks above 2920 cm^{-1} and symmetric C−H stretching peaks above 2852 cm^{-1}.[11,12] Figure 1 summarizes time-dependent storage experiments signifying the change in asymmetric C−H stretching peaks for low- and high-density MHA SAMs under various storage conditions. Figure 2 shows the corresponding data for the symmetric C−H stretches. The high-density SAMs (solid circles) do not experience significant IR band shifts over time under any of the storage conditions examined in this study. In contrast, significant variations were observed for the low-density SAMs over the studied time course. Both symmetric and asymmetric methylene stretches, which were initially at 2923 and 2852 cm^{-1}, decreased significantly during the course of the study and were found to be at 2919 and 2849 cm^{-1} after 4 weeks of storage. The direction of the peak shifts toward lower wavenumbers suggests that the alkyl chains of the LDSAMs increased their packing order. This effect is observed to be independent of the storage conditions (Figure 2b,c).

Possible explanations for this red shift of the symmetric and asymmetric methylene stretches may be as follows: (1) The

(21) Nuzzo, R. G.; Dubois, L. H.; Allara, D. L. *Langmuir* **1990**, *112*, 558−569.

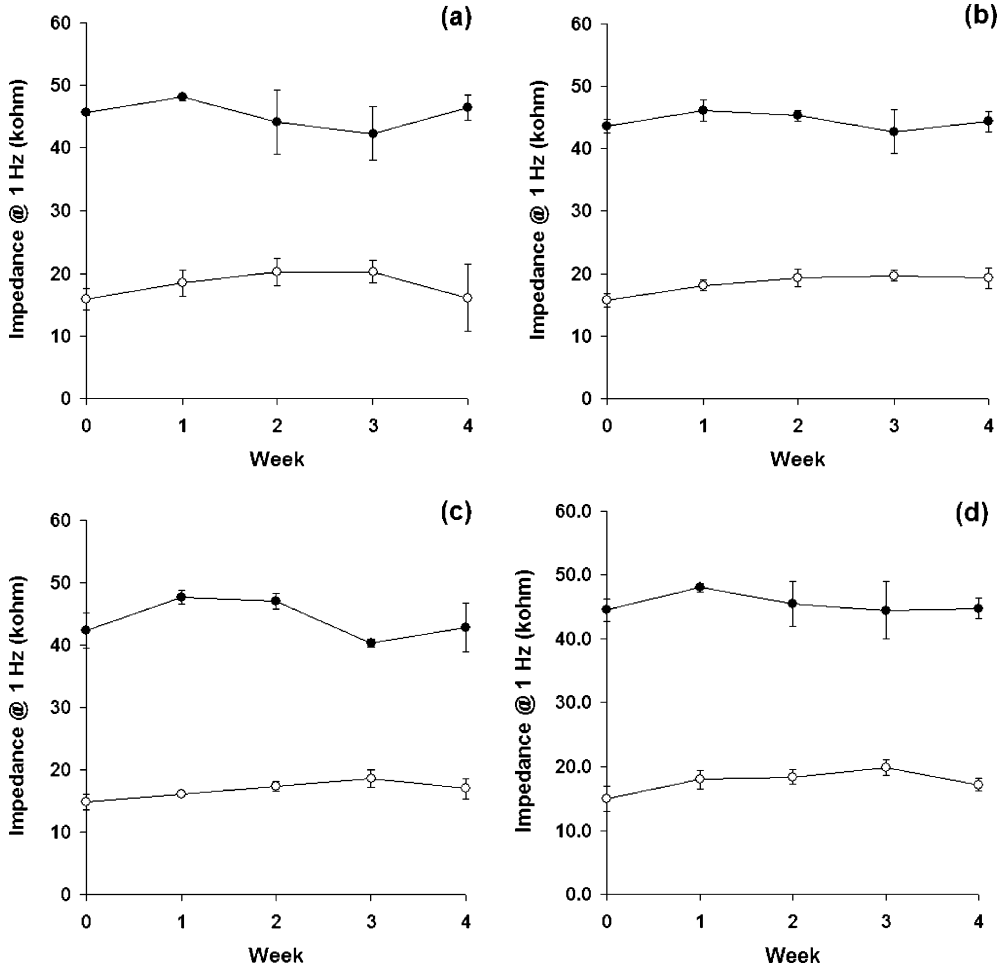

Figure 3. Impedance modulus at 1 Hz of high-density SAMs (●) and low-density SAMs (○) stored under various conditions: (a) 20 °C under air, (b) 20 °C under argon, (c) 4 °C under argon, and (d) 20 °C under ethanol.

Table 1. XPS C 1s Spectra Component Analysis for LDSAMs Stored for 4 Weeks under Different Storage Conditions

	theoretical	25 °C, air		25 °C, argon		4 °C, argon	
	%	area	%	area	%	area	%
$C-H_2$	82	5951	80	5368	84	4854	82
$C-S$, $C-CO_2H$	12	994	13	612	10	696	12
CO_2H	6	497	7	399	6	367	6

alkyl chains of LDSAMs undergo a thermodynamically driven ordering over time, which can be attributed to energetically favorable van der Waals interactions of individual alkyl chains. (2) Chemical modification of the monolayers due to thiol oxidation and/or intercalation of contaminants restricts alkyl chain flexibility and leads to the red shift of the methylene stretches. (3) Segregation of the initially homogeneously distributed MHA thiolates leads to the formation of dense, crystalline islands over time.

Whereas the phase segregation behavior (third hypothesis) has been well documented for high-density SAMs,[22−25] island formation should affect the electrochemical barrier properties of the monolayer because the formation of dense islands would inevitably result in areas where the gold surface is exposed. However, the exposure of uncovered gold areas should be detectable on the basis of decreased electrochemical impedance.

Electrochemical Impedance Spectroscopy. To probe this hypothesis, electrochemical impedance spectroscopy (EIS) data for low- and high-density MHA SAMs were measured for 1 Hz $< f <$ 100 kHz to assess the broad electrochemical response of samples in both the capacitance- and resistance-dominated regimes.[26] Because the contribution to the observed impedance due to monolayer capacitance is dominant only at lower frequencies ($f < \sim$1000) and impedance at 1 Hz is representative of impedance in this regime, $|Z|_{1\ Hz}$ has been reported to be a surrogate for the overall insulating properties exhibited by the SAMs.[26,27] For freshly prepared samples, $|Z|_{1\ Hz}$ of LDSAMs was 17 kΩ, which is significantly lower than the impedance measured for the corresponding high-density monolayers, which was consistently above 40 kΩ. These values are in agreement with previously reported data[12] and are an indication of reduced barrier properties of the LDSAMs as compared to their conventional high-density counterparts. However, the impedance values of the LDSAMs are significantly higher than the values measured for bare gold surfaces under identical conditions (<2 kΩ), suggesting that LDSAMs indeed exhibit homogeneous and robust coverage of the electrode surface.[11,12] After storage for

(22) Stranick, S. J.; Parikh, A. N.; Tao, Y. Y.; Allara, D. L.; Weiss, P. S. *J. Phys. Chem.* **1994**, *98*, 7636−7646.
(23) Chen, S.; Li, L.; Boozer, C. L.; Jiang, S. *Langmuir* **2000**, *16*, 9287−9293.
(24) Smith, R. K.; Reed, M. S.; Lewis, P. A.; Monnell, J. D.; Clegg, R. S.; Kelly, K. F.; Bumm, L. A.; Hutchison, J. E.; Weiss, P. S. *J. Phys. Chem. B* **2001**, *105*, 1119−1122.
(25)) Imabayashi, S.; Hobara, D.; Kakiuchi, T. *Langmuir* **2001**, *17*, 2560−2563.
(26) Boubour, E.; Lennox, R. B. *Langmuir* **2000**, *16*, 4222−4228.
(27) Boubour, E.; Lennox, R. B. *Langmuir* **2000**, *16*, 7464−7470.

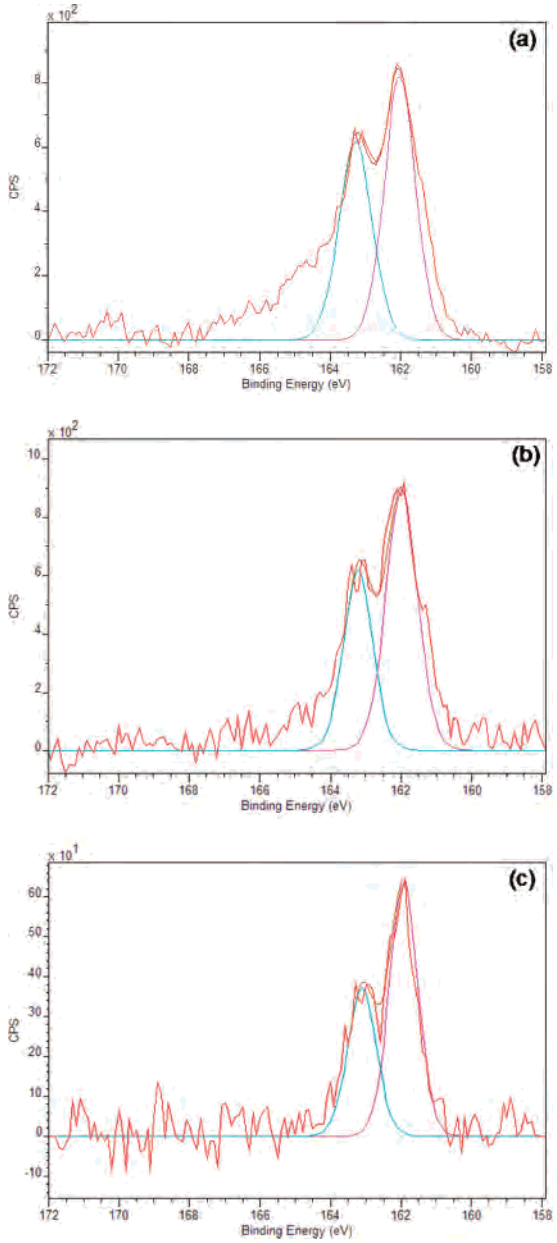

Figure 4. High-resolution S 2p XPS spectra of low-density SAMs before storage (a) after 4 weeks at 20 °C under air, (b) after 4 weeks at 20 °C under argon, and (c) after 4 weeks at 4 °C under argon.

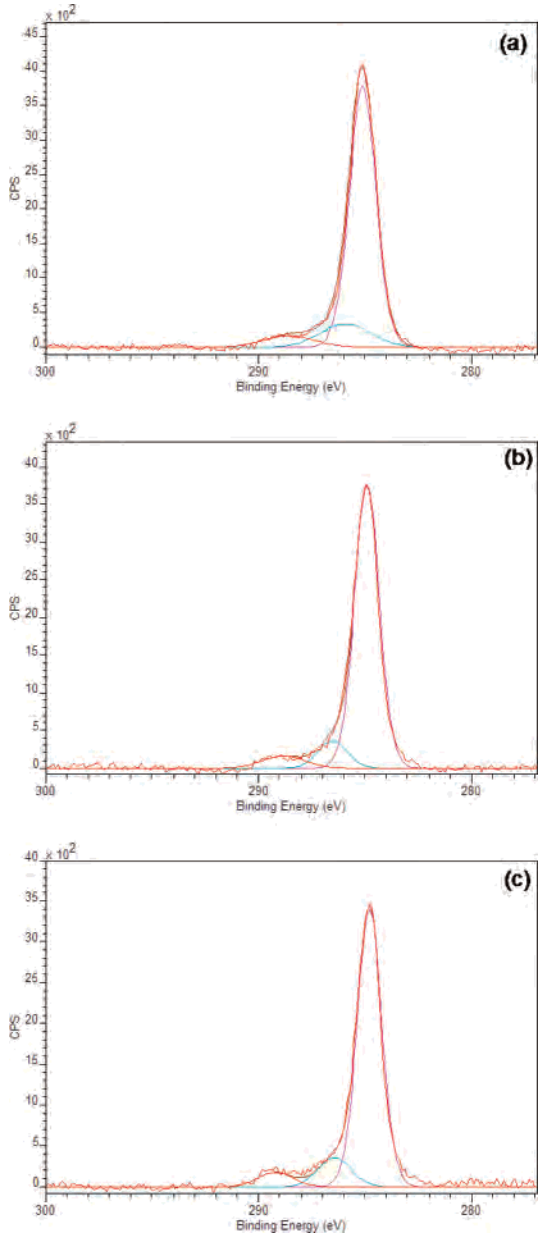

Figure 5. High-resolution C 1s XPS spectra of low-density SAMs before storage (a) after 4 weeks at 20 °C under air, (b) after 4 weeks at 20 °C under argon, and (c) after 4 weeks at 4 °C under argon.

up to 4 weeks in different environments and under two different temperatures, the electrochemical properties did not change significantly. Figure 3 shows the effect of extended storage over 1 month under different conditions for high- and low-density monolayers. Although LDSAMs are hypothetically more susceptible to oxidative degradation compared to their high-density counterparts, the LDSAM samples stored in air at room temperature (Figure 3a, open circles) did not show dramatically different changes in impedance than the samples stored in less stressful environments (although greater deviation was observed at week 4). The differences between samples stored under argon at room temperature versus those stored at 4 °C (Figure 3b,c, open circles) were also negligible. For all storage conditions examined in this study, the impedance data of LDSAMs were constant for 4 weeks, indicating a robust maintenance of the insulating properties over this time period, thereby effectively ruling out the possibility of phase segregation as the cause of the changes in the FTIR spectra.

Still, chemical changes such as oxidation or contamination could in principle contribute to the observed red shift in the FTIR spectra. In fact, it is important to recognize that oxidative degradation of SAMs under ambient conditions may occur without an adverse impact on electrochemical barrier properties. Schoenfisch et al.[5] demonstrated for high-density SAMs on gold that monolayer oxidation can concur with the maintenance of high impedance values. To assess changes in the chemical composition of the low-density monolayers under different storage conditions, XPS analysis was conducted for samples stored for 4 weeks, and the data were compared to those for freshly prepared samples.

X-ray Photoelectron Spectroscopy. XPS was performed to determine whether the different storage conditions had an effect on the oxidation of the LDSAMs, even beyond the level that may be detected by EIS. As shown in Table 1, the chemical compositions of both LDSAMs and conventional SAMs of MHA were in good agreement with the theoretically expected values. Table 1 summarizes the component model fitting for these spectra. The observed peak areas for aliphatic carbons, carbons adjacent

to the head and tail groups, and the carbonyl carbon correspond well with theoretical expectations. In addition, detailed analysis of the fine structure of the high-resolution S 2p spectra can reveal additional information regarding thiol oxidation. Figure 4a shows LD-MHA after 4 weeks of storage in air at room temperature. The high-resolution S 2p spectra of low-density SAMs show characteristic doublet signals at ∼162.5 eV, which can be attributed to surface-bound thiols.[28] In contrast, doublet signals at ∼167 eV, which are characteristic of oxidized sulfinate and sulfonate species,[6,29] are not present. Although a small shoulder on the left side of the original S $2p_{1/2}$ signal can be identified at ∼163.5 eV, the spectra do not indicate substantial amounts of oxidized species as expected for a widely oxidized monolayer. Likewise, for LD-MHA stored for 4 weeks in argon at room temperature (Figure 4b) and in argon at 4 °C (Figure 4c), characteristic oxidation peaks at ∼167 eV are not observed. Whereas storage under inert conditions (argon) can be expected to reduce oxidation significantly, the lack of oxidation for the sample kept in an air environment may be less intuitive. This can be elucidated, however, by the work of Willey et al., who observed the rapid (<24 h) oxidation of dodecanethiol SAMs exposed on a benchtop to ambient air, yet no significant oxidation when the samples were enclosed in sealed vials (as in this study).[8] It was suggested that the oxidation is driven by dilute atmospheric ozone,[5,28−29] which is rapidly depleted in sealed containers. To complement the high-resolution sulfur analysis, Figure 5 shows the corresponding high-resolution C 1s spectra of the low-density SAM samples. The high-resolution C 1s spectra reveal characteristic signals for aliphatic carbon (*C*−H) at 285.0 eV and carboxyl carbon (*C*−OOH) at 288.8 eV. In addition, there is a third signal at 286.6 eV that can be attributed to thiol-bond carbon (*C*−SH) as well as carbon in the α position with respect to the carboxyl group (*C*−COOH). Quantitative analysis of the spectra is given in Table 1 and is in excellent agreement with the theoretically expected values for all examined storage conditions. Given the intrinsic sensitivity limit of XPS, any change in the overall composition of the SAM of about 1 atom % or more can be expected to be detected by XPS and can be ruled out on the basis of this study.

Although the XPS data cannot entirely rule out oxidation and/or minimal contamination as the cause of the red shift observed in the FTIR study, these factors are most likely not the major contributors, given the XPS results. In addition, it is worthwhile to recognize that Figures 1d and 2d show the FTIR spectra of LDSAMs stored in ethanol solutions, which clearly provide different sources of contamination or oxidation than do samples stored under air or argon conditions, but the FTIR spectra show identical shifts of the methylene bands.

On the basis of the XPS and electrochemical impedance analysis, thermodynamically driven chain ordering due to an increase in van der Waals interactions appears to be the most likely cause of the structural changes observed with FTIR. Similar ordering effects have been observed for high-density monolayers at increased temperatures, which increase the fluidity of the monolayers.[30]

Conclusions

Low-density self-assembled monolayers of mercaptohexadecanoic acid on gold were stored under air, argon (25 and 4 °C), and ethanol. Analysis by electrochemical impedance spectroscopy showed no significant change in the electrochemical insulating properties of the air, argon, and ethanol samples over the course of 4 weeks. Oxidative degradation of these samples was also not observed by X-ray photoelectron spectroscopy. However, the fine structure of low-density SAMs as determined by Fourier transform infrared spectroscopy showed a trend toward decreasing alkyl chain fluidity over time. Increased ordering of MHA molecules on the surface is a possible cause of these observations. The robust chemical and electrochemical stability of low-density SAMs under a variety of practical storage conditions points toward the applicability of these systems in potential technological applications.

Acknowledgment. D.K.P. acknowledges support from a graduate fellowship from the National Institutes of Health through the University of Michigan Cellular Biotechnology Training Program. This project was funded by grants from the National Institutes of Health (5 R21 EB005732-02) and the Department of Defense (Idea award, W81XWH-06-1-0271).

LA701607E

(28) Lee, M. T.; Hsueh, C. C.; Freund, M. S.; Ferguson, G. S. *Langmuir* **1998**, *14*, 6419−6423.
(29) Tarlov, M. J.; Burgess, D. R. F.; Gillen, G. J. *J. Am. Chem. Soc.* **1993**, *115*, 5305−5306.
(30) Norrod, K. L.; Rowlen, K. L. *J. Am. Chem. Soc.* **1998**, *9*, 2656−2657.
(31) Zhang, Y. M.; Terrill, R. H.; Tanzer, T. A.; Bohn, P. W. *J. Am. Chem. Soc.* **1998**, *9*, 2654−2655.
(32) Delamarche, E.; Michel, B.; Kang, H.; Gerber, C. *Langmuir* **1994**, *10*, 4103.